ROBUST ADAPTIVE UNSCENTED KALMAN FILTERS FOR INTEGRATED NAVIGATION WITH NONLINEAR MODELS

YANG CHENG

Ph.D

The Hong Kong Polytechnic University

2017

The Hong Kong Polytechnic University

Department of Land Surveying and Geo-Informatics

Robust Adaptive Unscented Kalman Filters for Integrated Navigation with Nonlinear Models

YANG CHENG

A thesis submitted in partial fulfillment of the requirements for the degree of Doctor of Philosophy

March 2017

CERTIFICATE OF ORIGINALITY

I hereby declare that this thesis is my own work and that, to the best of my knowledge and belief, it reproduces no material previously published or written, nor material that has been accepted for the award of any other degree or diploma, except where due acknowledgement has been made in the text.

_________________________ (Signed)

YANG Cheng (Name of student)

Abstract

One of the key issues in navigation and kinematic positioning is to estimate state parameters from measurements and dynamics information with errors. The commonly used method for kinematic positioning and navigation is measurements from integrated Global Navigation Satellite System (GNSS) and Inertial Measurement Unit (IMU), and a Kalman filtering method can be used to fuse these two types of measurements with their uncertainties. The conventional Kalman filter is an optimal estimator for a linear system contaminated by Gaussian noises. In fact, most of the real-world dynamic systems tend to have a certain degree of nonlinearity, thus various filters have been proposed for dealing with nonlinear models, such as Extended Kalman filter (EKF), Unscented Kalman filter (UKF), and particle filter (PF). The optimality of these filter algorithms, however, is linked with the knowledge of the system noise and the quality of the measurements. The performance of the filters can be degraded or even diverged in the case that the stochastic model used in the estimation is largely different from the real dynamic system noise, or in the case that measurements containing outliers are used in the estimation process. This research investigates the method to improve the accuracy and robustness of state estimates in GNSS/IMU integrated navigation systems.

The main contributions of the thesis are:

(1) A common theoretical framework for both EKF and UKF is established by correlation inference.

A common theoretical framework of the two filters is established by correlation inference. The estimator expressed by the inference only depends on measurements, approximated

state, and predicted measurements as well as their covariance and cross-covariance matrices. The relationships and the performance differences between UKF and EKF are discussed in terms of theoretical foundation and algorithms, and are tested using both simulation and observation data. The results indicated the superiority of UKF for kinematic state estimation.

(2) Based on the above theoretical framework established, an adaptive UKF (AUKF) method is proposed to reduce the influence of the disturbance of a dynamic system.

An AUKF is rigorously derived based on the correlational inference method. The adaptive nonlinear estimator not only reduces the influence of those unpredictable dynamic disturbances, but also takes into account the effects of the nonlinear model. An adaptive mechanism is developed by using an innovation vector at the current measurement epoch, which avoids the storage of innovation sequences and is more sensitive to the discrepancy between those from the predicted system state and the measurements. Both simulation and field test have shown that the AUKF outperforms the conventional UKF in terms of accuracy of the positioning and velocity estimates in the case of dynamic disturbances.

(3) M-M estimation theory is applied and a robust M-M UKF (RMUKF) is developed to further reduce the influence of measurement outliers.

Since the estimate accuracy is improved by the aforementioned AUKF method in the case of dynamic disturbances. This study is then extended to further reduce the influence of measurement outliers, if any, for which the RMUKF method is proposed. The RMUKF estimator is robust and it applies the maximum likelihood (M-) principle to the errors in both functional model and measurements. The estimator of the RMUKF is also deduced and analysed. A weight matrix composed of bi-factor shrink elements is developed for the RMUKF for keeping the original correlation coefficients of predicted state elements unchanged. The RMUKF successfully attenuates both the dynamic model disturbances and the influence of measurement outliers.

(4) The theory developed above is verified by using an integrated IMU/GNSS navigation system in which the nonlinear IMU error model is treated as a dynamic model.

The conventional IMU error model is derived based on the assumption that a small angle exists in attitude errors only. Hence the coordinate transformation matrices in the positioning solution can be presented by approximated matrices. To illustrate the proposed nonlinear estimators, a nonlinear IMU error model derived by the Euler angle errors, is employed to integrate with GNSS in a loosely coupled integration strategy. The performance of the proposed estimators is evaluated by using both simulation and field data.

Acknowledgements

The doctoral degree completion to my satisfaction level has never been an easy task. I cannot express enough gratitude to my supervisors, Prof. Wenzhong Shi and Prof. Wu Chen, for their inspiring guidance and continued support. They have given me timely and scholarly suggestions with great kindness at every stage of my research, which has helped me enormously to accomplish this thesis.

I would also like to express my sincere gratitude to Prof. Gao Yang for the learning opportunities at the University of Calgary. His help and continuous advice even after the exchange period have given me great inspirations. My special thanks to Dr. Naser El-Sheimy as well, whose lecture on Inertial Techniques and INS/DGPS Integration has directly influenced the design of the integrated navigation in the dissertation.

My thanks go to my colleague Rui Xu for her significant support to my research, and Dr. Nan Gao from Beihang University for his comments during my programming. My thanks also go to all my fellow colleagues at the Hong Kong Polytechnic University for their assistance and encouragement, especially to Anshu Zhang, Wenzheng Fan, Xiaolin Zhou, Qiliang Liu, and Zi Yang.

Last but not least, I wish to express my deepest gratitude to my parents and my wife for their unconditional support and love, which helped me survive from all the stress during these years and made me be persistent on work. Their love has inspired me to go beyond what I thought I could go.

Contents

List of Figures

List of Tables

List of Abbreviations

AKF	Adaptive Kalman Filter
AUKF	Adaptive Unscented Kalman Filter
BDS	BeiDou Navigation Satellite System
CA	Constant Acceleration
CMT	Covariance Matrix Trace
CV	Constant Velocity
DCM	Direct Cosine Matrix
DD	Double Difference
DGPS	Differential GPS
DoD	Department of Defense
DR	Dead Reckoning
ECEF	Earth-Centered Earth-Fixed
EKF	Extended Kalman Filter
EU	European Union
GEO	Geostationary
GNSS	Global Navigation Satellite System

GPS	Global Positioning System
IGSO	Inclined Geosynchronous Orbit
IMU	Inertial Measurement Unit
INS	Inertial Navigation System
ITRF	International Terrestrial Reference Frame
LKF	Linearized Kalman Filter
LS	Least Squares
MEO	Medium Earth Orbit
MMSE	Minimum Mean Squared Error
NMEA	National Marine Electronics Association
PDF	Probability Density Function
PF	Particle Filter
PPP	Precise Point Positioning
PRN	Pseudo-random Noise
PVT	Position, Velocity, and Time
PZ 90	Parametry Zemli 1990
RAKF	Robust Adaptive Kalman Filter

RMSE	Root Mean Square Error
RMUKF	Robust M-M Unscented Kalman Filter
RTK	Real Time Kinematics
SD	Single Difference
SIS	Sequential Importance Sampling
SPP	Single Point Positioning
SUT	Scaled Unscented Transform
UKF	Unscented Kalman Filter
UT	Unscented Transform

Chapter 1 Introduction

1.1 Problem Description and Research Objectives

1.1.1 Problem Description

State estimation is to provide a complete representation of the internal status of a system at a given instant of time (Simon, 2006). Estimating the state is of paramount importance to the tracking of kinematic or dynamic systems, such as vehicle tracking and navigation. The aim of the state estimation is to solve state parameters from noisy signals or measurements collected from sensors (Yang et al., 2016). The sensors, in general, can be receivers of the Global Navigation Satellite Systems (GNSS), Inertial Navigation System (INS) and other geometric or physical measurement sensors. Signals from the sensors are subjected to errors including both systematic and random errors.

A Kalman filter is an optimal estimator and has been widely applied in real-time system state estimation under the assumptions that the errors in both measurements and dynamic models following normal (or Gaussian) distributions and the dynamic models are linear. However, the state estimation of a Kalman filter, may need to address the nonlinearity of the state space model (Yang et al., 2004), thus several extended Kalman filters have been proposed. For example, the Extended Kalman filter (EKF) and Linearized Kalman filter (LKF) are two approaches that use the first-order Taylor expansions to analytically deal with the nonlinearity of the state space models.

The Particle filter (PF) uses a sequential Monte Carlo sampling method based on a Bayesian theorem to approximate the posterior Probability Density Function (PDF) of the system state. However, for some real time applications, this method may not be feasible (Doucet et al., 2001). The Unscented Kalman filter (UKF), introduced by Julier and Uhlmann (1997), in which the functional models can be either linear or nonlinear, is also a probabilistic approach to approximate the state distribution by Gaussian random variables. The filter utilizes the Unscented Transform (UT) to estimate the system state, which then undergoes a nonlinear transformation (Wan & van der Merwe, 2000; Julier & Uhlmann, 2004).

The Kalman filter and its alternatives, however, are susceptible to outliers in measurements, if any, since the outlier contaminated data are inconsistent with the overall distribution pattern (Fitzgerald, 1971; Durgaprasad & Thakur, 1998). For practical systems, two types of outliers are often assumed, bad data in measurements and unpredictable disturbance of the dynamic models. The adaptive estimation proposed in this study is to handle the unpredictable disturbance of the dynamic model and also the biased prior stochastic information of the model. This approach adjusts the stochastic model in accordance with the real dynamic system noises. For the outliers in the measurements, a robust estimation is introduced to reduce the weight of those measurements that contain outliers (Yang, 1991). These two methods are under the assumption that only one type of outliers exists.

1.1.2 Objectives

This research aims to develop a robust and adaptive nonlinear filter for the application of a navigation system integrating the GNSS and Inertial Measurement Unit (IMU) to provide a continuous on-the-fly navigation state. This aim is achieved by realizing the following four research objectives:

1. Comparing the performances of the UKF and EKF under a common theoretical framework and various scenarios.

An alternative Kalman estimator derivation is presented with a correlational inference based on the cross-covariance matrices between measurements, predicted state and predicted measurements and a common Kalman filtering framework is established. A comparison between the UKF together with scaled unscented transform (SUT) and EKF is conducted based on theoretical analysis, simulation and field tests. The Taylor Expansion of an arbitrary nonlinear model is employed to analyze the performance of the filters. Integrated vehicle navigation, simulation and field tests are carried out using different state space models, different feedback modes and different integration strategies to assess the performance of the UKF and EKF.

2. Developing an adaptive Unscented Kalman filter based on correlational inference.

Based on the correlational inference, an adaptive Unscented Kalman filter (AUKF) is developed for reducing the influence of the dynamic model's disturbance. An adaptive factor introduced for the AUKF is the innovation vector at the present epoch. The use of the adaptive mechanism is mainly to effectively reduce the unpredictable disturbances of the dynamic model.

3. Developing a robust method for effectively addressing contaminated measurements.

A robust unscented Kalman filter based on the maximum likelihood estimation method is developed for the attenuation of those contaminated measurements and the disturbances of the dynamic model. Correlations between states are taken into consideration to prevent the error transform, and a weight matrix composed of bi-factor elements is introduced to keep the original state correlation coefficients unchanged.

4. Validating the proposed methods by using nonlinear state space model.

The effectiveness of the two proposed methods, i.e. AUKF and RMUKF, are tested using both simulation and field data collected from a GNSS/IMU integrated navigation system, in which the nonlinear IMU error model is employed for the system dynamic model. Both the simulation and field tests are proceed without initial alignment.

1.2 Dissertation Outline

The structure of the thesis is given in Figure 1.1 and its details are as follows:

Chapter 2 and **Chapter 3 present** literature review related to the study of this thesis and functional models respectively.

Chapter 4, an alternative expression for a Kalman filter based on a correlational inference is presented. A comparative study of the Kalman filter and UKF including an analytical analysis of the UKF and EKF based on Taylor expansions, and their prediction accuracy are given. The overall performance of the UKF and EKF is tested and compared using an integrated vehicle navigation system. A theoretical framework for the Kalman filtering is established, and the corresponding estimators are derived.

Chapter 5 addresses an unpredictable dynamic model's disturbances or use of improper stochastic information which could cause degradation in the filter's performance or even divergence. It mainly includes: 1) the construction of an adaptive factor based on the discrepancy of the current system to control the dynamic model disturbances, which is flexible for constructing the adaptive factor; 2) the nonlinear IMU error model is employed to perform the GNSS/IMU integration in a loosely coupled strategy.

Chapter 6 presents a robust M-M UKF (RMUKF) to handle the measurement outliers. The correlated bi-factor equivalent weight matrix for the RMUKF is determined by using the maximum likelihood (M-) principle. The robust mechanism suppresses the state outliers from both the dynamic model and measurements and so it can provide a robust solution in an iterative manner.

The major findings of this study and conclusions are summarized in **Chapter 7,** and recommendations for further research are also made in this chapter.

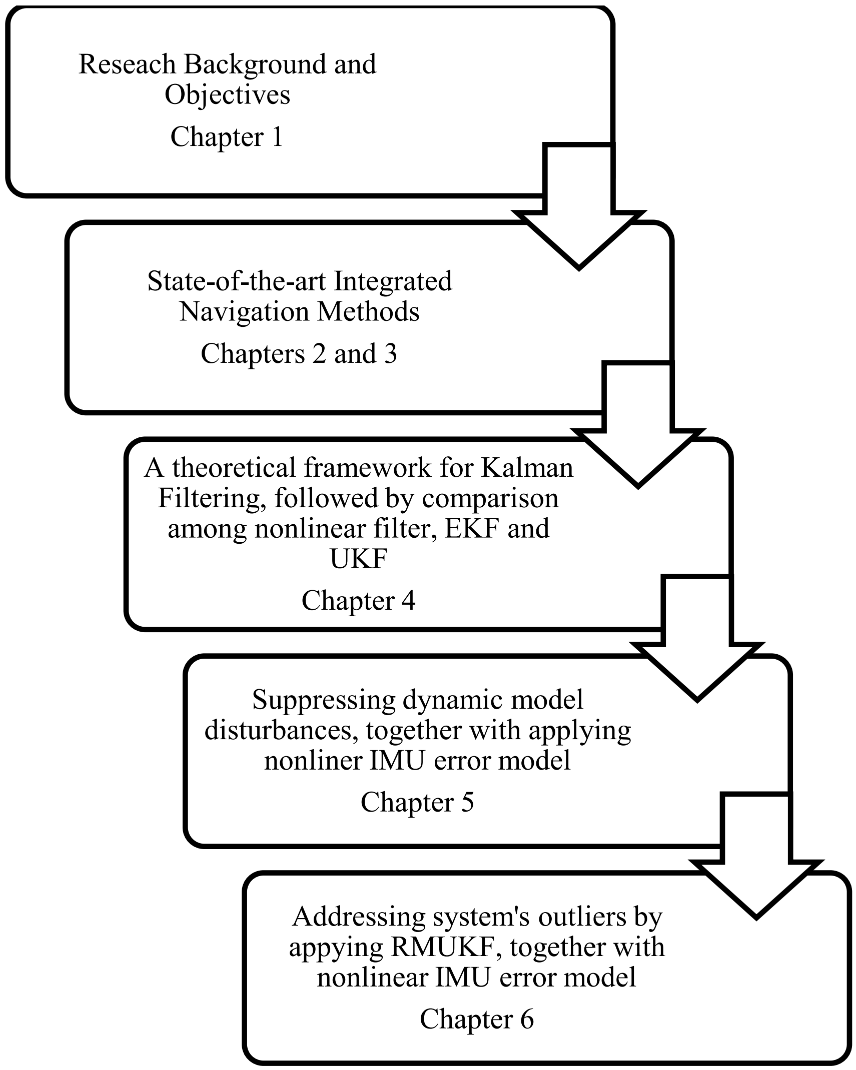

Figure 1.1 The organization of the thesis

Chapter 2 An Overview of Existing Filtering Methods

In this Chapter a brief history of the development for navigation systems, including GNSS and IMU development, together with their integration strategies is reviewed first. Various nonlinear estimation methods including the state-of-the-art research on adaptive estimators, robust estimators, and adaptive robust Kalman filters are then examined for the development of a robust adaptive estimator for this study.

2.1 Integrated Navigation System

Historically, navigation was primarily used for directing vessels upon the open seas and accomplished by the use of compasses and other observations such as those from the sun and stars. Nowadays, GNSS have been widely applied in many aspects of our lives. Using GNSS to navigate requires at least four light-of-sight measurements. In an urban canyon environment, however, the visibility of the GNSS satellites or the geometry of the observations are often poor, and even worse, the GNSS signals can be blocked. In addition, high-rise buildings may introduce multipath effects which degrade positioning accuracy. In this case, a single satellite navigation system can hardly provide continuous, accurate and robust state estimates for the user’s position. . A solution to this problem is an integration of GNSS with other types of sensors such as accelerometers and gyroscopes.

2.1.1 Global Navigation Satellite Systems

GNSS, a general term of satellite-based radio navigation systems, has played a fundamental role in positioning and navigation over 20 years. It is an all-weather system providing world-coverage information on position, velocity and time (PVT) 24 hours a day. The first GNSS, i.e. the Global Positioning System (GPS), was originally intended for military only, however, with the development of several other navigation systems, such as the Chinese BeiDou Navigation Satellite System (BDS), the European Galileo and Russian GLONASS, navigation applications have been largely extended to almost all location based services nowadays.

The principle of GNSS positioning is the use of the range measurements from several satellites with known positions to the receiver to estimate the position of the receiver (Hofmann-Wellenhof et al., 2003). The range is in fact measured according to the travel time of the signal from the satellite to the receiver. Ideally, the clocks in both the receiver and satellites need to be synchronized first, and then the range can be calculated by the travel time of the signal multiplied by the speed of light. The position of the receiver is at the spherical surface with the radius equal to the range. Since the range measurements are affected by the biases of the clocks, they are called pseudorange measurements. To solve the additional parameters for the bias between the clocks of the receiver and the satellite, the positioning solution requires at least four satellites.

2.1.1.1 Global Positioning System

GPS was developed by the Department of Defense (DoD) of the United States in the 1970s and declared operational in 1995 (Noureldin, Karamat, & Georgy, 2013). Currently, the system operates with 32 satellites, including 12 Block II R satellites, 7 Block II R-M satellites, and 12 Block II F satellites. The system can achieve a 10-meter-level positioning accuracy with single point positioning (SPP). To improve the services, next generation satellites, i.e. GPS Block III, is under development via GPS moderation. The new satellites signals in addition to the current ones will improve the accuracy and availability for all users (Betz et al., 2006).

2.1.1.2 BeiDou Navigation Satellite System

The BDS, developed in China, enables interoperation with other GNSS. Unlike GPS, the BDS has an additional message service and will consist of 35 satellites upon completion aiming to provide worldwide positioning services by 2020. The system includes 5 geostationary (GEO) satellites, 3 inclined geosynchronous orbit (IGSO) satellites, and 27 Medium Earth orbit (MEO) satellites. Until November 2016, 20 satellites were operational, including 6 GEO satellites, 8 IGSO satellitse, and 6 MEO satellites. Currently, the system is providing regional position services covering the Asia-Pacific region. The positioning and velocity accuracy of the system for free civilian users can be achieved within 10 m and within 0.2 m/s respectively.

2.1.1.3 Galileo

Galileo, developed by the European Union (EU), was first raised in 1999. The first two experimental satellites were launched in 2005 and currently it has 18 satellites in operation. With 30 satellites, it will become fully operational and provide worldwide navigation services for both civil and military users at a same level of accuracy by 2020. The system intends to interoperate with GPS, which enables the receivers to combine the signals from both Galileo and GPS constellations to increase the positioning accuracy (Jin et al., 2014). The Galileo system announced the initial services on December 15th, 2016 (European GNSS Agency, 2016). The initial stage is able to provide the following services: search and rescue service, precise time synchronization, and public regulated service.

2.1.1.4 GLONASS

GLONASS was introduced in 1976 by the former Soviet Union. The system was fully operational by 1995 with 24 satellites. However, only 6 satellites remained in 2001 due to the economic crisis of the country. By 2010, the GLONASS constellation consisted of 18 satellites and provided navigation support predominantly for the Russian territory. Currently, the system is again fully operational with 27 satellites and provides worldwide navigation information.

2.1.2 Inertial Measurement Unit

An Inertial Navigation System (INS) uses the dead reckoning (DR) method to determine navigation state, position, velocity and attitude. DR is a relative navigation method that estimates the position of an object based on the previously determined coordinates and the relative movement sensed at the present epoch, such as the velocity and attitude information. The navigation update of an INS is dependent on the internal hardware for 3-dimensinal navigation by means of a rigorous computation model, based on such as gyroscopes and accelerometers, rather than on the external guidance. An IMU, which consists of three orthogonal gyroscopes and three orthogonal accelerometers, is the core hardware for inertial measurements. The IMU measures the angular motion rate and the linear motion of an object. The sensors are mounted rigidly onto the device and formed a strapdown system so that the gyroscopes and accelerometers can sense the motion of the body frame with respect to the inertial frame. The velocity, position, and attitude of the object are then mathematically integrated from the measured data and projected to the local level frame.

Micro-Electro-Mechanical System (MEMS) technology enables the development of low-cost and small size integrated navigation systems for land vehicle and guidance applications. Despite the technological advances, MEMS-based IMUs inherit the error behavior of conventional inertial sensors, and also suffer from a variety of error sources which engender as a low performance device (Park & Gao, 2006). Thus, the IMU is difficult to be independently used as a navigation system, given that its estimation accuracy will degrade in a short period of time.

2.1.3 Integration Strategies

Based on the complementary characteristics of GNSS and IMU, positioning information derived from GNSS can be used to compensate IMU output; IMU can also provide position information between GNSS updates or satellite signal outages. An integrated system can become an enhanced navigation system that provides continuous and accurate position information. Typically, three commonly used strategies can be applied to the integrated system namely, loosely coupled strategy, tightly coupled strategy, and ultra-tightly coupled strategy (Petovello, 2003). The ultra-tightly coupled integration is conducted at the hardware level and hence is not included in this dissertation.

2.1.3.1 Loosely Coupled Integration

In the loosely coupled integration, both the raw GNSS measurements and IMU output are processed separately. Normally, the GNSS measurements are processed iteratively by the least squares or Bancroft method (Bancroft, 1985); and the IMU outputs are solved by the DR method. The differences between the GNSS and DR positions and velocities represent the filter's observations. The advantages of the loosely coupled integration are that the system is robust as two positioning systems work independently and the data processing of the filter is fast due to the separation of the two processing systems. Its main disadvantage is that at least 4 GPS satellites are needed for positioning and INS error accumulates over time. The scheme of this type of integration is presented in Figure 2.1.

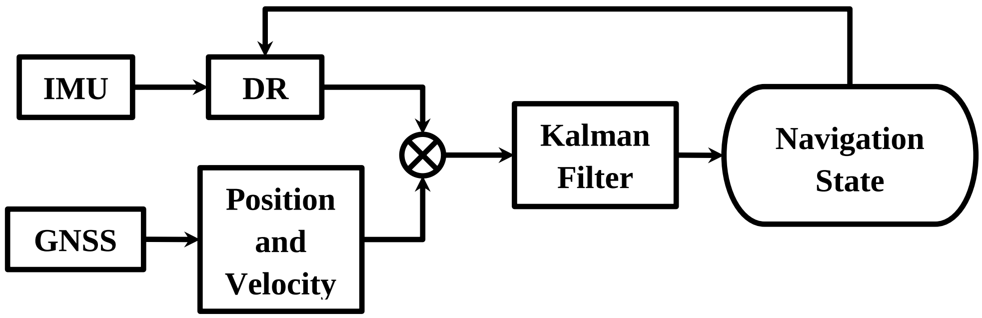

Figure 2.1 Loosely coupled integration

2.1.3.2 Tightly Coupled Integration

The tightly coupled integration process GNSS raw data and IMU output together. The position and velocity obtained from the DR approach are for predicting GNSS measurements using the position and velocity of the satellites. The advantage of the approach is that the system can provide navigation solutions when the number of satellites in view is less than 4. The major disadvantage of the tight integration is the increased dimension of the state vector, the clock bias, which results in heavy computational loads. The scheme of the tightly coupled integration is showed in Figure 2.2.

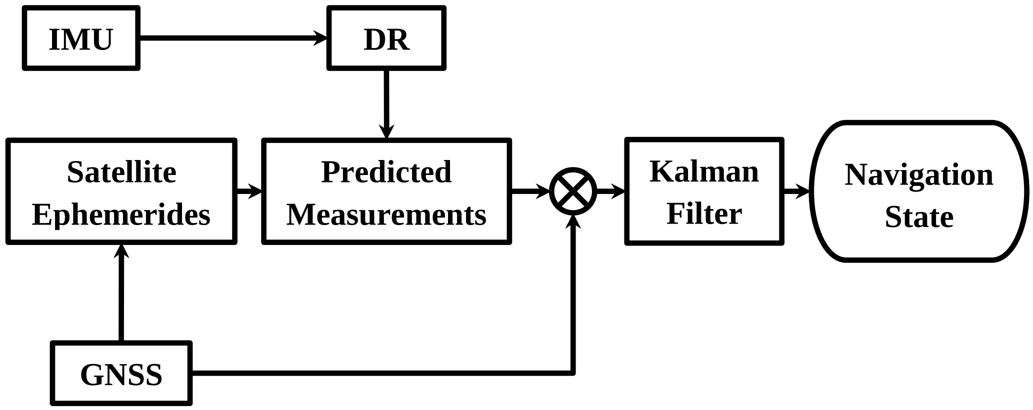

Figure 2.2 Tightly coupled integration

The main difference between the above two strategies is that different types of measurement data are used in the estimation. The loosely coupled integration uses processed measurements, in which the navigation states estimated by the GNSS receiver are integrated with the DR solution. However, the tightly coupled integration strategy employs raw GNSS measurements, such as pseudoranges and Doppler shifts, to conduct DR in a Kalman filter to estimate navigation states.

2.2 State Estimation

Filters to fuse noisy information from different sources are used to obtain an accurate state estimate of an integrated system. The Kalman filter is the most widely used method for state estimation (Gao et al., 2008; Challa, 2011). The filter provides an accurate estimated state based on the minimum mean squared error (MMSE). In reality, however, a dynamic system is generally nonlinear. Thus, the system has to be linearized by the first-order Taylor series expansion and further applied by the Kalman filter afterwards, namely EKF. The first order Taylor series expansion requires calculating the Jacobian matrix, while the reason to neglect the higher-order terms of the Taylor expansion is due to its large computation load, which introduces linearization errors and sometimes may cause filter divergence. To estimate the system state at a high accuracy, in recent years, two alternative methods, UKF and PF, have been proposed. The UKF method propagates the state mean and covariance through nonlinear functions without using a linearization process. The PF method employs a number of particles to approximate the state directly.

2.2.1 General State Space Model

State space model expresses measurements as a function of state that completely characterizes the dynamic of a system (Friedland, 1986; Hamilton, 1994). The model also depicts the probabilistic dependence between the latent state variable and the observed measurements (Zhe & Emery, 2013). A discrete-time state space model can be expressed as,

$$x_k = f(x_{k-1}) + w_k \tag{2.1}$$

$$y_k = h(x_k) + e_k \tag{2.2}$$

where f is the transition equation of the state evolution and h is the observation equation; f and h can be either linear or nonlinear functions. k is the time index or epoch; x_k is the n-dimensional system state at epoch k; y_k is the observation vector; w_k and e_k are the vectors of process noise and observation noise respectively.

The objective of the state space modelling is to estimate the PDF of the state vector using the observed data, which can be derived from a recursive process based on Bayes' rule (Zhe & Emery, 2013). The recursive process first predicts the system state at the current epoch based on the estimated state at the last epoch and the system evolution equation, and then corrects or updates the predicted result using the measurements of the current epoch to obtain the estimates of the current epoch (Orderud, 2005). The prediction stage propagates the current state distribution through function f , and then the predicted probability density function is obtained,

$$p(x_k|y_{k-1}) = \int p(x_k|x_{k-1})p(x_{k-1}|y_{k-1})\, dx_{k-1} \qquad (2.3)$$

where $p(x_k|x_{k-1})$ is the probability model of the state evolution specified by function f and the process noise distribution $p(w_k)$. The update stage corrects the predicted PDF based on the latest measurements via the Bayesian rule (Rigatos, 2012),

$$p(x_k|y_k) = \frac{p(y_k|x_k)p(x_k|y_{k-1})}{p(y_k|y_{k-1})} \qquad (2.4)$$

where the normalising constant,

$$p(y_k|y_{k-1}) = \int p(y_k|x_k)p(x_k|y_{k-1})dx_k \qquad (2.5)$$

depends on the likelihood function $p(y_k|x_k)$ which is fully specified by the observation function h and the observation noise distribution $p(e_k)$.

The general form of the Bayesian approach is difficult to be analytically resolved as the dominator of eq. (2.4) cannot be computed analytically (Doucet et al., 2000; Doucet et al., 2001). The state space model, if it is linear and the noise terms w_k, e_k are Gaussian distributed with zero mean, then the Kalman filer can be applied to estimate the PDF of the state. The particle filter, however, is able to implement the recursive Bayesian filter numerically.

2.2.2 Kalman Filter

Kalman filtering has been widely applied in multi-sensor integration for decades. It is an effective and versatile method to estimate the state from uncertain dynamics by combining noisy sensor outputs. Nevertheless, the state estimation of Kalman filtering, no matter what sensor outputs are used, has to address the nonlinearity of the state space model (Yang et al., 2004). Several methods for extending the standard Kalman filter to nonlinear state space model have been developed. For example, the EKF has been commonly used for nonlinear multi-sensor fusion (Grejner-Brzezinska & Yi, 2003; Wu & Yang, 2010). It propagates the first two moments of the density, mean and covariance of the system state, through the linearized model (Gordon et al., 1993; Huang & Wang, 2006), as given by:

$$x_k = f(\hat{x}_{k-1}) + f^{(1)}(\hat{x}_{k-1})(x_{k-1} - \hat{x}_{k-1}) + \frac{1}{2}(x_{k-1} - \hat{x}_{k-1})^T f^{(2)}(\hat{x}_{k-1})(x_{k-1} - \hat{x}_{k-1}) + \cdots \quad (2.6)$$

$$y_k = h(\bar{x}_k) + h^{(1)}(\bar{x}_k)(x_k - \bar{x}_k) + \frac{1}{2}\left((x_k - \bar{x}_k)\right)^T h^{(2)}(\bar{x}_k)(x_k - \bar{x}_k) + \cdots \quad (2.7)$$

where x_{k-1} and $\hat{x}_{k-1}$ are the true and estimated states vectors respectively at epoch $k-1$; $\bar{x}_k$ is the predicted state vector; $f^{(1)}(\cdot)$ denotes the Jacobian matrix of nonlinear function $f(\cdot)$; and $f^{(2)}$ denotes the Hessian matrix.

The detail of the derivation is presented in Chapter 3. The linear state space model with the first-order expansion can be written as,

$$x_k = Fx_{k-1} + w_k \quad (2.8)$$

$$y_k = Hx_k + e_k \quad (2.9)$$

where F and H are the linear transform matrices of the dynamic equation and the design matrix of the observation equation respectively, which are formed by the first two terms in eqs. (2.6) and (2.7) respectively; w_k and e_k are the two noise vectors following a Gaussian distribution with zero mean.

Let the covariance matrices of w_k and e_k are Σ_{w_k} and Σ_k respectively, the prediction state is,

$$\bar{x}_k = F\hat{x}_{k-1} \quad (2.10)$$

and its covariance matrix can be obtained from the error propagation,

$$\Sigma_{\bar{x}_k} = F\Sigma_{\hat{x}_{k-1}}F^T + \Sigma_{w_k} \tag{2.11}$$

The estimated state vector and its covariance matrix are,

$$\hat{x}_k = \bar{x}_k + K_k(y_k - H\bar{x}_k) \tag{2.12}$$

$$\Sigma_{\hat{x}_k} = (I - K_kH)\Sigma_{\bar{x}_k}(I - H^TK_k^T) + K_k\Sigma_kK_k^T \tag{2.13}$$

where K_k is the Kalman gain with the expression as,

$$K_k = \Sigma_{\bar{x}_k}H^T\left(H\Sigma_{\bar{x}_k}H^T + \Sigma_k\right) \tag{2.14}$$

The EKF approximates the posterior PDF by Gaussian, in which the first two moments of the density propagates through the linearized equations obtained by calculating the Jacobian matrices of the nonlinear functions f and h. This increases calculation complexity and inevitably introduces linearization errors.

2.2.3 Unscented Kalman Filter

The UKF, was introduced by Julier and Uhlmann (1997), is another probabilistic approach to approximate the state distribution using Gaussian random variables. The filter utilizes the Unscented Transform (UT) to estimate the system state which undergoes a nonlinear transformation (Wan & van der Merwe, 2000; Julier & Uhlmann, 2004). UKF samples a set of sigma points to match the current statistics properties and then propagates the points through the nonlinear function. The predicted mean and covariance are then estimated by the transformed and weighted sigma points and achieves at least to the second order of Taylor expansion (Julier & Uhlmann, 1997, 2002; Cui et al., 2005; Gustafsson & Hendeby, 2012).

The selection method of sigma points is based on the covariance matrix of the estimated state using a deterministic method,

$$\begin{aligned} \hat{x}_{0,k-1} &= \hat{x}_{k-1} \\ \hat{x}_{i,k-1} &= \hat{x}_{k-1} + \gamma S_i \quad i = 1,2,\cdots,n \\ \hat{x}_{i+n,k-1} &= \hat{x}_{k-1} - \gamma S_i \end{aligned} \tag{2.15}$$

where n is the dimension of the augmented state vector; γ is a scale factor,

$$\gamma = \sqrt{n+\kappa} \tag{2.16}$$

where the parameter κ fine tunes the sigma points. This affects the third- and higher-order terms of the Taylor expansion. It is possible for some of the fourth order-terms to be matched, when the state vector is Gaussian if $\kappa = 3 - n$. S_i in eq.(2.15) is the ith row or column of the square root of the state covariance matrix,

$$S_i = \sqrt{\Sigma_{\hat{x}_{k-1}}}_i \tag{2.17}$$

$\Sigma_{\hat{x}_{k-1}}$ is the state covariance matrix, and the subscript i is the ith column of the matrix square root. This formula can be solved by Cholesky decomposition.

The predicted state,

$$\bar{x}_{i,k} = f\left(\hat{x}_{i,k-1}\right) \tag{2.18}$$

$$\bar{x}_k = \sum_{i=0}^{2n}\left(w_i \bar{x}_{i,k}\right) \quad (2.19)$$

where w_i is the weight of the *ith* sigma point,

$$\begin{aligned} w_0 &= \frac{\kappa}{N+\kappa}, \quad i = 0 \\ w_i &= \frac{\kappa}{2(N+\kappa)}, \quad i \neq 0 \end{aligned} \quad (2.20)$$

where N is the number of the sigma points, $N = 2n + 1$.

The predicted covariance matrix can be calculated by the weighted transformed sigma points and the approximated mean values,

$$\Sigma_{\bar{x}_k} = \Sigma_{w_k} + \sum_{i=0}^{2n} w_i\left(\bar{x}_{i,k} - \bar{x}_k\right)\left(\bar{x}_{i,k} - \bar{x}_k\right)^T \quad (2.21)$$

The predicted measurement $\bar{y}$ and corresponding covariance are,

$$\bar{y}_{i,k} = h\left(\bar{x}_{i,k}\right) \quad (2.22)$$

$$\bar{y}_k = \sum_{i=0}^{2n} w_i\, \bar{y}_{i,k} \quad (2.23)$$

$$\Sigma_{\bar{y}_k} = \Sigma_k + \sum_{i=0}^{2n} w_i\left(\bar{y}_{i,k} - \bar{y}_k\right)\left(\bar{y}_{i,k} - \bar{y}_k\right)^T \quad (2.24)$$

The cross-correlated covariance is,

$$\Sigma_{\bar{x}_k\bar{y}_k} = \sum_{i=0}^{2n} w_i\left(\bar{x}_{i,k} - \bar{x}_k\right)\left(\bar{y}_{i,k} - \bar{y}_k\right)^T \quad (2.25)$$

The Kalman gain of the UKF is,

$$K_k = \Sigma_{\bar{x}_k\bar{y}_k}\Sigma_{\bar{y}_k}^{-1} \quad (2.26)$$

The estimated state vector is,

$$\hat{x}_k = \bar{x}_k + K_k(y_k - \bar{y}_k) \qquad (2.27)$$

and the estimated covariance is,

$$\Sigma_{\hat{x}_k} = \Sigma_{\bar{x}_k} - K_k \Sigma_{\bar{y}_k} K_k^T \qquad (2.28)$$

2.2.3.1 Scaled Unscented Transform

Unscented Transform (UT) is the key technique of the UKF and it determines sigma points to match the current statistical properties. The sampling strategy of the sigma points is not unique. Symmetric sampling, minimal skew sampling and spherical simplex sampling are popular methods. The symmetric sampling approach is widely used as it has the best estimation accuracy (Orderud, 2005). The bound radius of the sigma points are related to the state dimension. An increase in state dimension will lead to an increase in the bound radius of the sigma points, which may introduce the nonlocal effect, i.e. the filter may not guarantee the positive semi-definite of the covariance matrix (Julier, 1998). SUT is proposed to scale the bound radius of the sigma points to overcome the nonlocal effect as presented below,

$$\chi_i = \hat{x}_{k-1} \pm \sqrt{(n+\lambda)\Sigma_{\hat{x}_{k-1}}} \qquad (2.29\text{ a})$$

$$W_0^{(m)} = \frac{\lambda}{n+\lambda} \qquad (2.29\text{ b})$$

$$W_0^{(c)} = \frac{\lambda}{n+\lambda} + (1 - \alpha^2 + \beta) \qquad (2.29\text{ c})$$

$$W_i = \frac{1}{2(n+\lambda)} \tag{2.29d}$$

$$\lambda = \alpha^2(n+\lambda) - n \tag{2.29e}$$

where $0 \leq \alpha \leq 1$ is the scale factor that determines the bound radius of the sigma points; if the state is Gaussian, then $\beta = 2$; $\kappa \geq 0$ to guarantee positive semi-definiteness of the covariance matrix; W_i is the weight of the ith sigma point; and the superscripts m and c represent the mean and covariance respectively. The details of the derivation process can be found in Gustafsson and Hendeby (2012).

The scaled and non-scaled symmetric sampling approaches are presented in Figures 2.3 and 2.4, respectively. The two approaches propagate the sigma points through the system transition function expressed by eq.(2.30) and the parameters of scaled symmetric sampling are set as $\alpha = 0.01$, $\beta = 2$, $\kappa = 0$.

$$\begin{aligned} y_1 &= x_1 \sin\theta \\ y_2 &= x_2 \cos\theta \end{aligned} \tag{2.30}$$

Figures 2.3 (a) and 2.4 (a) are the mean and sigma points of the initial state. The transformed sigma points and the approximate mean are presented in Figures 2.3 (b) and 2.4 (b).

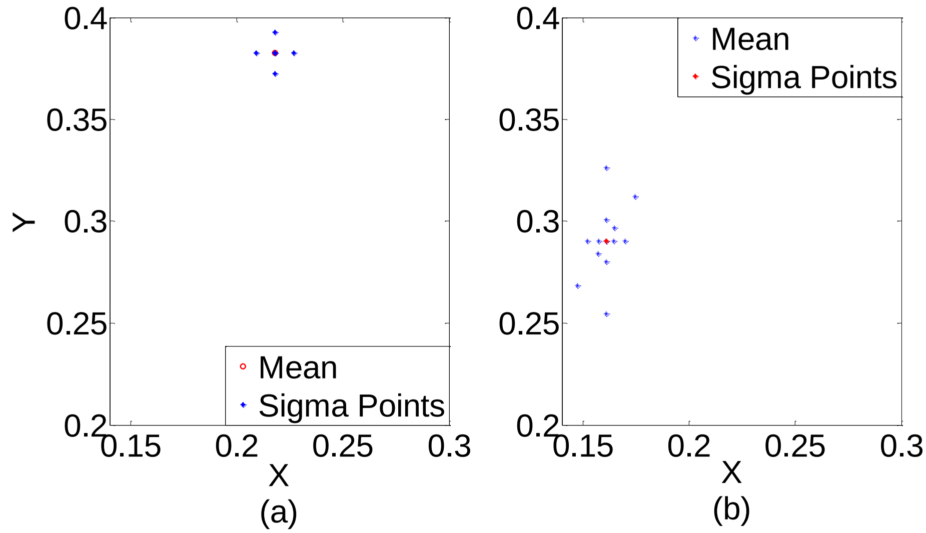

Figure 2.3 Scaled unscented transform

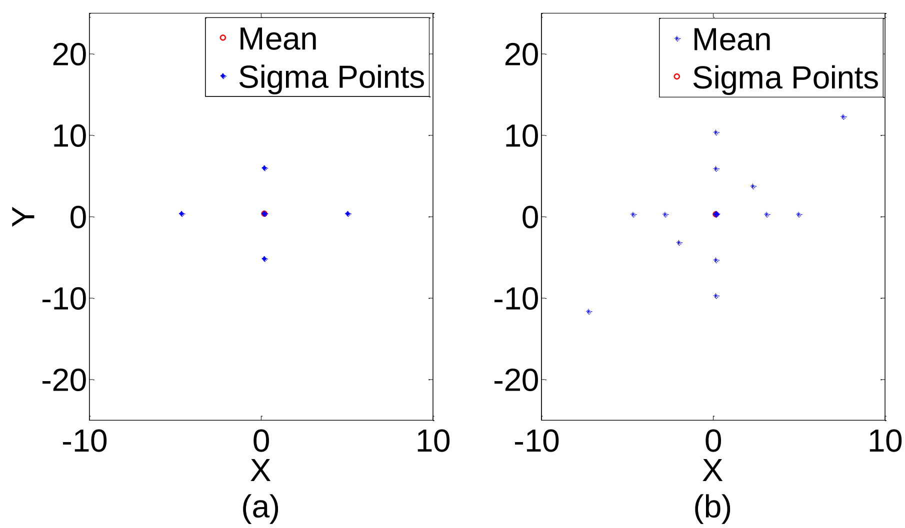

Figure 2.4 Unscented transform

Figure 2.5 shows the spread of the sigma points before and after propagation though the nonlinear equation with respect to $\hat{x}_{0,k-1}$ and $\bar{x}_{0,k}$, respectively.

$\hat{x}_{0,k-1}$ is the estimated state at epoch $k-1$; $\bar{x}_{0,k}$ is the prediction via the nonlinear model. The spread of the sigma points in SUT is noticeably smaller relative to that in UT, as shown in Figures 2.5(a) and 2.5(b). UT inevitably introduces nonlocal effects to the estimation of the system state. It is also found that the spread of the sigma points in SUT is affected by α. The spread of SUT is the same as that of UT when $\alpha = 1$. In this research SUT is considered in the system state estimation.

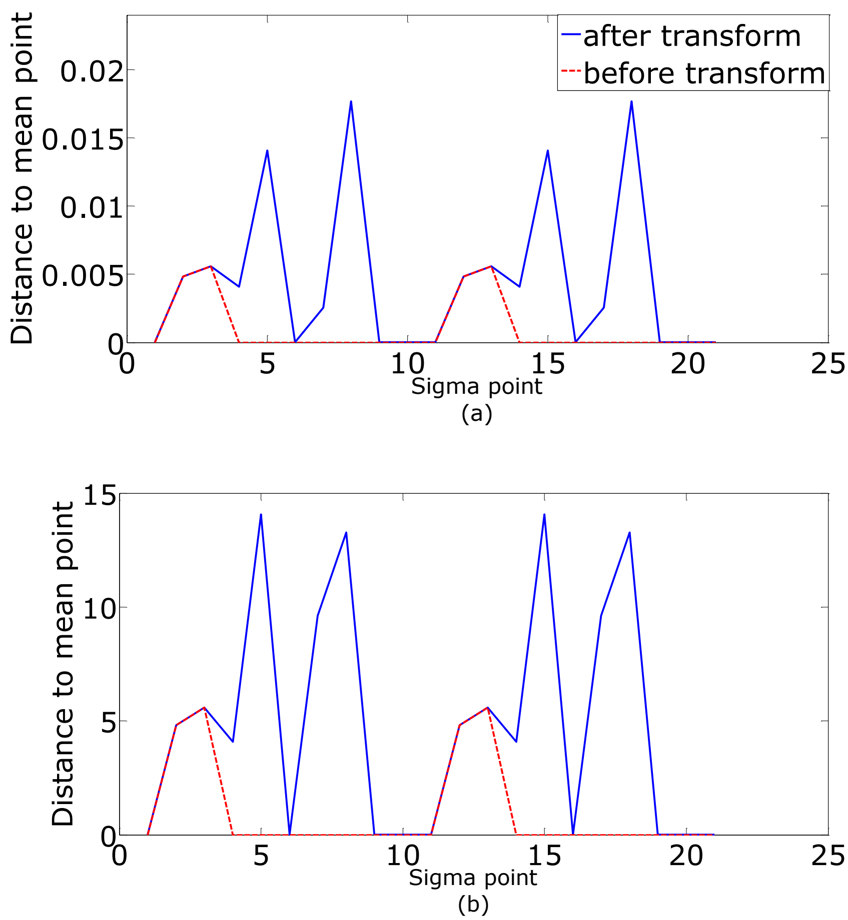

Figure 2.5 Comparison of sigma points spread distances with respect to the state mean value SUT (a) and UT (b)

2.2.4 Particle Filter

The Particle filter is a representative method and uses a sequential Monte Carlo sampling method based on a Bayesian theorem to approximate the posterior PDF of the system state (Gordon et al., 1993). The optimal estimation of the nonlinear and non-Gaussian state space model is provided by a large quantity of samples (Arulampalam et al., 2002; Gustafsson et al., 2002; Rigatos, 2012).

The PDF of the state vector can be expressed by $p(x_k|y_{1:k})$ with all available information. The PF prediction stage employs the system model and the PDF of the last epoch to obtain the prior information for the present epoch k, as shown in eq. (2.1). At the present epoch, the PDF of state vector can be estimated via the Bayesian rule eq. (2.4) with

$$p(y_k|y_{1:k-1}) = \int p(y_k|x_k)p(x_k|y_{1:k-1})dx_k \tag{2.31}$$

where the normalized constant depends on the likelihood function (2.32) which is determined by the observation model (Gordon et al., 1993)

$$p(y_k|x_k) = \int \delta\big(y_k - h_k(x_k)\big)p(e_k)de_k \tag{2.32}$$

Equation (2.4), however, is hard to be solved by any analytical method. Thus, the PF is commonly formulated as a Sequential Importance Sampling (SIS) method (Challa, 2011). The kernel of the method is to approximate the interest PDF based on a set of random samples $\left\{x_k^{(i)}, i = 1, \dots, N\right\}$ and the associated weights ω_k^i, which are normalized to $\sum_i \omega_k^i = 1$. The posterior density at present epoch k can be approximated as,

$$p(x_k|y_k) \approx \sum_{i=1}^{N} \omega_k^{(i)} \delta(x_k - x_k^{(i)}) \tag{2.33}$$

The weights are determined by importance sampling, with the samples being drawn from another distribution that has a support similar to the interest rather than the sample directly from the interest probability distribution. That is, the samples are drawn from the importance density $q(x_k^i|y_k)$ with the associated weight,

$$\omega_k^i \propto \frac{p(x_k^i|y_k)}{q(x_k^i|y_k)} \tag{2.34}$$

Factorize the importance density,

$$q(x_k^i|y_k) = q(x_k|x_{k-1}, y_k)q(x_{k-1}|y_{k-1}) \tag{2.35}$$

then the old particles $x_{k-1}^i \sim q(x_{k-1}|y_{k-1})$ can be augmented by $x_k \sim q(x_k|x_{k-1}, y_k)$ to obtain new particles $x_k^i \sim q(x_k^i|y_k)$.

The weight update is expressed as,

$$\omega_k^i \propto \omega_{k-1}^i \frac{p(y_k|x_k^i)p(x_k^i|x_{k-1}^i)}{q(x_k^i|x_{k-1}^i, y_k)} \tag{2.36}$$

Based on the SIS method, eq. (2.33) closes to the posterior density if the number of the particle is infinite. In practice, a prior transition density

$p(x_k|x_{k-1}^i)$ is chosen as the importance density, which is known as the bootstrap filter (Gordon et al., 1993).

Compared with the standard Kalman filter, the PF method has the advantages of no restriction being placed on the state space model or on the distribution of the system or on the measurements. However, the computation burden of the PF is heavy, especially in the case of high dimension state vector, and the exact distribution must be known (Daum, 2005; Chang & Liu, 2015).

2.3 Adaptive and Robust Estimation

The Kalman filter and its alternatives reduce error effects on the state estimates in a least squares sense, owing to the weighting information from different sources. The Kalman gain is the relative weight between the measurements and the system prediction obtained from the covariance matrices of the predicted state, measurements, and predicted measurements. In this sense, the state vector and its covariance matrix are obtained by solving a linear regression problem. It is well documented, however, the presented outliers, which refer to those data inconsistent with the overall pattern of the distribution, will degrade the estimation quality and render the estimate unreliable (Fitzgerald, 1971; Durgaprasad & Thakur, 1998). In general, two types of outliers are assumed, the uncertainties of the dynamic model and bad data in the measurements. An adaptive filter and robust filter have been developed for addressing the two types of outliers.

2.3.1 Adaptive Estimation

The accuracy of estimates from a Kalman filter relies on the knowledge of stochastic information and the dynamic model. Adaptive Kalman filtering is effective in resisting the effect of inaccuracy of the stochastic information (Ding et al., 2007; Hide et al., 2003; Hu et al., 2003; Wang et al., 2010). For the disturbances of the dynamic environment, a re-weighting technique is often used, in which the covariance matrices of the predicted state and the measurements are re-evaluated through the use of a moving window (Sage & Husa, 1969). A more flexible adaptive Kalman filter (AKF) that introduces an adaptive factor based on the discrepancy between the estimated and predicted states or based on the predicted residuals was proposed (Yang et al., 2001a; Yang & Gao, 2005). Furthermore, an optimal AKF was derived based on both the errors of the predicted state and the predicted residuals (Yang & Gao, 2006). A combination AKF based on the moving window variance estimate and the adaptive factors was proposed (Yang & Xu, 2003). The performance of the Kalman filter is improved after the adaptive variance estimation or adaptive factors are applied. However, due to the “crude” approximations of the nonlinear equation, the EKF can lead to poor representation of the probability distributions and nonlinear functions of interest (Chang et al., 2012).

The adaptation methods for the UKF have been discussed by many researchers. Han et al. (2009) analyzed two distinctive adaptive methods. In his first method, a cost function is constructed in order to minimize the difference between a theoretical covariance and actual innovation covariance; the Massachusetts

Institute of Technology (MIT) rule, which is developed in MIT and is firstly used in the Model Reference Adaptive Control (MRAC) approach (Markov & Tsankova, 2014), is used to derive the adaptive law, and the adaptive covariance matrix of the process noise is then estimated. The presented algorithm, however, needs to calculate partial derivatives. In the second method, two parallel UKFs run in a master and a slave manner, in which the master UKF estimates the system state while the slave UKF estimates the noise covariance matrix for the master UKF. Its computational demand is increased due to parallel UKFs. Hajiyev and Soken (2014) presented a robust adaptive Unscented Kalman filter (AUKF) based on a windowing approach. To adaptively estimate the covariance of the measurement noise, Gao et al. (2015) developed an AUKF using historical innovation sequence and the moving window approach.

2.3.2 Robust Estimation

The measurement outliers also can significantly degrade the state estimate of the Kalman filtering method. Statistical testing methods and robust estimations are two strategies to deal with the measurement outliers. The former strategy includes detection and isolation of the contaminated data, thus the classical least squares criterion can be applied to the remaining data. The statistical test method was initially founded by Baarda (1967, 1968) to detect the outliers in geodetic networks. The observation outliers are detected based on the residual vectors and isolated based on Baarda's w-test (Guo, 2015). The latter strategy applies the robust estimation criterion to the contaminated measurements directly to reduce the influences of the bad data. Several robust estimation methods have been proposed to improve the robustness of the Kalman filter in terms of resistance to the effect of measurement outlier on the estimation results, such as the Gaussian sum approach, H_∞ filter, and maximum likelihood (M-) technique. These algorithms are based on the concept of robust statistics. The H_∞ based Kalman filter minimizes the worst-case estimation error, and averages over all samples (He & Han, 2010). The filter treats modeling errors and uncertainties as bounded noise. In contrast, the Gaussian sum approach approximates non-Gaussian distribution analytically by several Gaussian distributions (Alspach & Sorenson, 1972; Caputi & Moose, 1993). The widely applied M- estimation technique improves the robustness of the Kalman filter by assuming that the observation errors follows Huber's distribution (Durgaprasad & Thakur, 1998), and then uses the M-estimation approach (Kovacevic et al., 1992; Durovic & Kovacevic, 1999). The approach down weights those contaminated measurements and conducts like least squares filters. For the correlated measurements or state elements, the Cholesky decomposition method is often used to de-correlate the correlations.

2.3.3 Robust Adaptive Estimation

In above methods, the dynamic model or the measurements are assumed to be accurate, that is both of the errors follow the Gaussian distribution. When the dynamic model has biases or/and the measurements contain outliers, the filter may yield unreliable results. A robust adaptive Kalman filter (RAKF) can overcome these limitations. Several new robust adaptive Kalman filters in which different adaptive factors were used to control the influences of both dynamic model disturbances and measurement outliers are proposed (Yang et al., 2001a; Yang et al., 2001b; Yang et al., 2004). These adaptive factors were constructed based on the robust state estimation only from measurements. Stochastic model adaptation methods, namely robust Maximum likelihood for measurements and the least squares estimation for the dynamic model (M-LS), the least squares estimation for measurements and Maximum likelihood for dynamic model (LS-M), and Maximum likelihood for both measurements and dynamic model (M-M) filters, were also developed to accommodate outliers or outlying disturbances by robust estimators using equivalent robust weights (Yang, 1991). In addition, a robust Kalman filter for a rank deficient observational model was derived by Koch & Yang (1998). A robust estimator for correlated measurements that employs the bi-factor reduction model of weight elements to suppress outliers was developed (Yang et al., 2002). By applying the M-estimator to the Kalman filter, the influences of dynamic model disturbances and measurement outliers have been effectively attenuated (Durovic & Kovacevic, 1999; Chan, et al., 2005; Gandhi & Mili, 2010). Wang et al. (2014) proposed a robust adaptive UKF that simultaneously deals with the dynamic model error and measurement outliers. In this method, Huber's robust function was used to adjust measurement weights based on the innovation vector, and the process noise matrix is adjusted by a fading factor based on the discrepancy between the predicted state and estimated state at the present epoch. Hajiyev & Soken (2014) developed a fault tolerant estimation algorithm based on UKF. This algorithm adaptively estimates covariance matrices of the process noise or measurement noise according to the type of the fault. Li et al. (2016) proposed a robust adaptive UKF that uses a moving window and matrix matching technology to adaptively estimate the uncertainties of the measurement noise and process noise, although the length of the moving window is not easy to be determined.

Chapter 3 Measurements and Dynamic Models for GNSS/INS Integration

As mentioned in Chapter 2, a Kalman filter predicts the system state based on the dynamic model and updates the predicted state vector using new measurements. In this Chapter, the details of the measurement model for difference data types, the dynamic model, and the coordinate frames, as well as the transformation between the different frames are discussed.

3.1 GNSS Measurement Models

3.1.1 GNSS Measurements

In a Kalman filtering process, the measurements at the current epoch are used to update or correct the predicted state for the stat estimate. The commonly used three types of GNSS measurements in civilian applications are carrier phases, Doppler shifts, and pseudoranges.

The carrier phase measurement is the sum of the fractional carrier phase and an unknown integer constant representing the number of full waves (Leick, 2004). The range of the satellite-receiver can be obtained by multiplying the carrier wavelength to the phase measurement. Due to the high accuracy of the carrier phase measurements, the position estimated from this type of measurements can achieve centimeter-level accuracy. However, the measurements contain unknown integer numbers of cycles, known as integer ambiguity, which needs to be estimated in the estimation process for a precise positioning application.

The real-time kinematic (RTK) positioning and precise point positioning (PPP) approaches use both carrier phase and pseudorange measurements (Hofmann-Wellenhof et al., 2003). RTK uses the double-differencing of four simultaneous GNSS measurements from two satellites and two ground receivers, one of which is the RTK user and the other is the so-called base station (with known position) located within a certain distance from the user. The double-differencing can largely reduce the atmospheric error effect in the four measurements so that the integer ambiguities can be quickly solved and fixed, which results in a high accuracy position solution. In the PPP approach, dual or even triple frequencies GNSS measurements and precise satellite orbit and clock products are used to obtain a decimeter level positioning accuracy solution.

Doppler measurements are instantaneous phase rates, which are derivatives of the carrier phase measurements. It represents the frequency shift caused by the relative motion between the receiver and the satellites (Kaplan & Hegarty, 2005).

The pseudorange is related to the satellite-receiver distance and is measured by the speed of light multiplied by the GNSS signal's travel time obtained by aligning the pseudo-random noise (PRN) code generated by the receiver together with an identical code in the signal to that in the satellite (Leick, 2004). The codes used to acquire the travel time of the signal, however, contain errors from both the receiver clock and satellite clock.

A variety of errors affect the quality of GNSS measurements. These errors can be classified into three categories: satellite related errors, receiver related errors, and signal propagation errors (Wang, 2006). The satellite related errors include satellite clock and ephemeris errors. The receiver related errors is the noise introduced by the receiver itself. The signal propagation errors are mainly caused by the troposphere, the ionosphere and multipath effect. In an urban environment, the multipath effect dramatically degrades the positioning accuracy.

Based on the above mentioned error sources, the measurement equation of pseudoranges can be expressed as (Leick, 2004),

$$P = \rho + d\rho + c(dt - dT) + d_{ion} + d_{trop} + \varepsilon_p \tag{3.1}$$

where P is the pseudorange measurement in meters; ρ is the geometric range between the satellite and the receiver antenna in meters; $d\rho$ is the satellite orbital error in meters; c is the speed of light; dt is the satellite clock error; dT is the receiver clock error; d_{ion} is the ionospheric delay; d_{trop} is the tropospheric delay; ε_p is the measurement noise including multipath effect. The geometric range is a function of the receiver and the satellite positions,

$$\rho = \sqrt{(x_r - x^i)^2 + (y_r - y^i)^2 + (z_r - z^i)^2} \tag{3.2}$$

where (x_r, y_r, z_r) are the receiver coordinates, and $\left(x^i, y^i, z^i\right)$ are the satellite coordinates obtained from the satellite ephemeris.

The measurement equation of the carrier phase is (Leick, 2004),

$$\lambda\phi = \rho + c(dt - dT) - \lambda N - d_{ion} + d_{trop} + \varepsilon_{\phi} \tag{3.3}$$

where ϕ is the carrier phase measurement in cycles; λ is the carrier wavelength; N is the integer ambiguity; and ε_{ϕ} is the carrier phase measurement noise and multipath effect.

The velocity can be solved from Doppler shifts. The equation can be expressed as following (Leick, 2004),

$$\dot{P} = \dot{\rho} + d\dot{\rho} + c\left(d\dot{t} - d\dot{T}\right) + \dot{d}_{ion} + \dot{d}_{trop} + \dot{\varepsilon_{p}} \tag{3.4}$$

where $\dot{P}$ is the observed range rate derived from Doppler shifts; $\dot{\rho}$ is the true range rate between the satellite and the receiver; $d\dot{t}$ and $d\dot{T}$ are the clock drift of the satellite and receiver respectively; $\dot{d}_{ion}$ is the ionospheric error drift; $\dot{d}_{trop}$ is the tropospheric error drift; and $\dot{\varepsilon_{p}}$ is the drift error caused by the measurement noise and multipath effect.

3.1.2 Differential GNSS

Error sources, such as satellite clock error, ionospheric delay and tropospheric delay in GNSS measurements are spatially correlated, i.e. the two delays slowly vary with spatial location. The closer two points, the smaller the difference between the delays of the two points. If two points are very close, e.g. a few kilometers apart, the atmospheric delays around the two locations can considered similar, or even the same. This is the reason why the differential

GNSS (DGNSS) is widely used to reduce the correlated error effects in the GNSS measurements for better and faster solutions (Grewal et al., 2007). DGNSS, which includes single difference (SD) and double difference (DD), has been widely applied in on-the-fly kinematic positioning and the details for them are introduced in the next sections

3.1.2.1 Single Difference

SD is operated on two measurements collected at two receivers simultaneously observing the same set of satellite and the satellite clock error and orbital errors are cancelled. The ionospheric and tropospheric delays can be also greatly reduced. This is under the assumption that the two receivers are located with the atmospheric spatially correlated region.

The pseudorange SD equation is (Leick, 2004),

$$\Delta P_{1,2} = \Delta\rho_{1,2} + \Delta d\rho - c\Delta T + \Delta d_{ion} + \Delta d_{trop} + \varepsilon_{\Delta p} \qquad (3.5)$$

where $\Delta P_{1,2}$ is the difference between the two observed pseudoranges and the subscripts denote the two receivers; $\Delta\rho_{1,2}$ the difference between the two geometric rages; ΔT is the difference between the two receiver clocks; Δd_{ion} and Δd_{trop} represent the differences in the ionospheric and tropospheric delays respectively; and $\varepsilon_{\Delta p}$ is the receiver noise.

$\Delta\rho_{1,2}$ can be expressed as,

$$\Delta\rho_{1,2} = \sqrt{(x_{r1} - x^i)^2 + (y_{r1} - y^i)^2 + (z_{r1} - z^i)^2} - \sqrt{(x_{r2} - x^i)^2 + (y_{r2} - y^i)^2 + (z_{r2} - z^i)^2} \quad (3.6)$$

where (x_{r1}, y_{r1}, z_{r1}) and (x_{r2}, y_{r2}, z_{r2}) are the positions of the rover and reference stations respectively .

Similarly, the SD phase measurement equation is (Leick, 2004),

$$\Delta\Phi = \Delta\rho + c\Delta dT - \lambda\Delta N - \Delta d_{ion} + \Delta d_{trop} + \varepsilon_{\Delta\phi} \quad (3.7)$$

where $\Delta\Phi$ is the SD phase measurement in the unit of length.

3.1.2.2 Double Difference

Double difference (DD) can be formed by two receivers simultaneously observing two satellites. The method can further eliminate the satellite and receiver clock errors, and reduce the atmospheric error. The DD pseudorange and carrier phase measurement equations are (Leick, 2004),

$$\Delta\nabla P = \Delta\nabla\rho + \Delta\nabla d\rho + \Delta\nabla d_{ion} + \Delta\nabla d_{trop} + \varepsilon_{\Delta\nabla p} \quad (3.8)$$

$$\Delta\nabla\Phi = \Delta\nabla\rho - \lambda\Delta\nabla N - \Delta\nabla d_{ion} + \Delta\nabla d_{trop} + \varepsilon_{\Delta\nabla\phi} \quad (3.9)$$

where the symbol $\Delta\nabla$ refers to the DD operator.

The drawbacks of the DGNSS methods are that the terms of the noise in the DD measurement equations is increased and the multipath effect still cannot be reduced; and the separation of the receivers, i.e. the length of the baseline, is limited to a certain range, depending on the regional atmospheric condition.

3.2 Dynamic Models

3.2.1 Constant Velocity Model

A vehicle's movement itself often gives information that may be used to establish a dynamic model for its positioning and navigation. The Constant Velocity (CV) model, as the simplest kinematic model, is often applied in low-speed vehicle navigation. It is expressed as:

$$r_{k+1} = r_k + \dot{r}_k \Delta t \tag{3.10}$$

where r_k and $\dot{r}_k$ denote the position and velocity vectors respectively at the kth epoch, Δt is the time interval between two consecutive epochs.

The CV model can be expressed as in a given geocentric coordinate system,

$$\begin{bmatrix} X_{k+1} \\ \dot{X}_{k+1} \end{bmatrix} = \begin{bmatrix} I & \Delta t I \\ 0 & I \end{bmatrix} \begin{bmatrix} X_k \\ \dot{X}_k \end{bmatrix} + w_k \tag{3.11}$$

where I is a 3×3 unit matrix; w_k is the error vector of the functional model; X_{k+1} and $\dot{X}_{k+1}$, are the position and velocity vectors respectively at epoch $k + 1$, which consist of three components as is expressed below,

$$X_{k+1} = [\delta x_{k+1} \quad \delta y_{k+1} \quad \delta z_{k+1}]^T \tag{3.12}$$

$$\dot{X}_{k+1} = [\delta \dot{x}_{k+1} \quad \delta \dot{y}_{k+1} \quad \delta \dot{z}_{k+1}]^T \tag{3.13}$$

The covariance matrix of w_k for a constant time interval Δt was given by (Mohamed & Schwarz, 1999). w_k can also be estimated by a variance component estimation (Yang & Xu, 2003).

If a geographic coordinate system is applied, the position vector is,

$$r = [\delta\phi \quad \delta\lambda \quad \delta h]^T \tag{3.14}$$

where $\delta\phi$, $\delta\lambda$, and δh are the corrections of the latitude, longitude, and altitude components respectively.

The velocity vector is then,

$$\dot{r} = [\delta V_N \quad \delta V_E \quad \delta V_U]^T \tag{3.15}$$

where δV_N, δV_E and δV_U are the corrections of the north, east and vertical components respectively.

The CV model can be expressed as,

$$\begin{bmatrix} r_{k+1} \\ \dot{r}_{k+1} \end{bmatrix} = \begin{bmatrix} I & \Delta t D \\ 0 & I \end{bmatrix} \begin{bmatrix} r_k \\ \dot{r}_k \end{bmatrix} + w_k \tag{3.16}$$

where D is given as,

$$D = \begin{bmatrix} \frac{1}{R} & & & \\ & \frac{1}{R\cos\phi} & & \\ & & 1 & \\ & & & 1 \end{bmatrix} \tag{3.17}$$

where R is the radius of the earth.

3.2.2 Constant Acceleration Model

If a constant acceleration (CA) is assumed for a vehicle's movement, the simplest dynamic model for the CV is usually expressed as,

$$\ddot{X}_{k+1} = [\delta\ddot{x}_{k+1} \quad \delta\ddot{y}_{k+1} \quad \delta\ddot{z}_{k+1}] \tag{3.18}$$

where $\ddot{X}_{k+1}$ denotes the acceleration vector at epoch $k+1$ consisting of three components: a$\ddot{x}_{k+1}$, $\ddot{y}_{k+1}$ and $\ddot{z}_{k+1}$.

The dynamic model is then,

$$\begin{bmatrix} x_{k+1} \\ \dot{x}_{k+1} \\ \ddot{x}_{k+1} \end{bmatrix} = \begin{bmatrix} I & I\Delta t & \frac{1}{2}\Delta t^2 I \\ & I & I\Delta t \\ & & I \end{bmatrix} \begin{bmatrix} x_k \\ \dot{x}_k \\ \ddot{x}_k \end{bmatrix} + \begin{bmatrix} 0 \\ 0 \\ I \end{bmatrix} w_k \tag{3.19}$$

where w_k is still the white noise vector of the model with the covariance matrix Σ_{w_k} expressed as

$$\Sigma_{w_k} = \sigma_a^2 \begin{bmatrix} \frac{\Delta t^4}{20} & \frac{\Delta t^3}{8} & \frac{\Delta t^2}{6} \\ \frac{\Delta t^3}{8} & \frac{\Delta t^2}{3} & \frac{\Delta t}{2} \\ \frac{\Delta t^2}{6} & \frac{\Delta t}{2} & 1 \end{bmatrix} \tag{3.20}$$

where σ_a^2 is a constant variance factor (Gelb, 1974).

In most cases, the CV or CA model may be integrated into a Kalman filter, which may enhance the continuity and reliability of the solution.

3.3 Inertial Measurement Models

3.3.1 Coordinate Frame and Transformation

GPS measurements are in the WGS 84 coordinate frame, which is similar to that of ITRF. At present, the difference between WGS 84 and ITRF is within millimeters. In contrast, INS measurements of orientation changes and the accelerations are expressed in the body frame. Thus, coordinate transformation is needed for the integration of GPS and INS measurements.

3.3.1.1 Essential Coordinate Frames

The most common reference frames used in this study are briefly examined in this section and more details can be found in (Petovello, 2003).

Inertial Frame

An inertial frame (i) can be a non-rotating and non-accelerating frame centered at the Earth's Centre of mass. Its Z-axis is parallel to the Earth's instantaneous spin axis; its X-axis points towards the mean equinoctial colure in the equatorial plane; and its Y-axis, orthogonal to the X- and Z-axes, is to complete a right-handed frame.

Earth-Centered Earth-Fixed Frame

The Earth-Centered Earth-Fixed (e) frame is centered at the Earth's Centre of mass. Its Z-axis is parallel to the Earth's mean spin axis; its X-axis points towards the mean meridian of Greenwich; and its Y-axis is orthogonal to the X- and Z-axes for completion of a right-handed frame.

Local Frame

A local frame (l), often referred as the East-North-Up (ENU) reference frame, is centered at the origin of the navigation system. Its Z-axis points upwards along the normal of the selected reference ellipsoid; Its X-axis points towards the geodetic East on the horizontal plane; and its Y-axis points towards the geodetic North on the horizontal plane.

Body Frame

The body frame (b) represents the orientation of the IMU axes. In a strapdown inertial system, IMU is rigidly mounted to the vehicle with arbitrary orientation. The axes are set to align with the roll, pitch and heading axes of that vehicle.

Platform Frame

The platform frame (p) is the frame in which the accelerations transformed from accelerometers and angular rates from the gyros are solved.

3.3.1.2 Coordinate Transformation

The coordinate transformation from one frame to another is accomplished by a rotation matrix, which is an orthogonal matrix and often named as the directional cosine matrix (DCM) of 3×3 dimension containing the cosine of the angles of a vector in the two frames (Savage, 2000). The DCM from the above defined e frame and l frame is obtained from the geodetic coordinate (El-Sheimy, 2012),

$$R_e^l = \begin{bmatrix} -\sin\lambda & \cos\lambda & 0 \\ -\sin\varphi\cos\lambda & -\sin\varphi\sin\lambda & \cos\varphi \\ \cos\varphi\cos\lambda & \cos\varphi\sin\lambda & \sin\varphi \end{bmatrix} \tag{3.21}$$

where φ and λ are the latitude and longitude respectively.

The DCM from the l frame to b frame is obtained from the Euler angles, which represent the rotation angles around the axes by yaw (A), pitch (p), and roll (r) (Shin, 2005). Yaw, pitch and roll are defined as the rotation angle around the Z-axis, X-axis and Y-axis respectively and all are in the counter-clockwise direction. The sequence of the successive rotations along the three axes is named rotation sequence. In this research, the rotation sequence adopted is: along the Y-axis is the first rotation, along the Z-axis is the second, and along the X-axis is the third rotation. The overall rotation matrix can be expressed as,

$$R_L^b = R(r)R(A)R(p) \tag{3.22}$$

The elements of the DCM are,

$$R_L^b(1,1) = cos\, r * cos\, A - sin\, r * sin\, A * sin\, p \tag{3.23a}$$

$$R_L^b(1,2) = cos\, r * sin\, A + sin\, r * cos\, A * sin\, p \tag{3.23b}$$

$$R_L^b(1,3) = -\, cos\, p * sin\, r \tag{3.23c}$$

$$R_L^b(2,1) = -\, sin\, A * cos\, p \tag{3.23d}$$

$$R_L^b(2,2) = cos\, A * cos\, p \tag{3.23e}$$

$$R_L^b(2,3) = sin\, p \tag{3.23f}$$

$$R_L^b(3,1) = cos\, A * sin\, r + sin\, A * sin\, p * cos\, r \tag{3.23g}$$

$$R_L^b(3,2) = sin\, A * sin\, r - cos\, A * sin\, p * cos\, r \tag{3.23h}$$

$$R_L^b(3,3) = cos\,p * cos\,r \tag{3.23i}$$

The vector in the body frame can be transformed to the local frame by,

$$p^l = R_b^l p^b \tag{3.24}$$

where p^l and p^b are the vectors expressed in the l frame and b frame respectively; and the rotation matrix R_b^l projects p^b from the b frame to the l frame.

3.3.2 Mechanization Equations

Mechanization equations are used to obtain navigation state from IMU measurements named specific force (f) and angular rate (ω). The equations model the motion of a moving object in the l frame can be expressed as follows (El-Sheimy, 2012),

$$\dot{r}^l = D^{-1} \cdot V^l \tag{3.25a}$$

$$\dot{V}^l = R_b^l f^b - \left(2\Omega_{ie}^l + \Omega_{el}^l\right) \cdot V^l + g^l \tag{3.25b}$$

$$\dot{R}_b^l = R_b^l\left(\Omega_{ib}^b - \Omega_{il}^b\right) = R_b^l \Omega_{il}^b \tag{3.25c}$$

Equation (3.25a) represents the relationships between the geographic coordinates and the velocity component in the l frame, where $r^l = [\varphi \quad \lambda \quad h]^T$ is the vehicle position denoted by geographic latitude, longitude and altitude in the l frame; D is the transform matrix projecting the velocity components to the geographic coordinates,

$$D = \begin{bmatrix} 0 & \frac{1}{M+h} & 0 \\ \frac{1}{(N+h)\cos\varphi} & 0 & 0 \\ 0 & 0 & 1 \end{bmatrix} \tag{3.26}$$

where M is the radius of curvature in the Meridian; and N is the curvature radius in the prime vertical.

In eq. (3.25b), $V^l = [V_E \quad V_N \quad V_U]^T$ is the velocity of the vehicle, composed of the East, North, and Up components in the l frame; R_b^l is the transformation matrix from the b frame to l frame and is a function of the attitude components; $\dot{V}^l$ is the acceleration of the vehicle in the l frame; f^b is the specific force vector in the b frame and is measured by accelerometers; $\Omega_{el}^l \cdot V^l$ is the centripetal acceleration of the l frame with respect to the e frame; $2\Omega_{ie}^l \cdot V^l$ is the Coriolis acceleration; g^l is the gravity vector including the gravitation term and the centripetal term related to the Earth rotation.

Equation (3.25c) is the attitude mechanization equation, where Ω_{ib}^b is the skew-symmetric matrix of the angular velocity vector ω_{ib}^b which is the rotation rate of the b frame with respect to the i frame, expressed in the b frame; Ω_{il}^b is the skew-symmetric matrix of the angular velocity vector ω_{il}^b which is the l frame rotation rate with respect to the i frame and expressed in the b frame; and ω_{il}^b is calculated by,

$$\omega_{il}^b = R_l^b \cdot \left(\omega_{ie}^l + \omega_{el}^l\right) \tag{3.27}$$

where ω_{ie}^{l} is the Earth rotation rate expressed in the l frame; ω_{el}^{l} is the rotation rate of in the local frame with respect to the e frame expressed in the l frame.

Before the estimation process for the state vector from the IMU measurements is performed, the orientation between the l frame and b frame needs to be determined, for which the initial alignment procedure is required. Gyroscope measurements include the Earth rotation rate and the orientation changes between both b and l frames. To obtain the angular rate of the moving object, the two terms should be removed, as shown in eqs. (3.25c) and (3.27).

3.3.3 IMU Error Model

The error of IMU sensors degrades the accuracy of the navigation state solved by eq. (3.25). The error in the state solution can be modeled by either a deterministic or a stochastic model in the estimation.

The performance of IMU can be indicated by bias, scale factor and noise. The bias consists of two parts: a deterministic part and a stochastic part. The deterministic part refers to the offset in the output of the sensors and the stochastic part refers to the rate at which the error in an inertial sensor accumulates with time (El-Sheimy, 2012). The scale factor, which is a deterministic error, indicates the relationship between the input and output of the inertial sensor. For a low-cost IMU, its deterministic error can be treated or modeled as a white noise component, due to its little contribution compared to its own measurement noise (Falco et al., 2012).

3.3.3.1 Linear IMU Error Model

The traditional deterministic error model is defined by perturbing the nominal differential of the above nonlinear eq. (3.25) with the assumption that the angle error is small (El-Sheimy, 2012). The two classic error analysis approaches are the phi angle approach and psi angle approach. The first approach solves the navigation equation and the error models in the l frame, while the second approach solves the navigation equation in the p frame (Kong, 2000). Thus, the initial alignment process, which establishes the relationship between the b and l frames, is needed to reduce the initial attitude error to fulfill the small angle assumption.

The errors of the state parameters are defined as:

$$\delta r^l = \tilde{r}^l - r^l \tag{3.28a}$$

$$\delta v^l = \tilde{v}^l - v^l \tag{3.28b}$$

$$\tilde{R}_b^l = R_b^l + \delta R_b^l = (I + E^l)R_b^l \tag{3.28c}$$

where δr^l and δv^l represent the perturbed position and velocity respectively; the elements with a tilde $(\tilde{\cdot})$ are calculated quantities, which contain errors.

If the Euler angles between the two frames are small, the following approximations hold,

$$\begin{aligned} \sin\theta &\approx \theta \\ \cos\theta &\approx 1 \end{aligned} \tag{3.29}$$

Thus, the rotation matrix between the two frames can be simplified as,

$$R_a^b = \begin{bmatrix} 1 & -\theta_z & \theta_y \\ \theta_z & 1 & -\theta_x \\ -\theta_y & \theta_x & 1 \end{bmatrix} = I + E \tag{3.30}$$

where E is the skew-symmetric matrix of the Euler angles.

Attitude Error Model

The derivation of the attitude error starts from differentiating eq. (3.28c), which is,

$$\dot{\tilde{R}}_b^l = \dot{R}_b^l + \dot{E}^l R_b^l + E^l R_b^l \Omega_{lb}^b \tag{3.31}$$

where Ω_{lb}^b is the is the skew-symmetric matrix of the angular velocity vector ω_{lb}^b which is the rotation rate of the b frame with respect to the l frame, expressed in the b frame. For eq. (3.25c) if the computed rotation matrix is assumed to contain errors, it can be written as,

$$\dot{\tilde{R}}_b^l = \tilde{R}_b^l \tilde{\Omega}_{lb}^b \tag{3.32}$$

Substituting eq. (3.28c) into the above equation and replacing the error term in the skew matrix, eq. (3.32) becomes,

$$\dot{\tilde{R}}_b^l = (I + E^l) R_b^l \left(\Omega_{lb}^b + \delta\Omega_{lb}^b\right) \tag{3.33}$$

Comparing this equation with eq. (3.25) and neglecting the second-order term $E^l R_b^l \delta\Omega_{lb}^b$, one can obtain,

$$\dot{E}^l R_b^l = R_b^l \delta \Omega_{lb}^b \quad (3.34)$$

Thus, the attitude error can be written as,

$$\dot{\varepsilon}^l = \tilde{R}_b^l \delta \omega_{lb}^b \quad (3.35)$$

where ω_{lb}^b is the angular velocity of the b frame with respect to the l frame, and can be calculated by,

$$\omega_{lb}^b = \omega_{ib}^b - R_l^b \omega_{il}^l \quad (3.36)$$

Linearizing the above equation and neglecting the second-order terms leads to the angular velocity error term $\delta\omega_{lb}^b$,

$$\delta\omega_{lb}^b = \delta\omega_{ib}^b - R_l^b \Omega_{il}^l \varepsilon^l - R_l^b \delta\omega_{il}^l \quad (3.37)$$

Substituting eq. (3.37) into eq. (3.35), the attitude error model in the l frame is,

$$\dot{\varepsilon}^l = R_b^l \delta\omega_{ib}^b - \Omega_{il}^l \varepsilon^l - \delta\omega_{il}^l \quad (3.38)$$

Velocity and Positioning Error Model

The velocity error model can be derived by differentiating eq. (3.25b),

$$\delta\dot{V}^l = \delta R_b^l f^b + R_b^l \delta f^b - \left(2\Omega_{ie}^l + \Omega_{el}^l\right) \cdot \delta V^l - \left(\delta\Omega_{ie}^l + \delta\Omega_{el}^l\right) V^l + \delta g^l \quad (3.39)$$

According to eq. (3.28c),

$$\delta R_b^l = E^l R_b^l \quad (3.40)$$

Thus, eq. (3.39) is,

$$\delta\dot{V}^l = E^l R_b^l f^b + R_b^l \delta f^b - \left(2\Omega_{ie}^l + \Omega_{el}^l\right) \cdot \delta V^l - \left(\delta\Omega_{ie}^l + \delta\Omega_{el}^l\right) V^l + \delta g^l \tag{3.41}$$

where δg^l is the error in the computation of normal gravitation.

The position error model can then be easily obtained,

$$\delta\dot{r}^1 = D^{-1}\delta V^l \tag{3.42}$$

3.3.3.2 Nonlinear IMU Error Model

IMU error models for large misalignment angles have been presented in literature recently. A quaternion-based error model, which does not rely on the assumption of small angle, is developed to solve the initial attitude uncertainties for in-motion alignment (Kong, 2004; Zhong et al., 2012). The quaternion method is more effective than the Euler angles and DCM methods. However, it increases the dimension of the state by estimate the quaternion vector instead of Euler angels. Yan et al. (2008) proposed a nonlinear error model based on the Euler angle errors and this model is used in this research.

In general, the DCM consists of Euler angles which contain large errors. The time derivative of the rotation matrix R_b^l is,

$$\dot{R}_b^l(1{,}1) = -\dot{r}\sin r\cos A - \dot{A}\cos r\sin A - \dot{r}\cos r\sin A\sin p - \dot{A}\sin r\cos A\sin p - \dot{p}\sin r\sin A\cos p \tag{3.43a}$$

$$\dot{R}_b^l(1,2) = -\dot{A}\cos p\cos A + \dot{p}\sin A\sin p \tag{3.43b}$$

$$\dot{R}_b^l(1,3) = -\dot{A}\sin A\sin r + \dot{r}\cos A\cos r + \dot{A}\cos A\sin p\cos r + \dot{p}\sin A\cos p\cos r - \dot{r}\sin A\sin p\sin r \tag{3.43c}$$

$$\dot{R}_b^l(2,1) = -\dot{r}\sin r\sin A + \dot{A}\cos r\cos A + \dot{r}\cos r\cos A\sin p - \dot{A}\sin r\sin A\sin p + \dot{p}\sin r\cos A\cos p \tag{3.43d}$$

$$\dot{R}_b^l(2,2) = -\dot{A}\sin A\cos p - \dot{p}\cos A\sin p \tag{3.43e}$$

$$\dot{R}_b^l(2,3) = \dot{A}\cos A\sin r + \dot{r}\sin A\cos r + \dot{A}\sin A\sin p\cos r - \dot{p}\cos A\cos p\cos r + \dot{r}\cos A\sin p\sin r \tag{3.43f}$$

$$\dot{R}_b^l(3,1) = \dot{p}\sin p\sin r - \dot{r}\cos p\cos r \tag{3.43g}$$

$$\dot{R}_b^l(3,2) = \dot{p}\cos p \tag{3.43h}$$

$$\dot{R}_b^l(3,3) = -\dot{p}\sin p\cos r - \dot{r}\cos p\sin r \tag{3.43i}$$

The matrix can be written as,

$$\dot{R}_b^l = R_b^l\left(\begin{bmatrix}\dot{p}\cos r - \dot{A}\cos p\sin r\\ \dot{r} + \dot{A}\sin p\\ \dot{p}\sin r + \dot{A}\cos p\cos r\end{bmatrix}\times\right) =$$

$$R_b^l\left[\begin{bmatrix}\cos r & 0 & -\cos p\sin r\\ 0 & 1 & \sin p\\ \sin r & 0 & \cos p\cos r\end{bmatrix}\begin{bmatrix}\dot{p}\\ \dot{r}\\ \dot{A}\end{bmatrix}\times\right] \tag{3.44}$$

where the $(\cdot\times)$ terms represent the skew matrix form of the elements.

Comparing with eq. (3.25c), then,

$$\omega_{lb}^{l} = \begin{bmatrix} \cos r & 0 & -\cos p \sin r \\ 0 & 1 & \sin p \\ \sin r & 0 & \cos p \cos r \end{bmatrix} \begin{bmatrix} \dot{p} \\ \dot{r} \\ \dot{A} \end{bmatrix} \tag{3.45}$$

As the error exists in the attitude angle, the rotation matrix projects the vector to a virtual frame, namely the platform frame (p). The difference between the p and l frames is,

$$\Delta R = R_b^p - R_b^l = R_b^p - R_p^l R_b^p \tag{3.46}$$

where R_b^p is the rotation matrix from the b frame to the p frame; and R_p^l is the rotation matrix from the p frame to the l frame.

Considering eq. (3.25c), the time derivative of the above equation is,

$$\dot{R}_b^l = \dot{R}_p^l R_b^p + R_p^l R_b^p \tilde{\Omega}_{lb}^b = R_b^l \Omega_{lb}^b \tag{3.47}$$

It can be further rewritten as,

$$R_p^l \Omega_{lp}^p R_b^p + R_p^l R_b^p \tilde{\Omega}_{lb}^b - R_b^l \Omega_{lb}^b = 0 \tag{3.48}$$

Multiplying R_l^p to the left, and multiplying R_p^b to the right side of the above equation leads to,

$$\Omega_{lp}^p + R_b^p \tilde{\Omega}_{lb}^b R_p^b - R_b^p \Omega_{lb}^b R_p^b = 0 \tag{3.49}$$

Thus,

$$\omega_{lp}^{p} = R_{b}^{p}\left(\omega_{lb}^{b} - \widetilde{\omega}_{lb}^{b}\right) \tag{3.50}$$

Substituting eq. (3.47) into eq. (3.50) and considering eq. (3.46),

$$\omega_{lp}^{p} = (I - R_{l}^{P})\omega_{il}^{l} + R_{l}^{p}\delta\omega_{il}^{l} - R_{b}^{p}\delta\omega_{ib}^{b} \tag{3.51}$$

Therefore, the attitude error can be expressed with the consideration of eq. (3.45)

$$\dot{\varepsilon} = \begin{bmatrix} \cos r & 0 & -\cos p \sin r \\ 0 & 1 & \sin p \\ \sin r & 0 & \cos p \cos r \end{bmatrix}^{-1} \left[(I - R_{l}^{P})\omega_{il}^{l} + R_{l}^{p}\delta\omega_{il}^{l} - R_{b}^{p}\delta\omega_{ib}^{b}\right] \tag{3.52}$$

Let

$$C_{\omega} = \begin{bmatrix} cos\, r & 0 & -cos\, p\, sin\, r \\ 0 & 1 & sin\, p \\ sin\, r & 0 & cos\, p\, cos\, r \end{bmatrix} \tag{3.53}$$

Then,

$$\mathrm{C}_{\omega}^{-1} = \frac{1}{\cos r}\begin{bmatrix} \cos p \cos r & 0 & \sin p \cos r \\ \sin p \sin r & \cos r & -\cos p \sin r \\ -\sin r & 0 & \cos p \end{bmatrix} \tag{3.54}$$

Thus, the attitude error model can be written as (Yan et al., 2008),

$$\dot{\varepsilon} = \mathrm{C}_{\omega}^{-1}\left[(I - R_{l}^{P})\omega_{il}^{l} + R_{l}^{p}\delta\omega_{il}^{l} - R_{b}^{p}\delta\omega_{ib}^{b}\right] \tag{3.55}$$

According to the derivative of eq. (3.39), the velocity error model is (Yan et al., 2008),

$$\delta\dot{v} = [(I - (R_l^p)^T)]R_b^p f^b + \left(R_l^p\right)^T R_b^p \delta f^b - \left(2 \cdot \delta\Omega_{ie}^l + \delta\Omega_{el}^l\right)V^l -$$

$$\left(2\Omega_{ie}^l + \Omega_{el}^l\right) \cdot \delta V^l + \left(2 \cdot \delta\Omega_{ie}^l + \delta\Omega_{el}^l\right) \cdot \delta V^l + \delta g^l \qquad (3.56)$$

The position error model remains the same as eq. (3.42).

The above derivation gives the navigation error model without the need for the assumption of small angle error.

3.4 Summary

In this chapter, general GNSS measurement models were described, and the differential techniques to eliminate the spatial related errors were introduced. The differential techniques are recognized as an effective method in reducing spatial and clock errors. Dynamic system models including the CV model, CA model, and IMU error models were reviewed. The CV and CA models can be applied to GNSS measurements to improve positioning performance in terms of accuracy, continuity and reliability. The IMU error models are often used as the dynamic model and the classical IMU error model was derived under the assumption of small misalignment angles. In reality, the environmental disturbances and sensors errors may not satisfy this assumption. In this case, nonlinear error models using a differential direction cosine matrix is needed. The concepts reviewed in this chapter will lay an important foundation for the work in the later chapters.

Chapter 4 Comparison between Kalman and Unscented Kalman Filters

An alternative derivation of the Kalman filter by using correlational inference concept predominantly for nonlinear state space models is presented in this Chapter. The inference is for the revelation of the relationships among the measurement vector, the predicted state vector, and also their cross-covariance matrices. Based on the correlational inference, a common Kalman filter framework is established and a comparison study of EKF and UKF is conducted under this framework using different methods and data including theoretical formulation, simulations and field tests. Different feedback control modes regarding integrated vehicle navigation are employed to evaluate the performance of UKF and EKF.

4.1 Kalman Filtering Framework Analysis Based on Correlational Inference

The Kalman filtering algorithm is derived using vector algebra as a minimum mean squared estimator. Its major advantages are less computational requirements, elegant recursive properties, and an optimal estimator for linear systems with Gaussian error statistics (Faragher, 2012). However, the filter requires a set of linear transformation to depict the time evolution of the system state, i.e., the dynamic model. The filter also needs a measurement model for the linear relationship between the state parameters and the observations. In practice, however, the dynamic systems are often in a nonlinear way to transition from one epoch to the next. In this case, the nonlinear models are linearized using the first-order Taylor expansion. Neglecting higher-order terms in the Taylor expansion can introduce linearization errors in the model. This will result in a low accuracy state solution (Gordon et al., 1993; Julier & Uhlmann, 1997). The UKF uses UT to approximate the transformed mean and covariance rather than approximates the nonlinear equations, is explored to deal with nonlinear state estimation in a different approach and achieves Taylor expansion at least to the second order.

4.1.1 Correlational Inference

Considering following the discrete nonlinear estimation system mentioned in Chapter 2,

$$X = f(X_{k-1}) + w_k \tag{2.1}$$

$$y_k = h(X_k) + e_k \tag{2.2}$$

where y_k is the $m \times 1$ measurement vector, X_k and X_{k-1} are $n \times 1$ state vectors at epoch k and $k-1$ respectively.

The equation for the error or residual of the measurement is,

$$V_k = h_k(\hat{X}_k) - y_k = \hat{y}_k - y_k \tag{4.1}$$

where $\hat{y}_k = h_k(\hat{X}_k)$; $\hat{X}_k$ is the estimated state vector; and V_k is the residual vector of y_k.

The predicted state vector $\bar{X}_k$ can be obtained by eq. (2.1),

$$\bar{X}_k = f_k(\hat{X}_{k-1}) \tag{4.2}$$

The predicted measurement vector $\bar{y}_k$ is given by,

$$\bar{y}_k = h_k(\bar{X}_k) \tag{4.3}$$

with the corresponding covariance matrix $\Sigma^*_{\bar{y}_k}$ at the epoch k. If the measurement vector y_k (at epoch k) is available, the innovation vector $\bar{V}_k$ can be obtained,

$$\bar{V}_k = y_k - h_k(\bar{X}_k) = y_k - \bar{y}_k \tag{4.4}$$

Given that two vectors y_k and $\bar{y}_k$ are independent, covariance matrix $\Sigma_{\bar{V}_k}$ can be calculated by,

$$\Sigma_{\bar{V}_k} = \Sigma_k + \Sigma^*_{\bar{y}_k} = \Sigma_k + H_k \Sigma_{\bar{X}_k} H_k^T \tag{4.5}$$

where H_k is the linearized form of the measurement model/function $h_k(\cdot)$; and $\Sigma_{\bar{X}_k}$ is the covariance matrix of the predicted state vector $\bar{X}_k$.

In theory, the following equation is valid,

$$\hat{y}_k - \hat{\bar{y}}_k = 0 \tag{4.6}$$

and considering the error equation form of $\hat{\bar{y}}_k$,

$$\hat{\bar{y}}_k = \hat{y}_k = h_k(\hat{X}_k) = \bar{y}_k + V_{\bar{y}_k} = y_k + V_k \tag{4.7}$$

where $\hat{\bar{y}}_k$ denotes the estimated vector of predicted measurements $\bar{y}_k$; $\hat{y}_k$ is the estimated measurement vector; $V_{\bar{y}_k}$ and V_k are the residual vectors with respect to $\bar{y}_k$ and y_k, respectively.

Thus,

$$V_k - V_{\bar{y}_k} + (y_k - \bar{y}_k) = 0 \tag{4.8}$$

Considering eq. (4.4), it becomes,

$$V_{\bar{y}_k} - \bar{V}_k - V_k = 0 \tag{4.9}$$

Eqs. (4.6) or (4.7) can be regarded as constraint equations. In addition, the residual vector of $\bar{X}_k$ is denoted by $V_{\bar{X}_k}$,

$$V_{\bar{X}_k} = \hat{X}_k - \bar{X}_k \tag{4.10}$$

Considering that $\bar{y}_k$ contains the predicted state $\bar{X}_k$ from a nonlinear function as shown in eq. (4.3), $\bar{y}_k$ and $\bar{X}_k$ are thus correlated with the cross-covariance matrix $\Sigma_{\bar{X}_k\bar{y}_k}$. To estimate the state vector $\hat{X}_k$ from the measurement vector y_k, $\bar{X}_k$ and $\bar{y}_k$with their covariance and cross-covariance matrices Σ_k, $\Sigma_{\bar{X}_k}$ and $\Sigma^*_{\bar{y}_k}$, as well as $\Sigma_{\bar{X}_k\bar{y}_k}$, the Lagrange objective function is firstly constructed by considering eqs. (4.6) and (4.9),

$$V_k^T \Sigma_k^{-1} V_k + \begin{bmatrix} V_{\bar{y}_k}^T & V_{\bar{X}_k}^T \end{bmatrix} \begin{bmatrix} \Sigma^*_{\bar{y}_k} & \Sigma_{\bar{y}_k\bar{X}_k} \\ \Sigma_{\bar{X}_k\bar{y}_k} & \Sigma_{\bar{X}_k} \end{bmatrix}^{-1} \begin{bmatrix} V_{\bar{y}_k} \\ V_{\bar{X}_k} \end{bmatrix} - 2\lambda^T \left(V_{\bar{y}_k} - \bar{V}_k - V_k \right) = min \tag{4.11}$$

where λ is the Lagrange multiple vector.

Taking the partial derivatives of eq. (4.11) with respect to V_k, $V_{\bar{y}_k}$, $V_{\bar{X}_k}$, and λ, and setting them to 0, one can obtain:

$$V_k = -\Sigma_k \lambda \tag{4.12}$$

$$\begin{bmatrix} V_{\bar{y}_k} \\ V_{\bar{X}_k} \end{bmatrix} = \begin{bmatrix} \Sigma^*_{\bar{y}_k} & \Sigma_{\bar{y}_k \bar{X}_k} \\ \Sigma_{\bar{X}_k \bar{y}_k} & \Sigma_{\bar{X}_k} \end{bmatrix} \begin{bmatrix} \lambda \\ 0 \end{bmatrix} = \begin{bmatrix} \Sigma^*_{\bar{y}_k} \lambda \\ \Sigma_{\bar{X}_k \bar{y}_k} \lambda \end{bmatrix} \tag{4.13}$$

From eq. (4.13), the solution is,

$$\begin{aligned} V_{\bar{y}_k} &= \Sigma^*_{\bar{y}_k} \lambda \\ V_{\bar{X}_k} &= \Sigma_{\bar{X}_k \bar{y}_k} \lambda \end{aligned} \tag{4.14}$$

Based on eqs. (4.12) and (4.14) and considering eq. (4.9), one can obtain

$$\Sigma_k \lambda + \Sigma^*_{\bar{y}_k} \lambda - \bar{V}_k = 0 \tag{4.15}$$

$$\lambda = \left(\Sigma^*_{\bar{y}_k} + \Sigma_k\right)^{-1} \bar{V}_k \tag{4.16}$$

Substituting eq. (4.16) into eq. (4.14), the residual vectors of the predicted measurements and predicted state vector are obtained respectively as follows,

$$V_{\bar{y}_k} = \Sigma^*_{\bar{y}_k} \left(\Sigma^*_{\bar{y}_k} + \Sigma_k\right)^{-1} \bar{V}_k \tag{4.17}$$

$$V_{\bar{X}_k} = \Sigma_{\bar{X}_k \bar{y}_k} \left(\Sigma^*_{\bar{y}_k} + \Sigma_k\right)^{-1} \bar{V}_k \tag{4.18}$$

Because of eq. (4.15),

$$V_{\bar{X}_k} = \Sigma_{\bar{X}_k \bar{y}_k} \Sigma_{\bar{V}_k}^{-1} \bar{V}_k \tag{4.19}$$

and,

$$\begin{aligned} \hat{X}_k &= \bar{X}_k + V_{\bar{X}_k} \\ &= \bar{X}_k + \Sigma_{\bar{X}_k \bar{y}_k} \left(\Sigma_{\bar{y}_k}^{*} + \Sigma_k \right)^{-1} (y_k - \bar{y}_k) \\ &= \bar{X}_k + K_k \bar{V}_k \end{aligned} \tag{4.20}$$

where K_k is the Kalman gain matrix,

$$K_k = \Sigma_{\bar{X}_k \bar{y}_k} \left(\Sigma_{\bar{y}_k}^{*} + \Sigma_k \right)^{-1} = \Sigma_{\bar{X}_k \bar{y}_k} \Sigma_{\bar{V}_k}^{-1} \tag{4.21}$$

It should be stressed that in the above equations, the estimated state vector $\hat{X}_k$ and its Kalman gain matrix K_k contain neither any Jacobian matrices of the nonlinear measurement model nor dynamic equations. Furthermore, since $\bar{y}_k$ and y_k are independent, then

$$\Sigma_{\bar{X}_k \bar{y}_k} = \Sigma_{\bar{X}_k \bar{V}_k} \tag{4.22}$$

Thus, from eq. (4.19),

$$\hat{X}_k = \bar{X}_k + \Sigma_{\bar{X}_k \bar{V}_k} \Sigma_{\bar{V}_k}^{-1} \bar{V}_k = \bar{X}_k + K_k \bar{V}_k \tag{4.23}$$

The posterior covariance matrix of the estimated state vector reads,

$$\Sigma_{\hat{X}_k} = \Sigma_{\bar{X}_k} - K_k \Sigma_{\bar{V}_k} K_k^T \tag{4.24}$$

The above expression shows that the covariance matrix of the estimated state vector is smaller than that of the predicted state vector. Also, the posterior covariance matrix of the state vector is not related to any linearization process since K_k is obtained from eq. (4.21). Therefore, the latter is not related to linearization.

4.1.2 Theoretical Analysis

The following facts of interest are obtained from the above derivations:

(i) The derivation presented in the section illustrates the Kalman filtering theoretical framework. In this framework, the estimated state vector relates to the innovation vector and its covariance matrix, the cross-covariance matrix of the predicted vectors, and the predicted state vector; yet the methods to gain these covariance matrices are not limited. Thus, the state estimated from the prior covariance and cross-covariance matrices makes Kalman filtering process more flexible and more extensible. In the new expression (4.23), the predicted state vector $\overline{\mathrm{X}}_{\mathrm{k}}$ with $\Sigma_{\overline{\mathrm{X}}_{\mathrm{k}}}$ can be obtained by approximation method, such as, UT (Julier and Uhlmann 1997). Additionally, the correlational inference has proved that the state estimate is not difficult to obtain by the approximation method, and furthermore the estimate does not need any computation of Jacobian matrix for measurement equation or dynamic equation.

(ii) The estimators of $\hat{X}_k$ and $\Sigma_{\hat{X}_k}$ are expressed in the eqs. (4.20) and (4.24), in which the predicted state vector $\bar{X}_k$ and innovation vector $\bar{V}_k$ with its covariance matrix $\Sigma_{\bar{V}_k}$ can be derived by (4.2), (4.4) and (4.5). The innovation vector $\bar{V}_k$ reflects the consistency between the predicted state and the measurement. The

Kalman gain matrix K_k is determined by $\Sigma_{\bar{X}_k \bar{y}_k}$ and $\Sigma_{\bar{V}_k}^{-1}$. Hence, the cross-covariance matrix between $\bar{X}_k$ and $\bar{V}_k$ as well as the weight matrix $\Sigma_{\bar{V}_k}^{-1}$ of $\bar{V}_k$ are crucial in determining the gain matrix K_k. The estimated state vector $\widehat{\mathrm{X}}_{\mathrm{k}}$ can also be easily obtained when the cross-covariance matrices $\Sigma_{\bar{X}_k \bar{y}_k}$ or $\Sigma_{\bar{X}_k \bar{V}_k}$ are determined. In UKF, $\Sigma_{\bar{X}_k \bar{y}_k}$ is generated according to the sample dispersion of $\bar{X}_k$ and $\bar{y}_{\mathrm{k}}$, of which the predicted state vectors are not related to the actual linearized models, while $\Sigma_{\bar{X}_k \bar{y}_k}$ is usually much more accurate than that propagated from the linearized equations (Yang et al., 2016).

(iii) The eq. (4.19) expresses the relationship between the two correlated stochastic vectors $V_{\bar{X}_k}$ and $\bar{V}_k$. This relationship illustrates that the stochastic unknown vector $V_{\bar{X}_k}$, which does not appear in the system model can be derived from the related estimated vector $\overline{\mathrm{V}}_{\mathrm{k}}$, by using cross-covariance matrix $\Sigma_{\bar{X}_k \bar{y}_k}$. This relationship is also appeared in collocation (Moritz 1980; Koch 1977; Yang et al. 2009). If two correlated stochastic vectors s and s_1 with expectations $E(s) = 0$ and $E(s_1) = 0$ and also with the covariance matrices Σ_s and Σ_{s_1} as well as cross-covariance matrix $\Sigma_{ss_1} = \Sigma_{s_1 s}^T$ exist, the relationship between the two estimated vectors $\hat{\mathrm{s}}$ and $\hat{\mathrm{s}}_1$ is then,

$$\hat{\mathrm{s}} = \Sigma_{\mathrm{ss}_1} \Sigma_{\mathrm{s}_1}^{-1} \hat{\mathrm{s}}_1 \text{ or } \hat{\mathrm{s}} = \Sigma_{\mathrm{s}_1 \mathrm{s}} \Sigma_{\mathrm{s}_1}^{-1} \hat{\mathrm{s}} \tag{4.25}$$

(vi) If the state space model is linear, the basic expression of the new derived estimator from the correlational inference is equivalent to Kalman filter. Both the linearized form of the error expressed in eq. (4.1) and the form of the predicted state expressed in eq. (4.2) are,

$$V_k = H_k \hat{X}_k - y_k \tag{4.26}$$

$$\bar{X}_k = F_{k,k-1} \hat{X}_{k-1} \tag{4.27}$$

with the covariance matrix $\Sigma_{\bar{X}_k}$,

$$\Sigma_{\bar{X}_k} = F_{k,k-1} \Sigma_{\hat{X}_{k-1}} F_{k,k-1}^T + \Sigma_{w_k} \tag{4.28}$$

where, $F_{k,k-1}$ is the transition matrix.

Thus, the Kalman filter solution is obtained (Koch & Yang, 1998),

$$\hat{X}_k = \bar{X}_k + \Sigma_{\bar{X}_k} H_k^T \left(H_k \Sigma_{\bar{X}_k} H_k^T + \Sigma_k \right)^{-1} (H_k \bar{X}_k - y_k) \tag{4.29}$$

It is noted that the innovation (or predicted residual) vector in the linearized form is expressed as,

$$\bar{V}_k = H_k \bar{X}_k - y_k \tag{4.30}$$

and the corresponding predicted measurement is,

$$\bar{y}_k = H_k \bar{X}_k \tag{4.31}$$

The following equations can be easily obtained from eqs. (4.28) and (4.31),

$$\Sigma_{\bar{X}_k \bar{V}_k} = \Sigma_{\bar{X}_k \bar{y}_k} = \Sigma_{\bar{X}_k} H_k^T \tag{4.32}$$

$$\Sigma_{\bar{V}_k} = \Sigma_{\bar{y}_k}^* + \Sigma_k = H_k \Sigma_{\bar{X}_k} H_k^T + \Sigma_k \tag{4.33}$$

The conventional Kalman gain matrix then reads,

$$K_k = \Sigma_{\bar{X}_k} H_k^T \left(H_k \Sigma_{\bar{X}_k} H_k^T + \Sigma_k \right)^{-1} = \Sigma_{\bar{X}_k \bar{V}_k} \Sigma_{\bar{V}_k}^{-1} \qquad (4.34)$$

This derivation suggests that the state estimator (4.20) derived by the correlational inference is equivalent to the standard Kalman filter estimator (4.29) in the case that the system model is linear.

This correlational inference deduces Kalman filter by the relationship among the predicted measurement vector y_k and the predicted state vector $\overline{\mathrm{X}}_{\mathrm{k}}$, as well as the cross-covariance matrix $\Sigma_{\bar{X}_k \bar{y}_k}$. The deduction avoids the linear model requirements of Kalman filter. With the use of the new expression of Kalman filter, different methods can be deduced in the same framework based on the revealed relationships between the measurement and the state vectors. If the state space model is linear, the relationship of the measurement vector y_k and the state vector X_k can be easily obtained with variance propagation law, Kalman filter estimator is then obtained; If the state space model is nonlinear, and the first order Taylor expansion is used to approximate the nonlinear equation, the covariance matrix can also be obtained by variance-covariance propagation, then the EKF estimator is derived; or UT is employed to approximate the covariance matrix, then the UKF is expressed.

4.2 Comparison of EKF and UKF Nonlinear Techniques

As mentioned before, the EKF and UKF use different techniques to approximate nonlinear estimations. The EKF uses the first-order Taylor expansion to approximate nonlinear equations, while UKF uses the sigma points to approximate the mean and its covariance matrix of the transformed state vector. In this section, the performance of the UKF and EKF are analysed and compared.

4.2.1 Linearization of Nonlinear Equations

Let an arbitrary nonlinear equation be,

$$x_k = f(x_{k-1}) \tag{4.35}$$

where $f(\cdot)$ is the nonlinear model expressing the state transition of time; x_{k-1} is the one dimensional system state at time epoch $k-1$, and it is a random variable with the mean $\hat{x}_{k-1}$ and variance $\sigma^2_{\hat{x}_{k-1}}$. To predict the state mean and variance using a Kalman filter, the nonlinear equation must be linearized, and is commonly by use of Taylor expansion about $\hat{x}_{k-1}$,

$$f(x_{k-1}) = f(\hat{x}_{k-1} + \delta x) = f(\hat{x}_{k-1}) + f^{(1)}\delta x + \frac{1}{2} f^{(2)}\delta x^2 + \frac{1}{3!} f^{(3)}\delta x^3 + \frac{1}{4!} f^{(4)}\delta x^4 + \cdots \tag{4.36}$$

where δx is the difference between the true state and the estimated state, with a zero mean Gaussian and variance $\sigma^2_{\hat{x}_{k-1}}$; $f^{(i)}$ is the ith order term of a partial derivative operator with respect to $\hat{x}_{k-1}$.

The transformed mean $\bar{x}_k$ can be obtained by taking expectations of eq. (4.36), and considering $E(\delta x) = 0$, and $Cov(\delta x) = \sigma^2_{\hat{x}_{k-1}}$,

$$\bar{x}_k = f(\hat{x}_{k-1}) + \frac{1}{2} f^{(2)} \sigma^2_{\hat{x}_{k-1}} + \frac{3}{4!} f^{(4)} \sigma^4_{\hat{x}_{k-1}} \cdots \tag{4.37}$$

The covariance of $\bar{x}_k$ then, can be obtained by,

$$\begin{aligned} \Sigma_{\bar{x}_k} &= E[(x-\bar{x}_k)(x-\bar{x}_k)^T] \\ &= f^{(1)}\sigma^2_{\hat{x}_{k-1}}[f^{(1)}]^T + \frac{1}{3!}E\left[(f^{(1)}\delta x)(f^{(3)}\delta x^3)^T\right] + \frac{1}{3!}E\left[(f^{(3)}\delta x^3)(f^{(1)}\delta x)^T\right] \\ &\quad + \frac{1}{4!}E\left[(f^{(2)}\delta x^2)(f^{(2)}\delta x^2)^T\right] - \frac{1}{4!}E[f^{(2)}\delta x^2]E[f^{(2)}\delta x^2]^T \end{aligned} \tag{4.38}$$

Recalling that the Jacobian matrix F is the first order partial derivative of nonlinear equation $f(\cdot)$, then eq. (4.38) can be written as,

$$\begin{aligned} \Sigma_{\bar{x}_k} &= F\sigma^2_{\hat{x}_{k-1}}F^T \\ &\quad + \frac{1}{3!}E\left[(f^{(1)}\delta x)(f^{(3)}\delta x^3)^T\right] + \frac{1}{3!}E\left[(f^{(3)}\delta x^3)(f^{(1)}\delta x)^T\right] \\ &\quad + \frac{1}{4!}E\left[(f^{(2)}\delta x^2)(f^{(2)}\delta x^2)^T\right] + \frac{1}{4!}E[f^{(2)}\delta x^2]E[f^{(2)}\delta x^2]^T \end{aligned} \tag{4.39}$$

Due to the complexity of computation, the first order of the expansion is used to propagate the mean and the variance of the state. The higher order terms of the expansion are ignored, which introduced linearization error. Furthermore, if the approximation point (or the approximate value of the parameter) is far away from the true value, then the first-order approximation of the nonlinear equation will introduce large linearization errors. Thus, the EKF is not an optimal estimator. The filter may diverge quickly if the initial state or the process uncertainties are not accurately known or have not been carefully dealt with. It should be mentioned that if the curvature of the nonlinear equation is not large enough, the EKF may result in reasonable estimates of the state parameters. It means that the dynamic model is near to the linear one. Furthermore, if the approximation point is sufficiently close to the true value, then neglecting the high-order terms would not significantly affect the state estimates.

4.2.2 Unscented Transform

The UT was proposed by Julier and Uhlmann (1997) on the intuition that the approximation of a Gaussian distribution being easier than approximating an arbitrary nonlinear equation. By this means that the Gaussian statistical properties of random variables which propagate through a nonlinear transformation can be more easily approximated. To analyze the transformation, the nonlinear eq. (4.35) and its expansion are used again by propagating a sigma point,

$$\bar{x}_{i,k} = f\left(\hat{x}_{i,k-1}\right) + f^{(1)}\delta x_i + \frac{1}{2}f^{(2)}\delta x_i^2 + \frac{1}{3!}f^{(3)}\delta x_i^3 + \frac{1}{4!}f^{(4)}\delta x_i^4 + \cdots \tag{4.40}$$

The mean of the predicted state is a weighted mean of the sigma points as expressed below,

$$\bar{x}_k = w_0\bar{x}_{0,k} + \sum_{i=1}^{2n}\left(w_i\bar{x}_{i,k}\right) \tag{4.41}$$

Substituting the weight of the sigma points expressed in eqs. (2.29b) and (2.29d) into eq. (4.6), and taking the expectation of all the sigma points, the predicted mean is,

$$\bar{x}_k = \frac{\lambda}{n+\lambda} E(\bar{x}_{0,k}) + \frac{1}{2(n+\lambda)} E(\bar{x}_{1,k}) + \frac{1}{2(n+\lambda)} E(\bar{x}_{2,k}) + \cdots + \frac{1}{2(n+\lambda)} E(\bar{x}_{i,k}) \tag{4.42}$$

Substituting eq. (4.40) into (4.42), the following can be obtained,

$$\bar{x}_k = f(\bar{x}) + \frac{1}{2(n+\lambda)} \sum_{i=1}^{2n} \left(\frac{1}{2} f^{(2)} \tilde{\sigma}_{i,k-1}^2 + \frac{1}{4!} f^{(4)} \tilde{\sigma}_{i,k-1}^4 + \cdots \right) \tag{4.43}$$

where $\tilde{\sigma}_{i,k-1}^2$ is the element of the weighted covariance of the state in eq. (2.29a), and,

$$\tilde{\sigma}_{i,k-1} = \sqrt{(n+\lambda)\sigma_{i,k-1}^2} \tag{4.44}$$

Thus, eq. (4.43) is written as,

$$\bar{x}_k = f(\bar{x}_k) + \frac{1}{2} f^{(2)} \sigma_{i,k-1}^2 + \frac{1}{2(n+\lambda)} \sum_{i=1}^{2n} \left(\frac{1}{4!} f^{(4)} \tilde{\sigma}_{i,k-1}^4 + \frac{1}{6!} f^{(6)} \tilde{\sigma}_{i,k-1}^6 \dots \right) \tag{4.45}$$

The covariance matrix of the above transformed state can be obtained by following eq. (2.21),

$$\Sigma_{\bar{x}_k} = \frac{1}{2(n+\lambda)} \left(\sum_{i=1}^{2n} (\bar{x}_{i,k} - \bar{x}_k)(\bar{x}_{i,k} - \bar{x}_k)^T \right) \tag{4.46}$$

Similar to eq. (4.39),

$$\Sigma_{\bar{x}_k} = F\sigma^2_{\hat{x}_{k-1}}F^T + \frac{1}{2(n+\lambda)}\sum_{i=1}^{2n} E\left[\frac{1}{3!}\left(f^{(1)}\delta x_i\right)\left(f^{(3)}\delta x_i^3\right)^T + \frac{1}{3!}\left(f^{(3)}\delta x_i^3\right)\left(f^{(1)}\delta x_i\right)^T + \frac{1}{4!}\left(f^{(2)}\delta x_i^2\right)\left(f^{(2)}\delta x_i^2\right)^T + \cdots\right] \quad (4.47)$$

From the above derivations, it can be found that the UT is able to achieve the accuracy similar to that of the third-order Taylor expansion. .

4.2.3 Performance Comparison

To compare the prediction precision of UT and first-order Taylor Expansion, the same model as expressed in eq. (2.30) in Chapter 2 is selected,

$$\begin{aligned} y_1 &= x_1 \sin\theta \\ y_2 &= x_2 \cos\theta \end{aligned} \quad (2.30)$$

The system state is denoted by $X = [x \quad y \quad \theta]^T$ with a covariance matrix $\Sigma = 1 * 10^{-2} * diag([(1m)^2 \quad (1.4m)^2 \quad (3m)^2])$. Figures 4.1(a) and 4.1(b) present the initial mean and predicted mean, as well as their 1-σ error ellipse which is derived from the covariance matrix. The error ellipse is used for presenting the error bound of the estimated states. The dot-dash line in the dark colour shown in Figure 4(b) is the Monte Carlo approach with 10^7 samples used to provide the reference for the prediction results. It can be seen that the UT results are more close to the reference, while the first-order Taylor expansion predicted mean is biased and its error ellipse is enlarged and biased. The Root Mean Square Error (RMSE) of UT and first-order Taylor expansion is presented in Table 4.1.

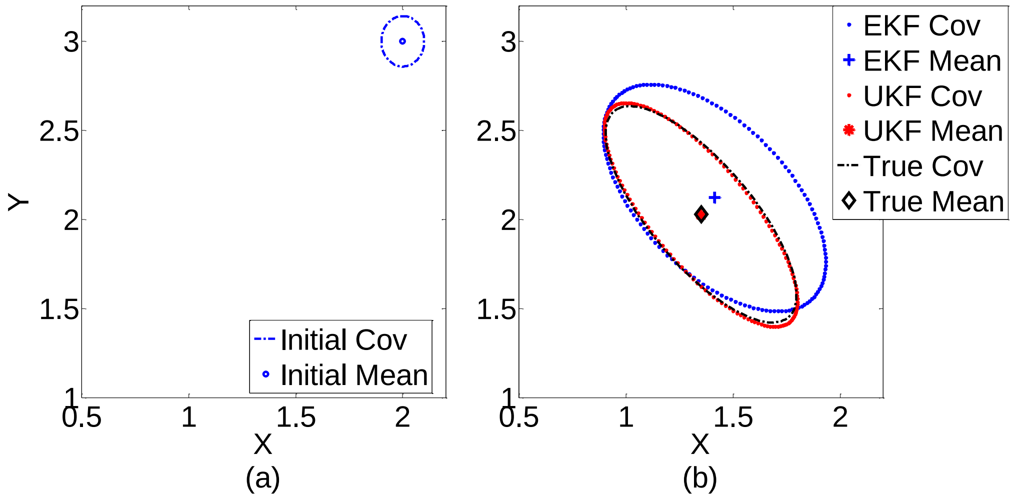

Figure 4.1 Performance comparisons of prediction precision (a) is the initial state with 1-σ error ellipse, and (b) is predicted state mean with 1-σ error ellipses by UT, first-order Taylor expansion, and Monte Carlo approach

Table 4.1 Comparisons of RMSEs [m] of UT and the first-order Taylor expansion prediction

	UKF	EKF
X	0.001	0.062
Y	0.002	0.093

4.3 Theoretical Relation between Extended and Unscented Kalman Filters

The correlational inference in section 4.1 was used to establish the common framework for the UKF and EKF. From the derivations and state estimators, some theoretical relationships between UKF and EKF are found as follows,

(i) Both the UKF and EKF can be operated within the Kalman filtering framework. The accuracy of the estimated state depends on the accuracy of predicted state $\bar{x}_k$, the predicted measurement $\bar{y}_k$ and the Kalman gain matrix.

(ii) The UKF has better prediction accuracy than the EKF in most nonlinear state cases as illustrated in Figure 4.1. The mean and covariance matrix of the state estimate resulting from the UKF are obtained by the weighted sigma points propagated through the nonlinear function. The UT used in the propagation process avoids the problem with introducing the linearization error which degrades the filter performance.

(iii) The accuracy of the predicted measurement vector $\bar{y}_k$ resulting from the UKF is more accurate than that of the EKF. In the UKF, a set of sigma points propagated through the nonlinear system dynamic model and the observation model are used to approximate the predicted measurements. The first propagation obtains system predicted state and its covariance matrix, as mentioned in point (2), and the second propagation uses re-sampled sigma points propagate through the nonlinear observation model to obtain the predicted measurements and its covariance matrix, as well as the cross-covariance matrix between the predicted state vector and predicted measurement vector. The EKF, however, uses the linearized models, system model and observation model to obtain the predicted state and measurement vectors, as well as their covariance matrices; hence it introduces a linearization error in both predicted state information and predicted measurement information.

(iv) The reliability of the estimated state $\hat{x}_k$ from a Kalman filter relies on quality of the Kalman gain matrix K_k. In the EKF, the Kalman gain is calculated using the predicted covariance matrix $\Sigma_{\bar{x}_k}$, measurement noise covariance matrix Σ_k, and the linearized design matrix H_k. A linearization error exists in all these three items. However, in the UKF, the cross-covariance matrix $\Sigma_{\bar{x}_k \bar{y}_k}$ and the predicted measurement covariance matrix $\Sigma_{\bar{y}_k}$ are obtained from weighted sigma points. This result can be used to calculate the projected mean and its variance up to the second order (Julier & Uhlmann, 2004).

(v) Unlike the EKF, the Jacobian matrix for a nonlinear equation system is not needed in the UKF estimation process.

(vi) The UKF iteratively propagates the sigma points through nonlinear functions, while the EKF only calculates the Jacobian matrix once for the whole estimation process. The former is more close to the reality of a dynamic system and thus leads to a better solution.

(vii) For the matching of the current statistic properties, the UKF uses the UT to capture the stochastic information the estimated state. The UT calculates the square root of the state covariance matrix by Cholesky decomposition which requires a positive-definite matrix (Agarwal & Mehra, 2014). However, the decomposition requires numerical stability of the process, since the UKF cannot guarantee a positive-definite matrix resulting from iterations.

4.4 Comparison Using Simulated and Field Data

To comprehensively evaluate the performance difference between the UKF and EKF applied to vehicle navigation, a simulation test and two field tests were carried out. Data for the three cases were processed on a PC with Intel Core i7-3770 CPU at 3.40 GHz, 16-GB RAM equipped with Windows 7, and the Matlab R2010a 64-bit program was used.

For the first case, a moving vehicle with a constant turning behaviour under the open-loop mode was adopted. The second test was carried out in Hong Kong, for which GPS and IMU were integrated with the loosely coupled strategy, and estimated errors were fed back to the estimation system compensate the errors of the IMU sensors. The third test was conducted in Beijing, in which GPS observations with a constant velocity model were conducted to form a tightly coupled integration system. It was for an analysis of the effectiveness of these different state space models and feedback modes used in the EKF and UKF.

4.4.1 Case 1: Open Loop Constant Turn Model

Constant turning is a form of behaviour where a vehicle turns with a constant angular rate ω. A nonlinear dynamic model with respect to the vehicle's heading velocity is commonly used to express the system state. In the aforementioned simulation, a constant turning at an angular rate of 2.54°/s with a heading velocity of 81 km/h was selected for the test. The trajectory of the vehicle was designed on a 500 m radius and its coordinates are shown in Figure 4.2. It was assumed that the observations were sampled at every 1 s while the states were updated every 0.1 s. The simulation period was 141 s. Figure 4.3 shows the implementation scheme of the data processing.

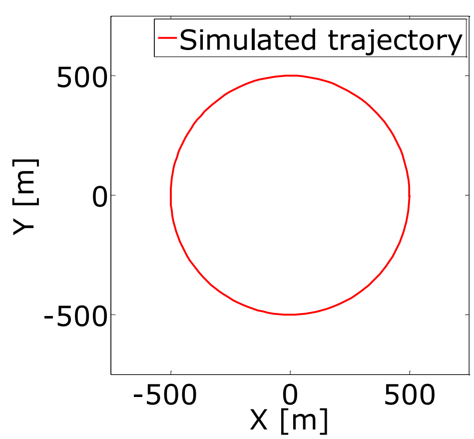

Figure 4.2 Designed vehicle trajectory

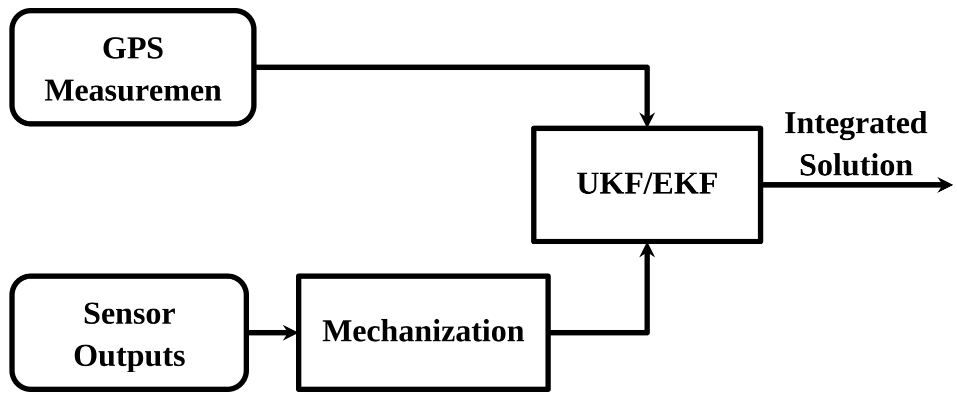

Figure 4.3 Open loop implementation scheme of filter integration

The discrete dynamic model with the state vector is,

$$f(x_k \quad y_k \quad v_k \quad \omega_k \quad \theta_k) = \begin{bmatrix} x_{k-1} + v_{k-1} t \sin\theta_{k-1} \\ y_{k-1} - v_{k-1} t \cos\theta_{k-1} \\ v_{k-1} \\ \omega_{k-1} \\ \theta_{k-1} - \omega_{k-1} t \end{bmatrix} + w_{k-1} \qquad (4.48)$$

where x_k, and y_k are the vehicle's position in the selected two-dimensional coordinate system; $v_{k,}$ ω_k and θ_k are the heading velocity, angular velocity and heading of vehicle, respectively; w_{k-1} is the Gaussian noise with zero mean and covariance matrix $\Sigma_{w_{k-1}}$; and the subscript k indicates time epoch.

The observation function is,

$$y_k = H_k X_k + e_k \qquad (4.49)$$

where H_k is an identity matrix, and e_k is the uncorrelated observation noise with covariance matrix $\Sigma_k = diag[(1m)^2\ (1m)^2\ (0.5m/s)^2\ (0.001rad/$

$s)^2$ $(0.01rad)^2]$.

The initial state was set to $X = [498.93 \quad -0.94 \quad 22.62 \quad 0.045 \quad -0.016]^T$. The state estimates resulting from both the UKF and EKF were compared against the simulated value (the reference or truth) for the validation and comparison of their performances. The difference of the estimate from the reference indicates in the error of the estimation results. Figures 4.4(a) and 4.4(b) show the errors of the UKF and EKF estimates in the X and Y components respectively. Figure 4.5 shows the heading error of the vehicle. Figure 4.6 shows the estimated angular velocity and their reference values. The RMSE of all epochs of the UKF EKF are listed in Table 4.2 for the overall accuracy of the time period.

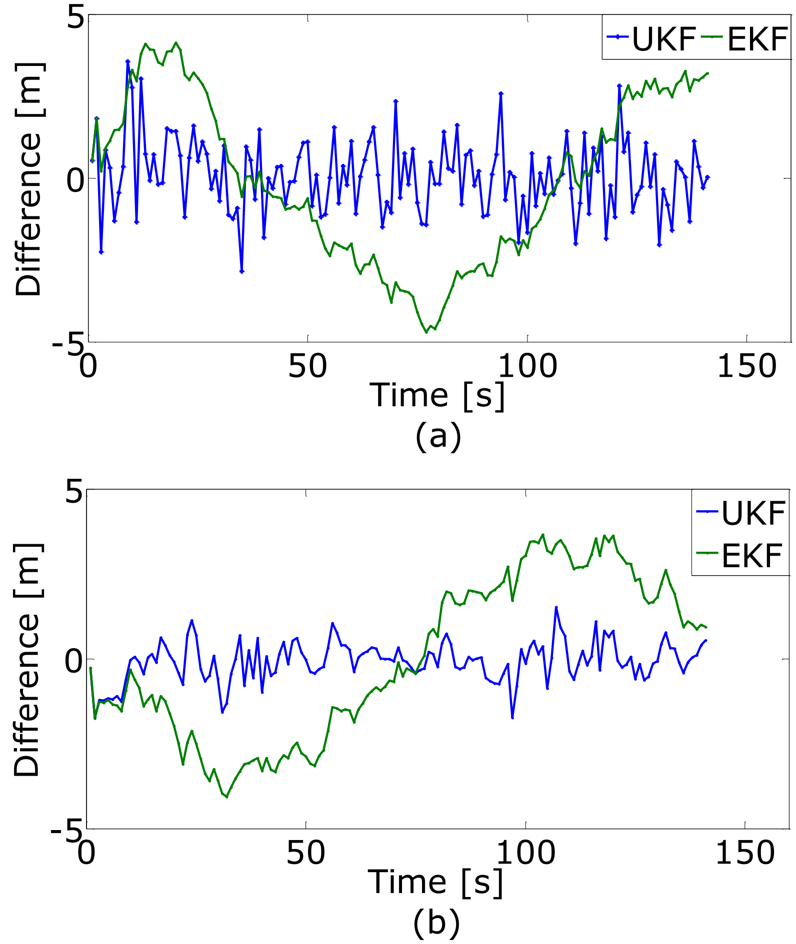

Figure 4.4 Difference between the UKF and EKF estimates and the truth for the X component (a) and the Y component (b)

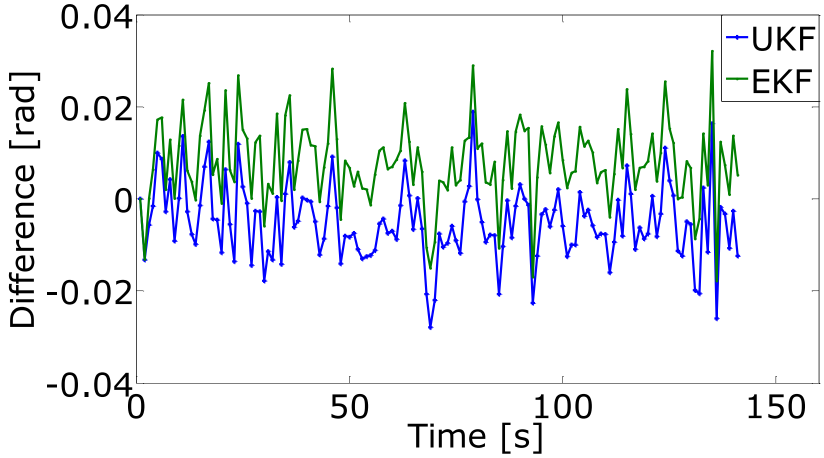

Figure 4.5 Error of the estimated heading

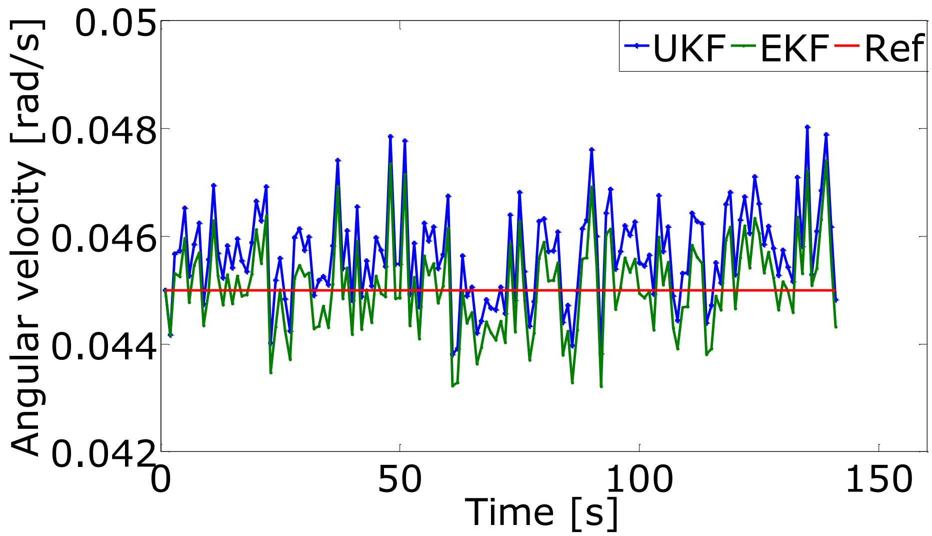

Figure 4.6 Estimated and reference angular velocities

Table 4.2 RMSE of all filter epochs

	UKF	EKF
X [m]	0.98	2.19
Y [m]	0.54	2.51
V [m/s]	0.17	0.17
ω [rad/s]	0.001	0.0008
θ [rad]	0.009	0.012

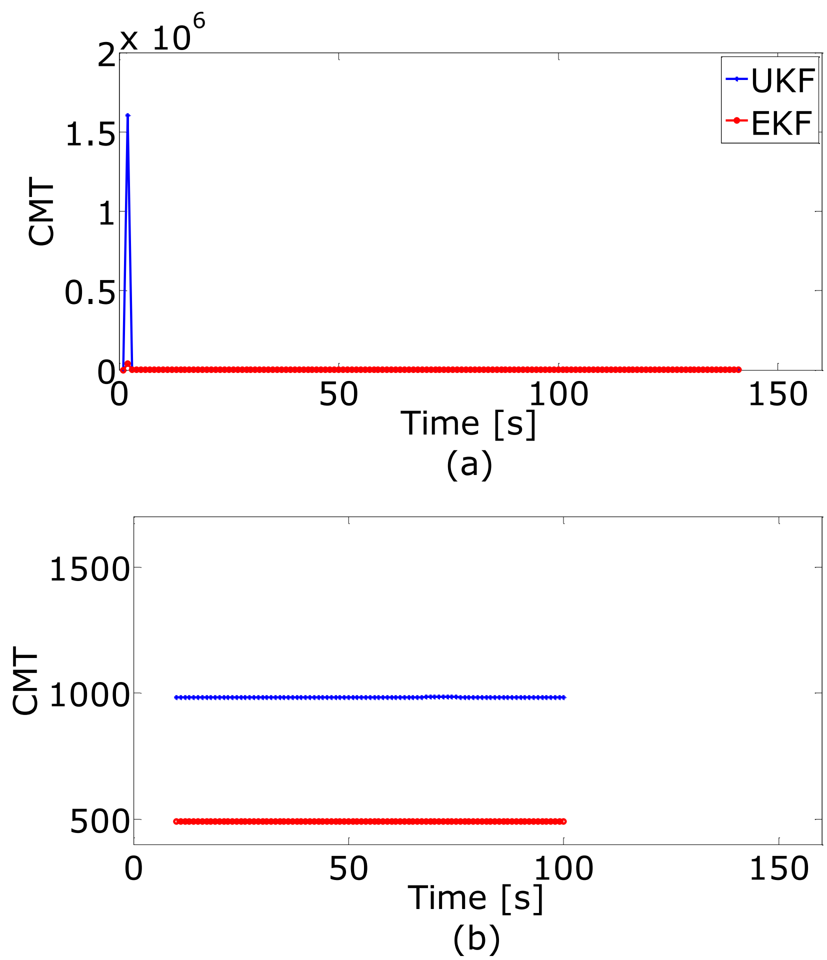

Figure 4.7 Predicted covariance matrix trace of UKF (a) and EKF (b)

The trace of the predicted covariance matrix is presented in Figure 4.7. Figure 4.7(a) shows the covariance matrix trace (CMT) of the predicted state resulting from the UKF and EKF respectively. The difference between the two estimators from epoch 10 to 100 s is presented in Figure 4.7(b).

From the two figures we can see that:

(i) In Figure (4.6) The RMSE of the UKF for the X and Y components are 0.98 m and 0.54 m respectively, which are significantly less than the EKF results of 2.19 m and 2.51 m. This indicates that the UKF significantly outperforms the EKF.

(ii) From Figure 4.7, the trace of the covariance matrix of the predicted state resulting from the UKF is larger than that of EKF, $tr\left(\Sigma_{\bar{x}_k}^{UKF}\right) > tr\left(\Sigma_{\bar{x}_k}^{EKF}\right)$. This suggests that the UKF is less affected by historical data, which leads the estimate close to the observation.

4.4.2 Case 2: Closed-Loop GPS/IMU Integrated Navigation System

In the second test case, which was the field test conducted in Hong Kong, the closed-loop mode was selected for the GPS/IMU integrated navigation system. The route of the vehicle was through dense building areas with many overpasses and viaducts. The position of the vehicle represented is in the Hong Kong 80 Grid coordinate system. The test duration was about 15 minutes and the data were collected from a Hitachi H48C 3-axis accelerometer and Analog Devices ADXRS300 gyroscope at 100 Hz (Analog Devices Inc., 2004; Hitachi, 2007). The accelerometer was for measuring the acceleration in the heading direction and the gyroscope measured the change in the heading of the vehicle. A GPS module was equipped for position and velocity measurements every 1.4 s. The GPS and IMU were loosely coupled and the system provides state information including position, timing, velocity, acceleration and heading in the National Marine Electronics Association (NMEA) 0813 standard. This standard is a specification for communication between marine electronics equipment.

In this case, the error state is used to establish the system dynamic model. The estimated result is used for compensating the error of the IMU measurements. The schematic of the close-loop implementation is shown in Figure 4.8, with the state vector $X = [\delta x\ \delta y\ \delta v\ \delta\theta\ b\ \delta\omega\ s]^T$, and the nonlinear dynamic model being expressed by the following equations,

$$
\begin{aligned}
&X_{k+1} = f\left(X_k\right) + w_k \\
&= \begin{bmatrix} \delta x_k + \delta v_k T \sin\theta_k + v_k T \cos\theta_k \delta\theta_k + 0.5\delta a_k T^2 \sin\theta_k + 0.5\delta a_k T^2 \cos\theta_k \delta\theta_k \\ \delta y_k + \delta v_k T \cos\theta_k - v_k T \sin\theta_k \delta\theta_k + 0.5\delta a_k T^2 \cos\theta_k - 0.5\delta a_k T^2 \sin\theta_k \delta\theta_k \\ \delta v_k + \delta a_k T \\ \delta\theta_k + d_k T \\ e^{\frac{-T}{\tau_g}} b \\ e^{\frac{-T}{\tau_g}} \delta\omega \\ e^{\frac{-T}{\tau_g}} s \end{bmatrix}
\end{aligned}
\tag{4.50}
$$

where δx and δy are the positioning errors in the two coordinate components; δv is the error of the velocity with respect to the heading direction; $\delta\theta$ is the heading error; b is the acceleration bias; $\delta\omega$ is the angular rate bias; s is the accelerometer scale factor; τ_g is the correlation time of the accelerometer and the gyroscope; T is the time interval, the system noise was defined as $w_k = [0\ 0\ 0\ 0\ w_b\ w_{\delta\omega}\ w_s]^T$ and white noise with a covariance matrix Σ_{w_k} were assumed.

The observation equation is,

$$y_k = H_k X_k + e_k \tag{4.51}$$

where,

$$H_k = \begin{bmatrix} 1 & 0 & 0 & 0 & 0 & 0 & 0 \\ 0 & 1 & 0 & 0 & 0 & 0 & 0 \\ 0 & 0 & 1 & 0 & 0 & 0 & 0 \\ 0 & 0 & 0 & 1 & 0 & 0 & 0 \end{bmatrix} \tag{4.52}$$

$$y_k = \left[P_{gps} - P_{INS}, V_{gps} - V_{INS}, Head_{GPS} - Head_{INS}\right]^T \tag{4.53}$$

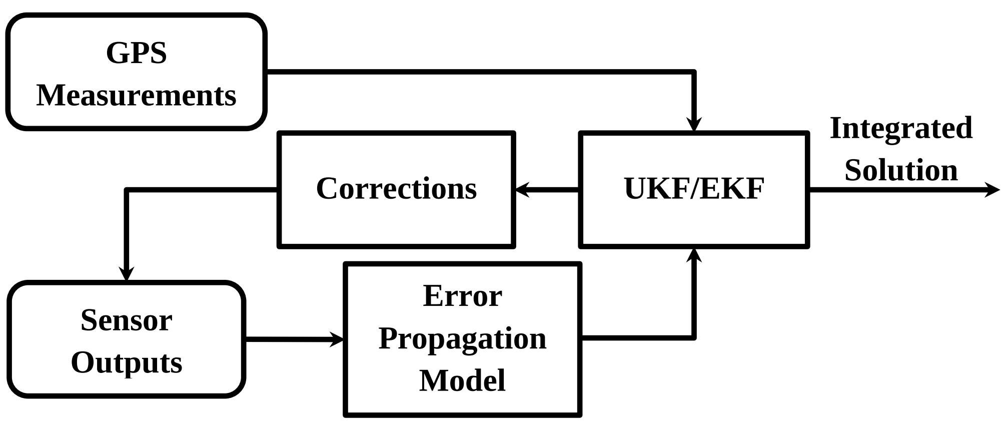

Figure 4.8 Close loop implementation scheme of UKF/EKF

The positioning trajectory estimated from the UKF and EKF, along with the positioning resulting from the SD approach of GPS measurements as the reference is shown in Figure 4.9. The positioning errors in the X, Y components and their overall accuracy in the time series are depicted in Figures 4.10(a), (b) and (c). The dash line denotes the UKF and the solid line for the EKF. The RMSE of these results are listed in Table 4.3.

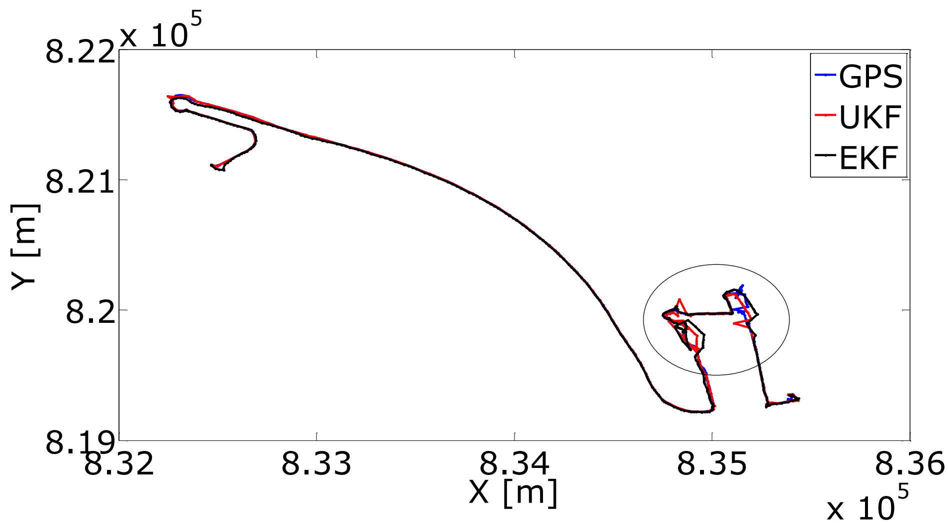

Figure 4.9 Estimated trajectory of the vehicle resulting from UKF, EKF and GPS (as the reference)

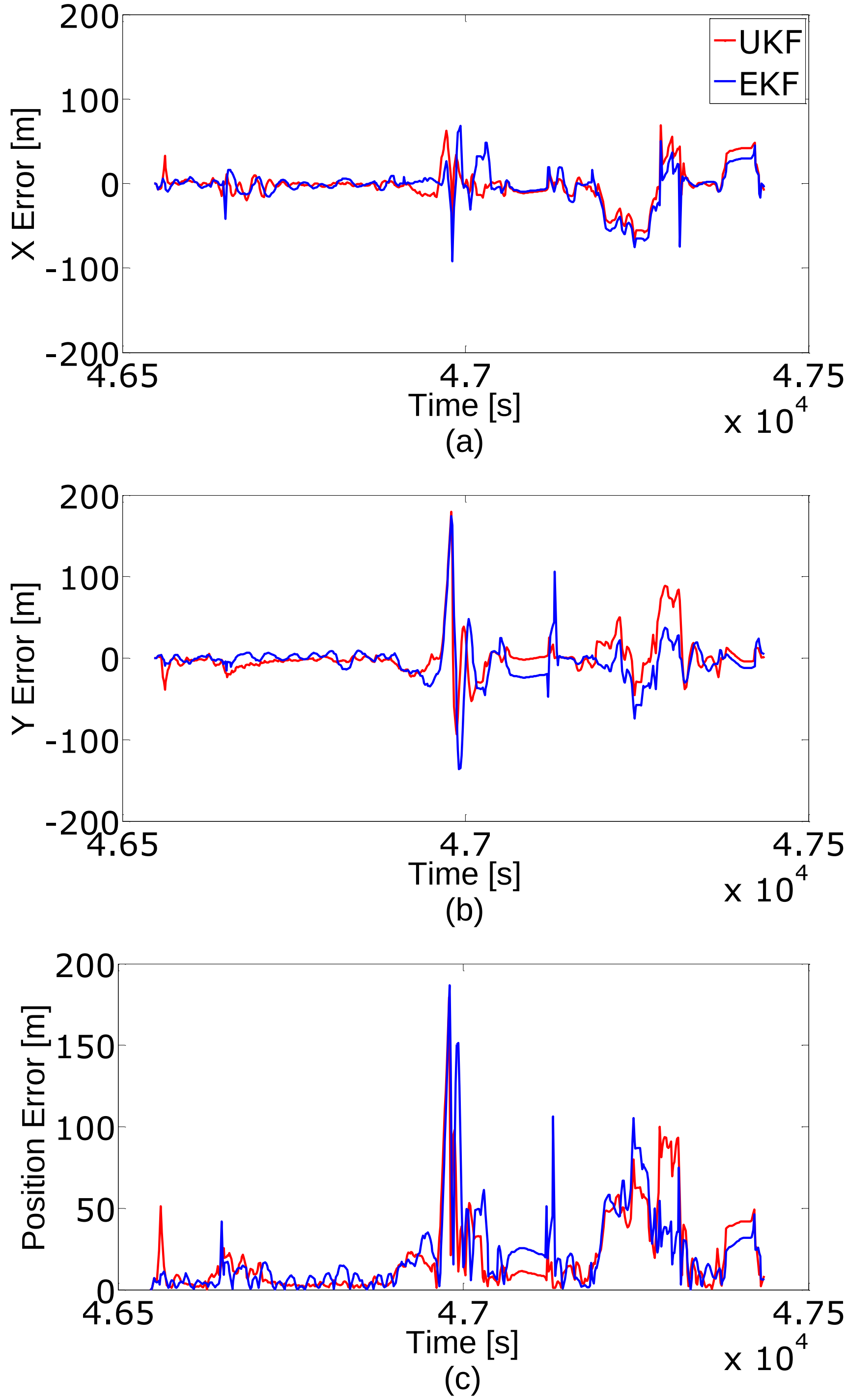

Figure 4.10 Positioning error of UKF and EKF in the, X components (a), Y components (b), and overall Position error (c) (GPS SD positioning results were used as the reference).

Table 4.3 Comparison of the position results of RMSEs [m] from UKF and EKF

	UKF	EKF
X	16.30	21.59
Y	20.64	26.18

Those peak values shown in Figure 4.10(c) correspond to the area marked by the circle in Figure 4.9, which were caused by the fact that the number of visible satellites was under four. Figure 4.11 presents the velocity solved by GPS measured Doppler shifts and estimated by the UKF and EKF.

From this test case, it can be seen that the UKF outperforms the EKF in terms of positioning accuracy. The reason is that the error model moderates the nonlinearity of the state space model. The UKF estimated result is closer to the measurements than those of EKF, even though the measurements are contaminated.

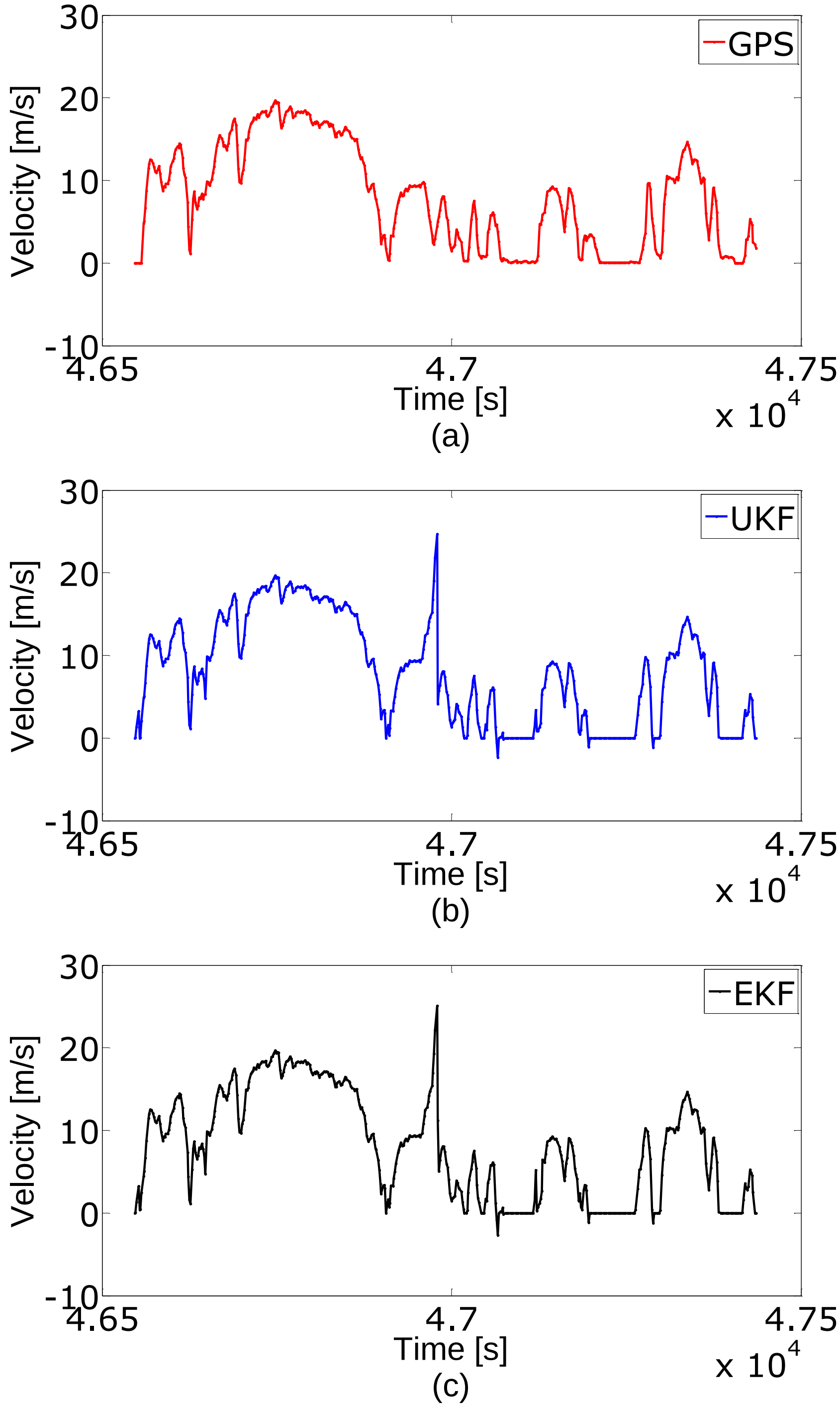

Figure 4.11 Velocity estimated by GPS (a), UKF (b) and EKF (c)

4.4.3 Case 3: Constant Velocity Model

In the third test scenario, conducted along the Beijing's Fifth Ring Road in a suburban environment for testing the constant velocity model for the system dynamic model, the GPS receiver was equipped to collect the position and velocity of the vehicle at a 1 second sampling rate. The driving time was about 3 hours. The predicted position and velocity were transferred to nonlinear GPS observation model. The integration architecture is presented in Figure 4.12. The state vector is $X = \left[x, y, z, v_x, v_y, v_z, \delta t, \delta\dot{t}\right]^T$, where $[x, y, z]^T$ are the coordinates of the vehicle in the WGS84 coordinate system; $\left[v_x, v_y, v_z\right]^T$ are the corresponding velocity components; δt is the receiver clock bias, and $\delta\dot{t}$ is the clock bias rate. The system observed the pseudorange and Doppler shift directly, thus the observation vector is $y_k = [\rho_i, \dot{\rho}_i]^T$, where ρ_i is the pseudorange of the ith satellite and $\dot{\rho}_i$ is its Doppler shift. The initial states were set to zero.

The vehicle trajectory measured by the GPS SD approach with pseudorange measurements is illustrated in Figure 4.13. The positioning solution from carrier phase measurements was used as the reference.

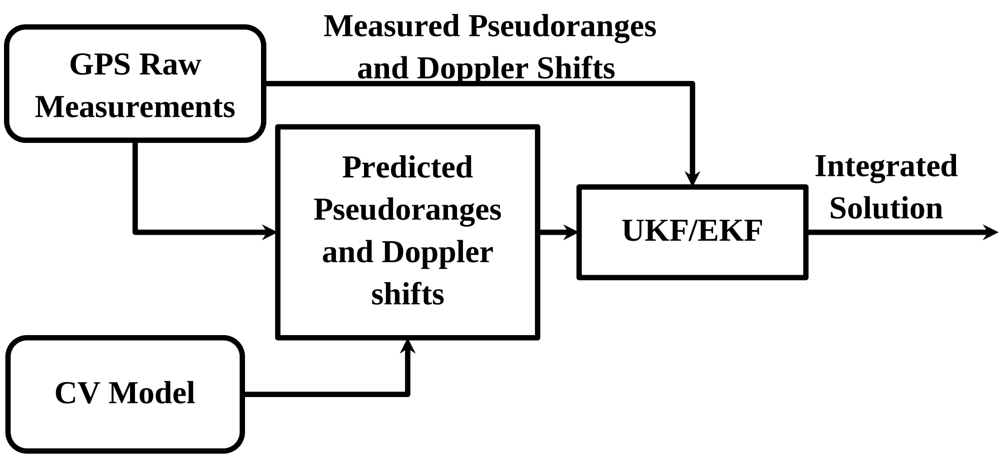

Figure 4.12 Tightly Integration scheme of UKF/EKF

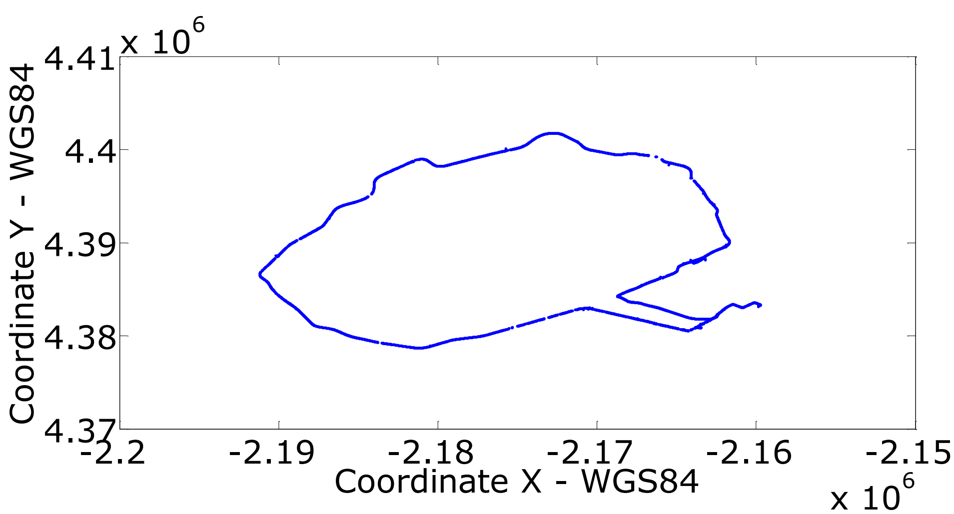

Figure 4.13 Vehicle trajectory

The errors of the estimated position resulting from the UKF and EKF for the time series are shown in Figures 4.14 and 4.15 respectively. The large peak values shown at the beginning epochs in Figure 4.15 were caused by the zero initial state. The spikes in time series are mainly caused by the multipath effect of GPS measurements. The RMSE of position estimation is listed in Table 4.4. The velocity results are plotted in Figures 4.16 and 4.17; and the convergence time is shown in Figure 4.18.

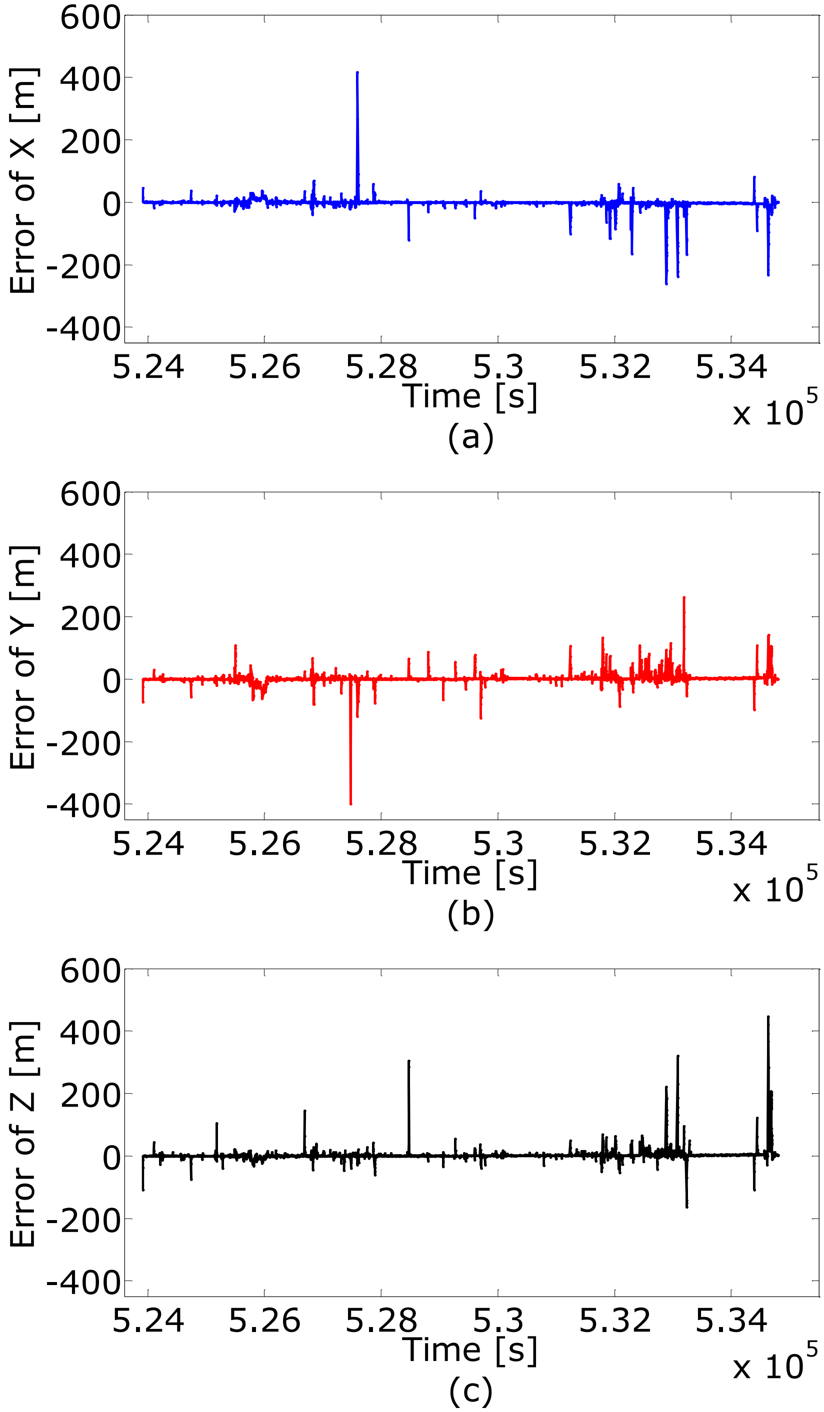

Figure 4.14 UKF positioning error (in the X component (a), Y component (b), and Z component (c) (GPS carrier phase solution is the reference)

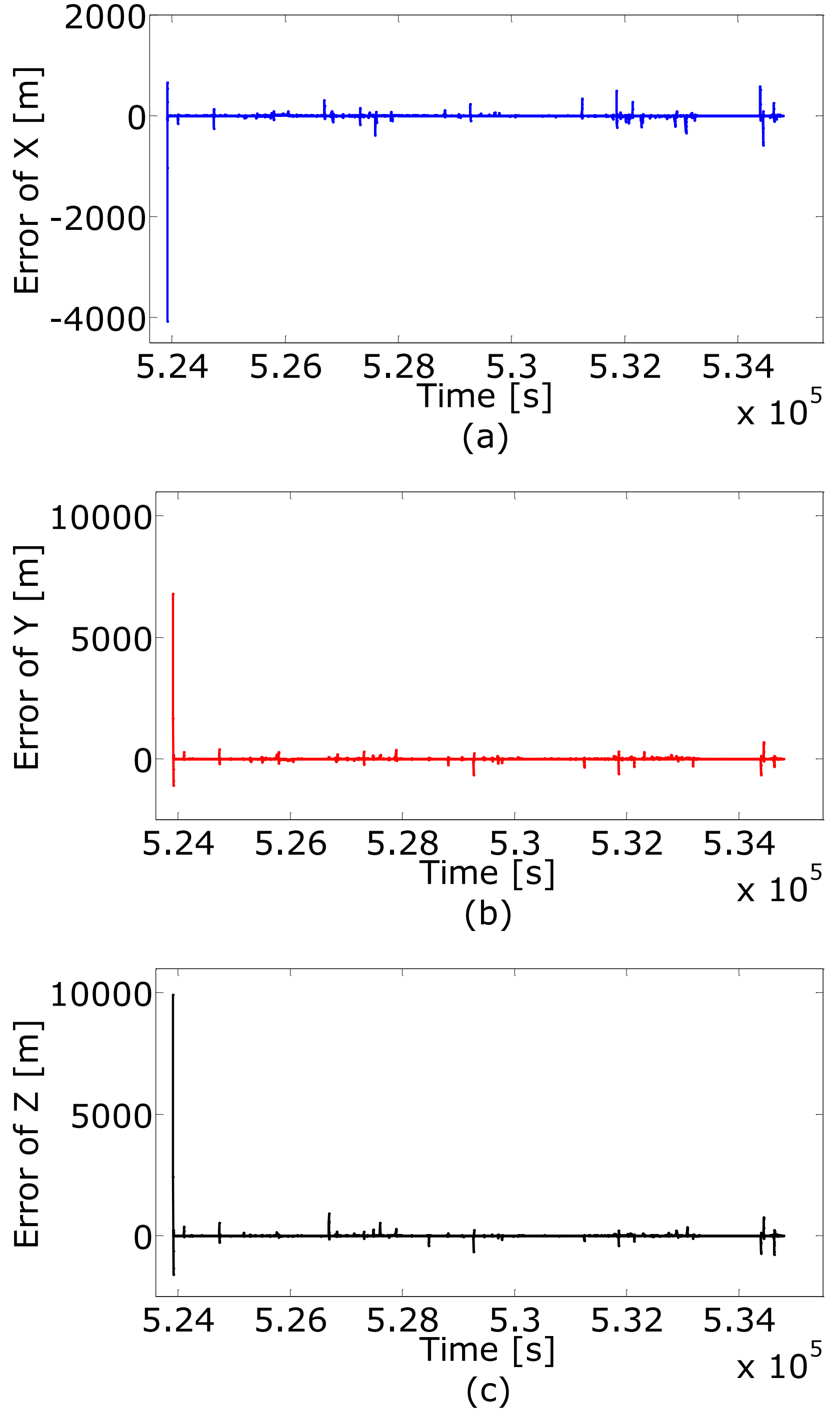

Figure 4.15 Error of EKF position in the X component (a), Y component (b), and Z component (c)

Table 4.4 The RMSE of UKF and EKF positioning [m]

	UKF	EKF
X	0.10	0.22
Y	0.12	0.27
Z	0.14	0.42

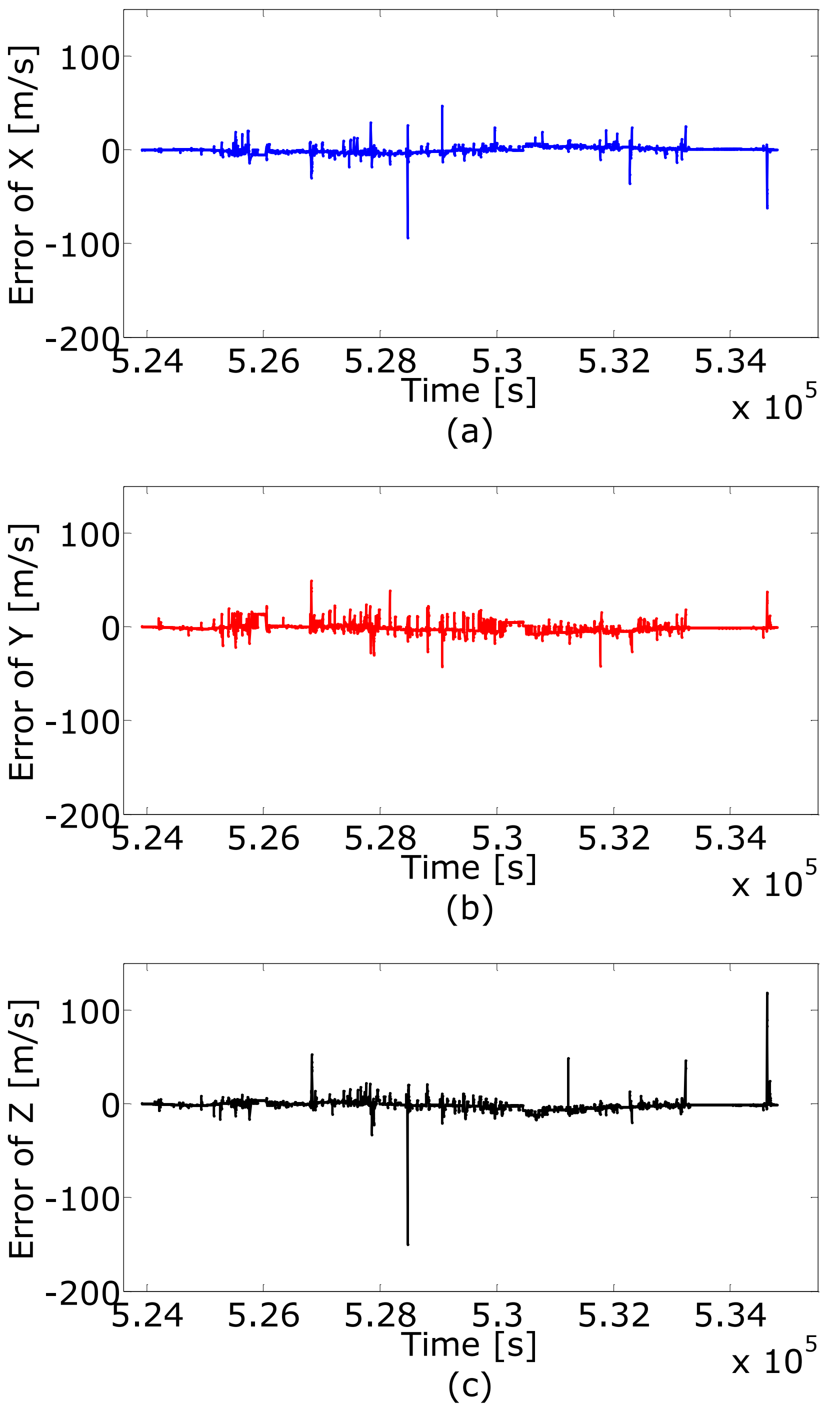

Figure 4.16 Velocity error of UKF with respect to the GPS Doppler measurement, in X components (a), Y components (b), and Z components (c)

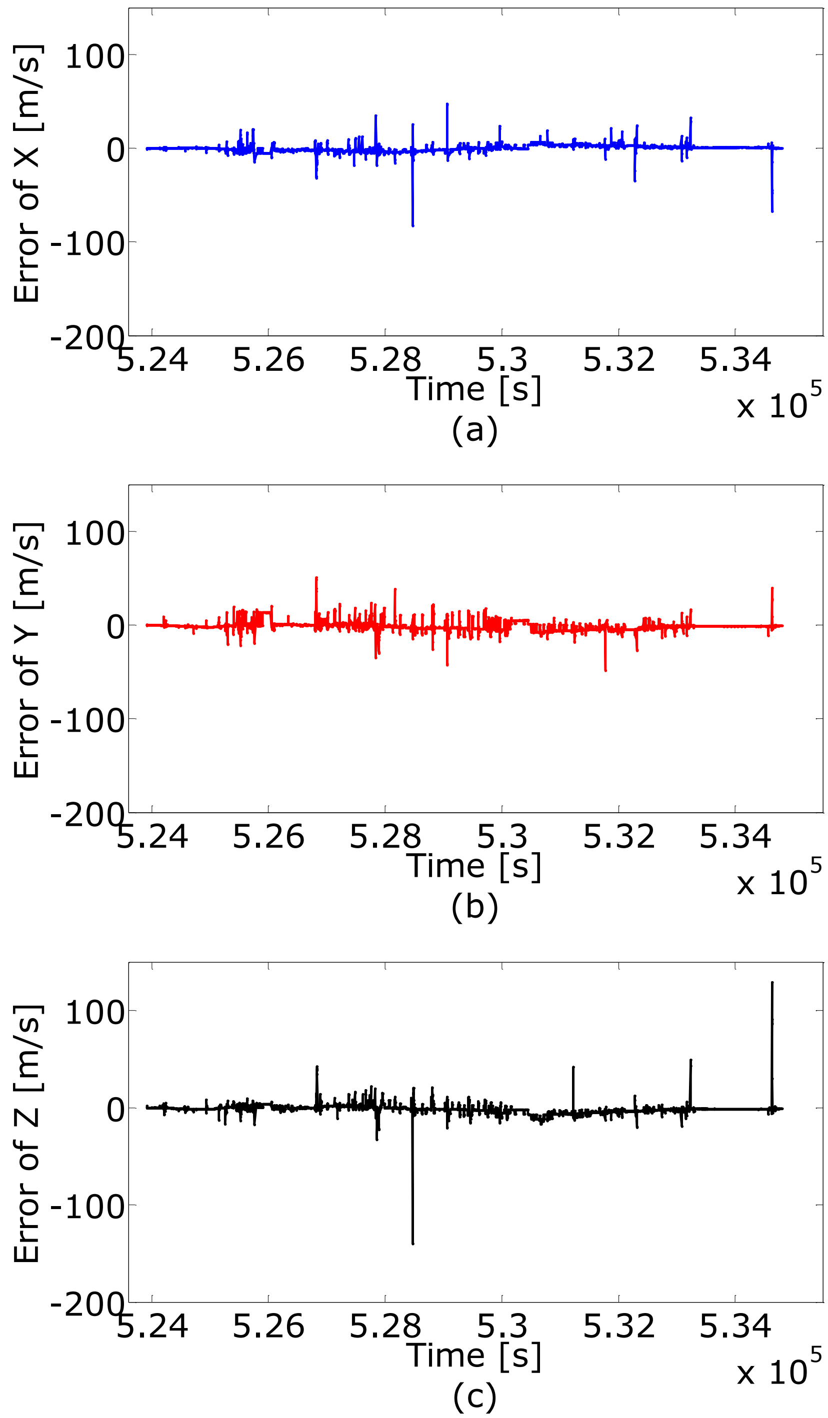

Figure 4.17 Velocity error of EKF with respect the GPS Doppler measurements, X components (a), Y components (b), and Z components (c)

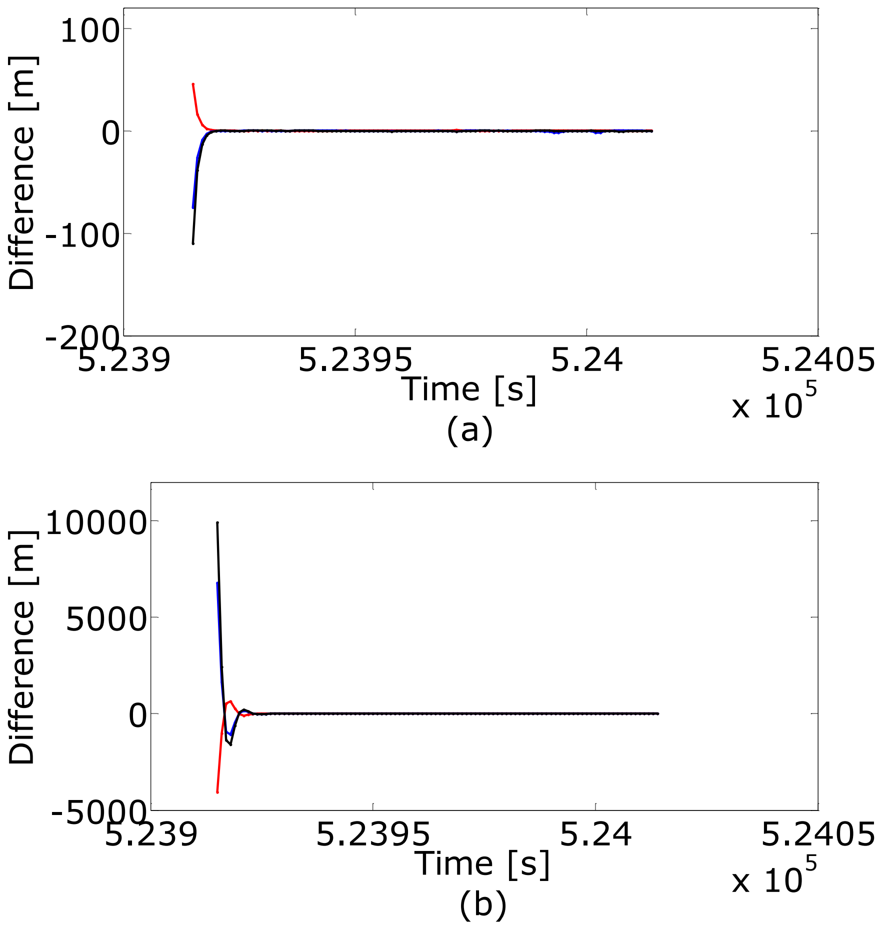

Figure 4.18 Converge time of UKF (a) and EKF (b)

With the zero value of the initial state, the UKF converges faster than the EKF. However, both have no resistance to measurement outliers (i.e. multipath effect). The test results of the above three cases again confirmed that the UKF outperforms the EKF in terms of accuracy and consistency of positioning and velocity.

4.5 Summary

In this Chapter, the theoretical framework of Kalman filtering was established based on the correlational inference and the statistical relationship between the UKF and standard Kalman filter was obtained by the inference. The performance of the UKF and EKF were tested using both simulation and field tests with different feedback modes. From the derivation of the Taylor expansions, the UKF could achieve at least the second-order accuracy; while the EKF propagates the mean and covariance of the state estimate by the first order expansion. In the tests, the vehicle state vector is estimated from the UKF and EKF and different state space models were adopted. The behaviour of the filters combined with different feedback modes and integration strategies were tested. The first test simulated the vehicle trajectory in the open-loop model. The nonlinear equations act as the system model directly in the UKF, while the EKF calculates the Jacobian matrix to linearize the equation. The RMSE of UKF for the X component is 0.98 meter and 0.54 meter for the Y component with respect to the simulated true position. EKF achieved 2.19 meter and 2.51 meter RMSE for the respective X and Y components. The second test was a field test, in which the IMU and GPS were integrated in the closed loop mode, and the error model was used as the system dynamic model. The model moderated the nonlinearity of the equations. The third test used a linear CV model as the system dynamic model, and the tightly coupled strategy was adopted to estimate the position and velocity. The measurement model is nonlinear. The RMSE of UKF for the X, Y and Z components are 0.10 meter, 0.12 meter, and 0.14 meter; while the RMSE of those of EKF are 0.22 meter, 0.27 meter, and 0.42 meter. The performances of the UKF and EKF from all the three tests are acceptable. The UKF performed better in terms of accuracy and consistency, especially with nonlinear equations.

Chapter 5 Correlational Inference-based Adaptive Estimation

The superiority of the UKF to nonlinear state estimation was presented in Chapter 4. The estimation accuracy of the UKF is affected by the level of knowledge of the stochastic model. In the GNSS/IMU integrated navigation, the knowledge of measurement model noise is obtained by the GNSS positioning solution, while the process noise as priori information is time-varying. Additionally, the uncertainty of the dynamic model disturbances can distort the process noise information. Incorrect noise information degrades the filter performance and can even lead to diverge of the estimation. In this study, an AUKF based on correlational inference was developed for addressing the dynamic system disturbance influences, and an adaptive factor was introduced for the AUKF to adjust the contribution of the dynamic model and the measurement model.

5.1 Adaptive Unscented Kalman Filtering Based on Correlational Inference

5.1.1 Adaptive Unscented Kalman Filter

The UKF described in Chapter 2 depends on the approximation method for nonlinear system models. The approximation method is very difficult to accurately predict the distribution or the dynamic errors. Additionally, the inaccurate estimation of the last epoch will affect the selection of the sigma points at the present epoch. Thus, the state prediction vector $\bar{X}_k$ is influenced, in the same way as the predicted measurement vector $\bar{y}_k$ from eq. (4.3). To control the influence of the dynamic model disturbances, an adaptive factor α_k $(0 < \alpha_k < 1)$ is introduced. The adaptive UKF estimator can be obtained based on the correlational inference. The predicted state vector is assumed to be contaminated by some kinematic disturbance phenomenon; the contribution of $\bar{X}_k$ therefore should be weakened. Thus, eq. (4.11) can be rewritten with the adaptive factor α_k, similar to Yang et al. (2001a),

$$V_k^T \Sigma_k^{-1} V_k + \begin{bmatrix} V_{\bar{y}_k}^T & V_{\bar{X}_k}^T \end{bmatrix} \cdot \alpha_k \cdot \begin{bmatrix} \Sigma_{y_k}^* & \Sigma_{\bar{y}_k \bar{X}_k} \\ \Sigma_{\bar{X}_k \bar{y}_k} & \Sigma_{\bar{X}_k} \end{bmatrix}^{-1} \begin{bmatrix} V_{\bar{y}_k} \\ V_{\bar{X}_k} \end{bmatrix} - 2\lambda^T \left(V_{\bar{y}_k} - \bar{V}_k - V_k \right) = min \qquad (5.1)$$

and eq. (4.14) is updated as,

$$\begin{aligned} V_{\bar{y}_k} &= \frac{1}{\alpha_k} \Sigma_{y_k}^* \lambda \\ V_{\bar{X}_k} &= \frac{1}{\alpha_k} \Sigma_{\bar{X}_k \bar{y}_k} \lambda \end{aligned} \qquad (5.2)$$

The adaptive UKF estimator is (Yang, et al., 2001b; Yang & Gao, 2005, 2006),

$$\begin{aligned} \hat{X}_{AK} &= \bar{X}_k + \frac{1}{\alpha_k} \Sigma_{\bar{X}_k \bar{y}_k} \left(\frac{1}{\alpha_k} \Sigma_{y_k}^* + \Sigma_k \right)^{-1} (\mathrm{y}_k - \bar{y}_k) \\ &= \bar{X}_k + \Sigma_{\bar{X}_k \bar{y}_k} \left(\Sigma_{y_k}^* + \alpha_k \Sigma_k \right)^{-1} (y_k - \bar{y}_k) \end{aligned} \qquad (5.3)$$

This equation can also be expressed as,

$$\hat{X}_k = \bar{X}_k + \widetilde{K}_k (y_k - \bar{y}_k) \qquad (5.4)$$

where $\widetilde{K}_k$ is the adaptive Kalman gain matrix, which is expressed as,

$$\widetilde{K}_k = \Sigma_{\bar{X}_k \bar{y}_k} \tilde{\Sigma}_{\bar{V}_k}^{-1} \quad (5.5)$$

and,

$$\tilde{\Sigma}_{\bar{V}_k} = \sum_{i=0}^{2n} w_i [(\tilde{y}_k)_i - \bar{y}_k] [(\tilde{y}_k)_i - \bar{y}_k]^T + \alpha_k \Sigma_k \quad (5.6)$$

where $\tilde{\Sigma}_{\bar{V}_k}$ is the innovation covariance matrix of the adaptive estimation.

The larger the errors of $\bar{X}_k$ generated from the sigma points, the larger the covariance matrices, $\Sigma_{\bar{X}_k \bar{y}_k}$ and $\Sigma_{\bar{V}_k}$. Thus, the adaptive factor α_k plays a valuable role in weakening the contribution of disturbed or contaminated predicted state vector $\bar{X}_k$, or strengthens the contribution of the measurement vector y_k.

The adaptive factor can be constructed as (Yang & Gao, 2006),

$$\alpha_k = \begin{cases} 1 & tr\left(\hat{\Sigma}_{\bar{X}_k}\right) < tr\left(\Sigma_{\bar{X}_k}\right) \\ \frac{\sum_{i=1}^{n} \sigma_{\bar{X}_{k_i}}^2}{\sum_{i=1}^{n} \Delta \bar{X}_{k_i}^2} & otherwise \end{cases} \quad (5.7)$$

where, $\Delta\bar{X}_k$ marks the discrepancy between the predicted state and the estimated state; and

$$\Delta\bar{X}_k = \tilde{X}_k - \bar{X}_k \quad (5.8)$$

$$tr\left(\hat{\Sigma}_{\bar{X}_k}\right) \approx tr(\Delta\bar{X}_k \Delta\bar{X}_k^T) = \Delta\bar{X}_k^T \Delta\bar{X}_k = \sum_{i=1}^{n} \Delta\bar{X}_{k_i}^2 \quad (5.9)$$

where $\tilde{X}_k$ is the estimate from the measurement information at the present epoch. The estimate can be derived from the linearized measurement model by the robust least squares method (Yang et al., 2002),

$$V_k = H_k\hat{X}_k - y_k \tag{5.10}$$

where H_k is the Jacobian matrix of h_k, which is the nonlinear design matrix, the state robust estimate from the measurements is then,

$$\tilde{X}_k = (H_k^T \bar{P}_k H_k)^{-1} H_k^T \bar{P}_k y_k \tag{5.11}$$

where $\bar{P}_k$ denotes the equivalent weight matrix of y_k, the latter is determined by the robust estimation principle.

The robust state is estimated by the linearized measurement model, by which the calculation burden of the estimation with a nonlinear state space model is increased. Thus, another adaptive factor was given by (Yang & Gao, 2006),

$$\alpha_k = \begin{cases} 1 & tr\left(\hat{\Sigma}_{\bar{V}_k}\right) < tr\left(\Sigma_{\bar{V}_k}\right) \\ \frac{\sum_{i=1}^{n_k} \sigma_{\bar{V}_{k_i}}^2}{\sum_{i=1}^{n_k} \bar{V}_{k_i}^2} & otherwise \end{cases} \tag{5.12}$$

where n_k represents the number of the measurements; $\hat{\Sigma}_{\bar{V}_k}$ is the estimated covariance matrix of the predicted residual vector $\bar{V}_k$, which can be calculated by either the windowing method, eq. (5.13) or the predicted residual vector at the present epoch, eq. (5.14); $\Sigma_{\bar{V}_k}$ is the covariance matrix of the innovation vector and can be obtained by eq. (4.33) by means of the linearized measurement model or unscented transformation of the nonlinear equation. The above two approaches lead to the same result as the vector solution is a linear equation.

$$\hat{\Sigma}_{\bar{V}_k} = \frac{1}{m-1}\sum_{i=1}^{m}\bar{V}_{k-i}\bar{V}_{k-i}^{T} \tag{5.13}$$

$$\hat{\Sigma}_{\bar{V}_k} = \bar{V}_k\bar{V}_k^{T} \tag{5.14}$$

where m is the length of the window; and $\sigma_{\bar{V}_{k_i}}^2$ in eq. (5.12) can be calculated as,

$$\sigma_{\bar{V}_{k_i}}^2 = \sigma_{\bar{y}_{k_i}^*}^2 + \sigma_{k_i}^2 \tag{5.15}$$

where $\sigma_{\bar{V}_{k_i}}^2$, $\sigma_{\bar{y}_{k_i}^*}^2$ and $\sigma_{k_i}^2$ are the ith diagonal element of $\Sigma_{\bar{V}_k}$, $\Sigma_{\bar{y}_k}$ and Σ_k respectively. When the discrepancy between the predicted measurement and the measurement is large, the value of α_k is less than 1. Therefore, the contribution of the predicted state to the estimation results from the unscented transform is weakened.

5.1.2 Discussions

Window-based adaptive estimation methods have been proposed in several studies (Gao et al., 2015; Hajiyev & Soken, 2014). The core of the approaches is the matching of calculated covariance matrices with the theoretical ones. The latter are derived by windowing approximation. Hajiyev and Soken (2014) employed an adaptive matrix to scale the covariance matrix of measurement noise and an adaptive factor to adjust the covariance matrix of process noise. The adaptive matrix is estimated based on the covariance matching principle, i.e. the calculated covariance matrix $\Sigma_{\bar{y}_k}$ is equal to the theoretical covariance matrix $\hat{\Sigma}_{\bar{y}_k}$. The theoretical covariance matrix $\hat{\Sigma}_{\bar{y}_k}$ is obtained by innovation sequences. The adaptive factor can also be estimated with residual sequences via the window approach. The calculation of the adaptive matrix involves matrix inversion. The adaptive factor is then calculated by the trace of the covariance matrices. In the window-based adaptive estimation approach proposed by Gao et al. (2015), historical innovation sequences or residual sequences were also used to calculate the theoretical covariance matrix for the adjustment of the covariance matrices of the measurement or process noise. The theoretical covariance matrix is calculated based on the randomly weighted historical information rather than the simple moving average.

The adaptive factor was constructed by exploiting the relationships among the covariance matrices revealed in the correlational inference. The inference established the theoretical equivalence between the UKF and Kalman filter. Unlike the window-based adaptive scheme, the proposed adaptive scheme is designed to weaken the contribution of the priori information based on the disturbances of the system, whereas, the window based adaptive schemes balance the noise information of the dynamic or measurement model. The adaptive estimator, which does not need any functional model linearization, was analytically derived, based on the relationships between the covariance matrices of the innovation vector and the predicted state vector. The adaptive factor is obtained by the innovation vector at the present epoch, which avoids the need to store the historical information. Additionally, the adaptive mechanism is sensitive to the discrepancy of the filter at the give epoch.

5.2 Numerical Experiment and Analysis

Both simulation and field tests were also conducted for the performance assessment of the AUKF applied to an integrated GNSS/IMU navigation system, and a comparison between AUKF and UKF was also conducted. The integrated system used a nonlinear IMU error model as the dynamic model. This is different from the classical linear IMU error model which is derived under the assumption of small misalignment angles. In reality, the environmental disturbances and sensors errors may not satisfy this assumption thus the nonlinear error model presented in Chapter 3 was used in this study. The loosely coupled configuration was employed in the integration of the IMU and GPS. Data were processed in the Matlab R2010a 64-bit program on a PC with Intel Core i7-3770 CPU at 3.40 GHz, 16-GB RAM equipped with Win 7.

5.2.1 Simulation Result

The simulation was based on the moving vehicle with different driving behaviors. The simulation duration is 3000s. The configuration of the simulation is shown in Table 5.1. The simulation was processed without any initial alignment.

Table 5.1 Simulation settings and initial conditions

gyro constant drift	100°/h
angular random walk	5°/√h
velocity random walk	1000 ηg/√Hz
accelerometer bias	2000 ηg
Initial position	[22.31° 114.18° 41 m]
Initial positioning error	[1 m 1 m 3 m]
Initial velocity error	[0.2 m/s 0.2 m/s 0.2 m/s]
Initial Misalignment angle	[-20° 34° 80°]

The estimated results are compared with the simulated value (the reference) as shown in Figure 5.1 for the positioning error. The red dotted line indicates the AUKF estimate error, and the blue dotted line represents the UKF estimate error. It can be observed that the UKF estimate is affected by the dynamic model error. The overall RMSE of the UKF estimate in the East, North, and Altitude components are 1.94 m, 2.45 m, and 26.14 m respectively; while that of AUKF are 1.04 m, 0.98 m, and 1.61 m. In addition, the largest error of UKF for the East, North, and Altitude components are 12.87 m, 19.12 m and 75.94 m, respectively; while those estimated by the AUKF are 3.70 m, 5.01 m, and 7.93 m. It is also found that the UKF estimate in the altitude component has a bias, caused by both measurement noise and disturbed predicted information. The

AUKF reduced the weight of the predicted information by an adaptive factor, driving the estimate to the measurements.

The velocity errors of the two filters are illustrated in Figure 5.2. The errors presented a similar pattern to that of the positioning error. The oscillations of the AUKF estimates are much smaller than that of the UKF, and the velocity estimate in the altitude direction is divergent. This can be explained below: The predicted information of the filter is disturbed by the IMU sensor error, hence causing a biased UKF estimate. The AUKF, however, used an adaptive factor to weaken the predicted information which weakens the bias. The result illustrates that the AUKF has outperformed the UKF under the disturbances of the dynamic model, which is presented in Table 5.2.

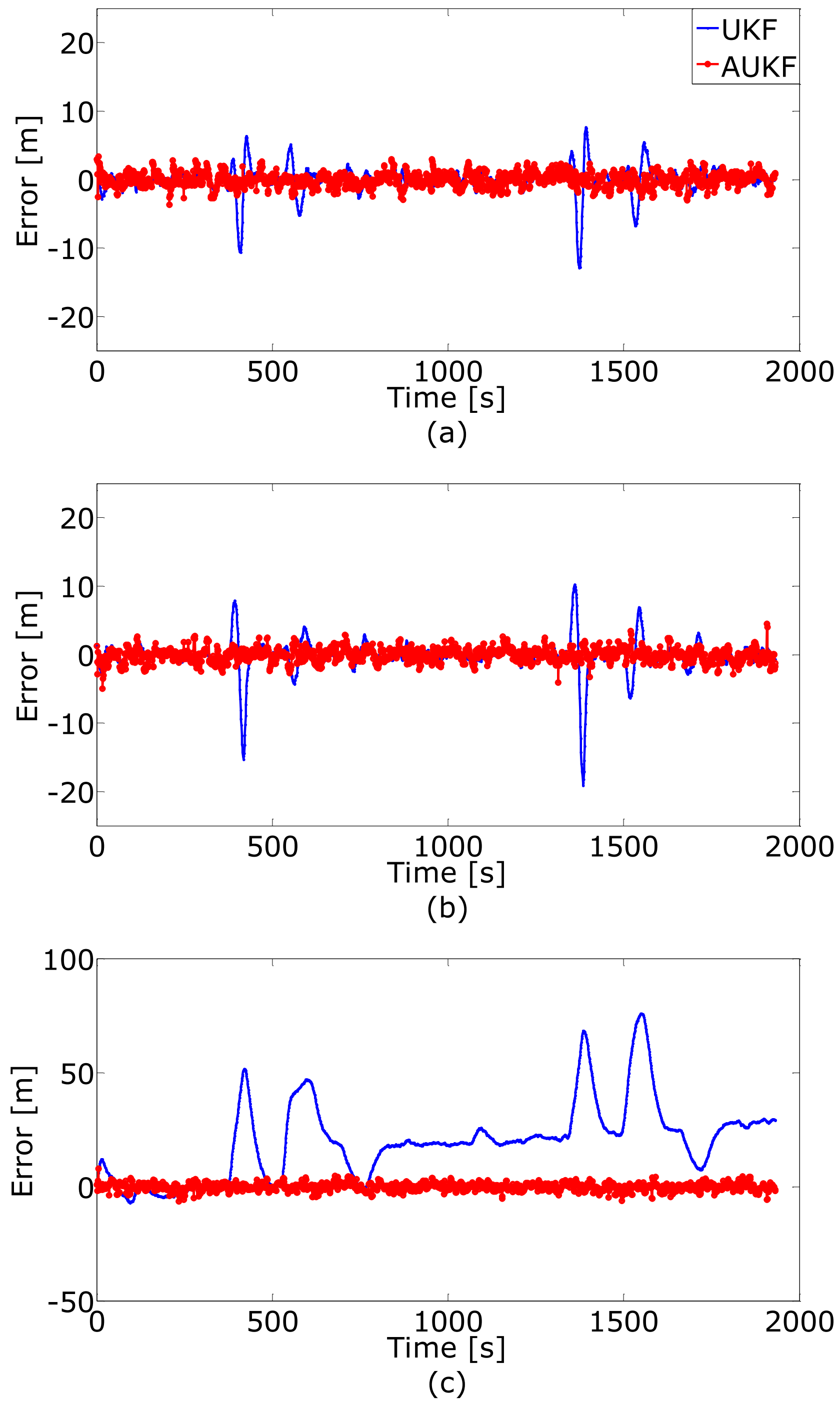

Figure 5.1 Position error of two filters in East (a), North (b), and Altitude (c)

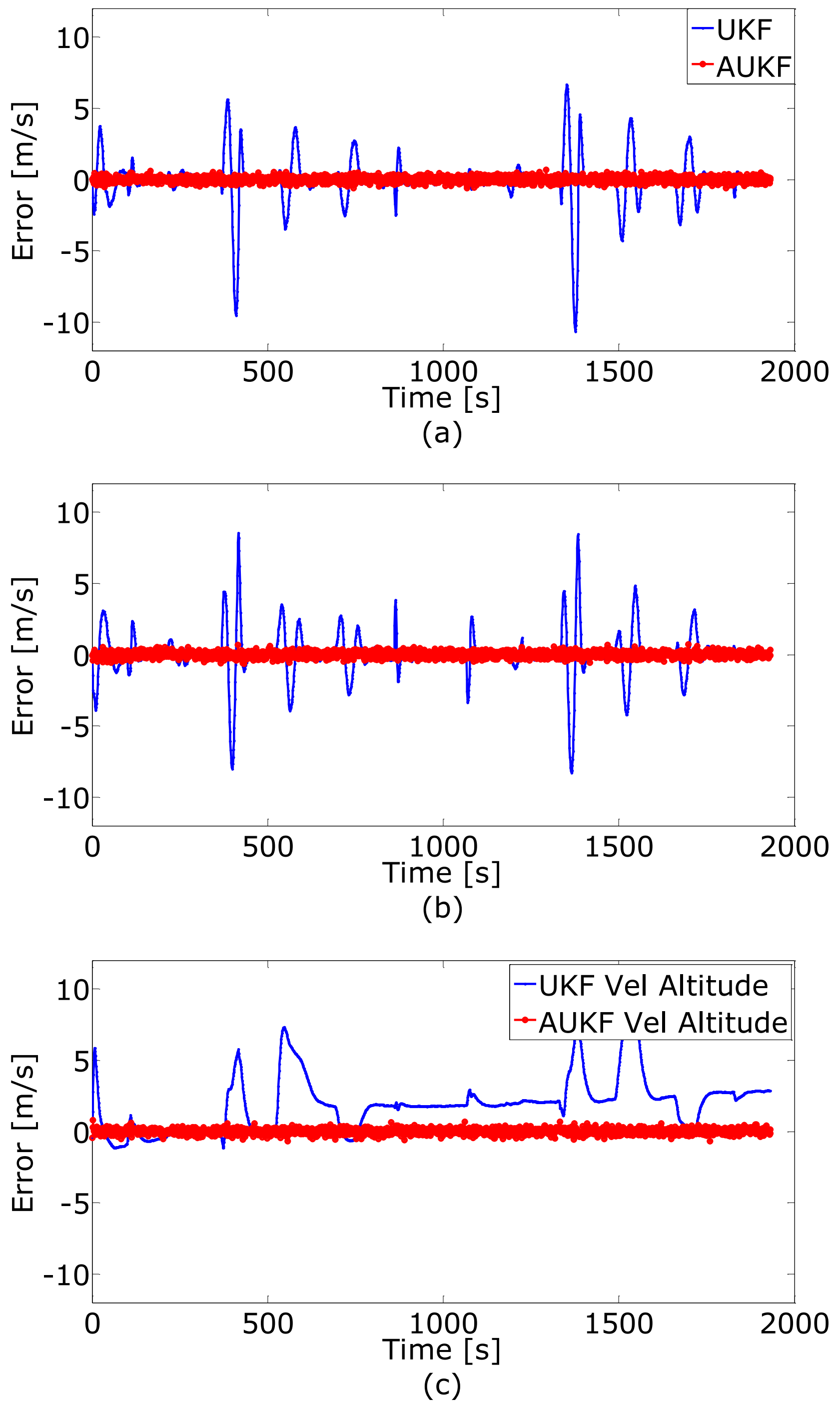

Figure 5.2 Velocity error of two filters in East (a), North (b), and altitude (c)

Table 5.2 RMSE of two filter solutions

		UKF	AUKF
Position [m]	East	1.94	1.04
	North	2.45	0.98
	Altitude	26.14	1.61
Velocity [m/s]	East	1.64	0.19
	North	1.60	0.20
	Altitude	2.73	0.19

5.2.2 Field Test Results

This experiment and analysis subsection presents experimental results to demonstrate the performance of positioning solution. The proposed adaptive filter applied to IMU/GPS integrated vehicle navigation was tested in field for a period lasting approximately one and half an hour. The IMU and GPS parameters and initial c

onditions are listed in Table 5.3.

Table 5.3 IMU and GPS parameters and initial conditions

IMU Sampling Frequency	100 Hz
GPS Sampling Frequency	10 Hz
IMU Accelerometer bias	500 μg
IMU gyro bias	1 deg/h
Initial Position Error	[7 m, 7 m 7 m]
Initial Velocity Error	[0.1 m/s 0.1 m/s 0.1 m/s]
Initial Attitude Error	[10° 20° -15°]

The estimation results were compared with the robust SPP solution which is used as the reference. From the position errors shown in Figure 5.3, it can be seen that the position estimated from the AUKF is much closer to the GPS measured position The AUKF constrained the errors at the East component during the process period. The peak value of the UKF estimate error during the time period between 283980 s and 284070 s is 2.66 m, while that of the AUKF is 1.30 m. The error UKF estimate errors in the altitude direction fluctuate in the range between -40 m and 58 m during the process time, while that of the AUKF vary between -22 m and 17 m. This means a large improvement is achieved by the AUKF. The remaining oscillation around epoch 283300 s to 283600 s and 283900 s to 284200 s are caused by poor GPS measurements.

From the velocity errors shown in Figure 5.4, one can see that the UKF has no resistance to outliers in the dynamic model and that the AUKF retrains the error of the velocity. It is also noticed that the AUKF converges faster than the UKF.

Since the UKF operates under the Kalman framework and employs the unscented transform to deal with the nonlinear equations, the disturbances in the dynamic model may bias the predicted information. The AUKF dynamically adjusts the statistics of the measurements during the filtering process so that the contribution of the inaccurate prior information can be reduced. Therefore, the AUKF can effectively resist the disturbances of the dynamic model, leading to much higher accuracy than that the standard UKF. Table 5.4 illustrates the RMSE of the position and velocity errors, which indicate that the AUKF is superior to UKF.

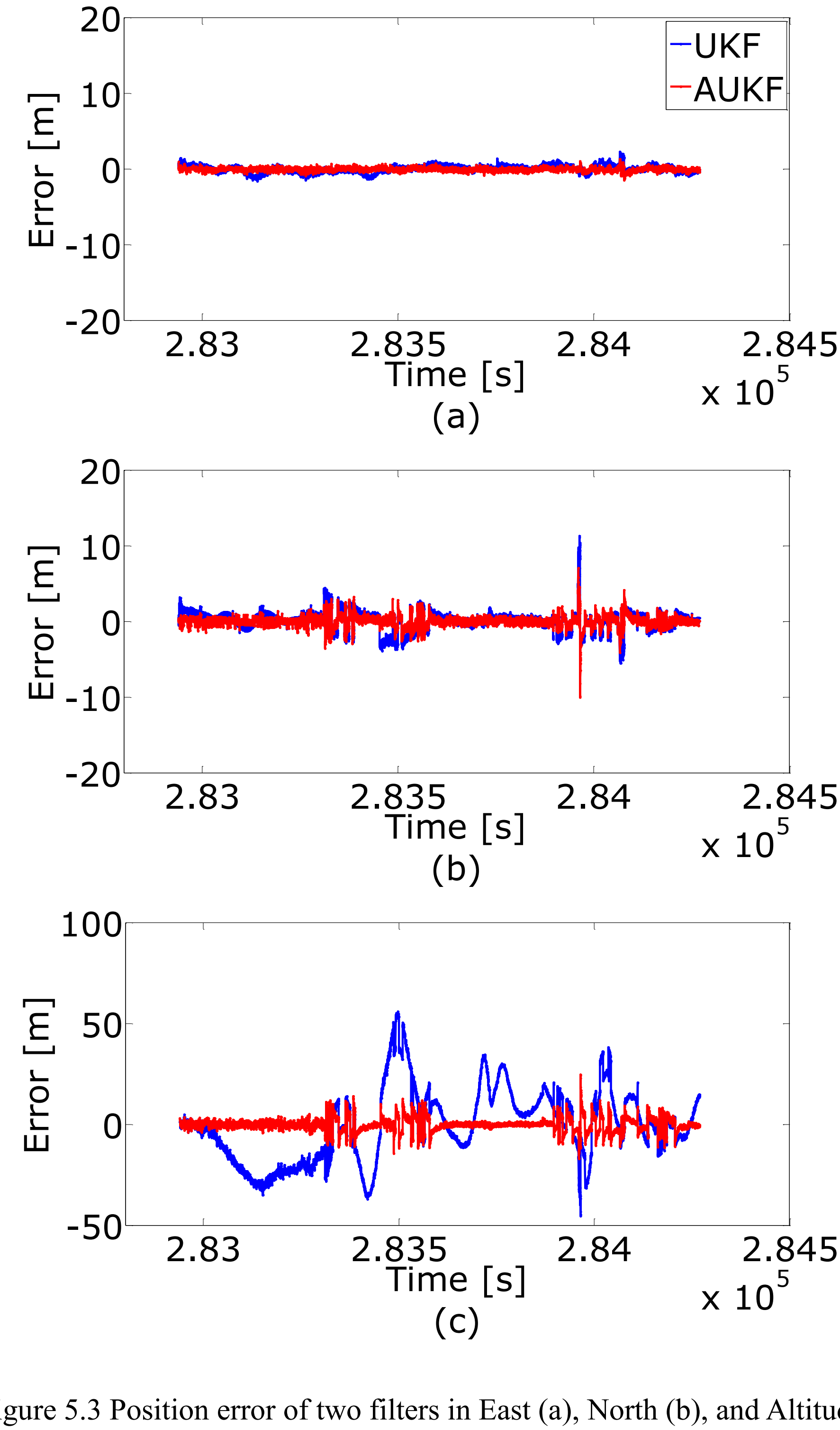

Figure 5.3 Position error of two filters in East (a), North (b), and Altitude (c)

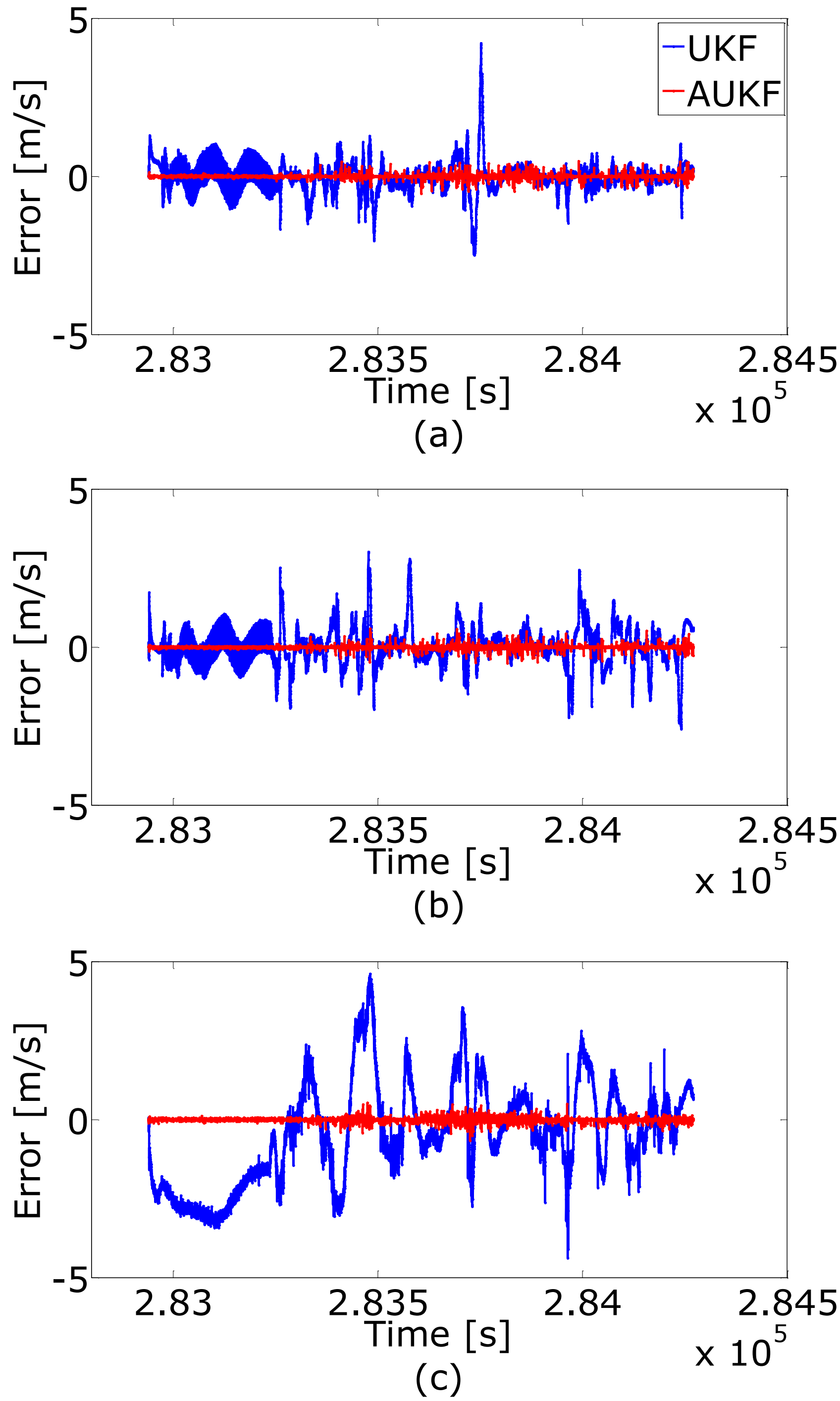

Figure 5.4 Velocity error in East (a), North (b), and altitude (c)

Table 5.4 RMSE of two filter solutions

		UKF	AUKF
Position [m]	East	0.49	0.24
	North	1.30	0.72
	Altitude	18.24	3.23
Velocity [m/s]	East	0.50	0.04
	North	0.61	0.04
	Altitude	1.66	0.05

5.3 Summary

In this Chapter, an adaptive Unscented Kalman filter (AUKF) based on the correlational inference was proposed and its performance was tested. The adaptive mechanism improves the performance of the filter in dealing with contaminated predicted state and nonlinear models. The adaptive factor is obtained from the innovation vector at the present epoch, which avoids the storage of innovation sequences and is more sensitive to the discrepancy of the predicted system state from the measurements. In both simulation and the field tests, the loosely coupled configuration and nonlinear dynamic model were used and results showed that the AUKF outperformed the UKF in terms of velocity and positioning accuracy. In the simulation, the UKF RMSE in East, North, and Altitude components estimation are 1.94 meter, 2.45 meter, and 26.14 meter correspondingly; while the RMSE of those of AUKF are 1.04

meter, 0.98 meter, and 1.61 meter. In the field test, the UKF RMSE in positioning estimation are 0.49 meter, 1.30 meter, and 18.24 meter; while the RMSE of those of AUKF are 0.24 meter, 0.72 meter, and 3.23 meter.

Chapter 6 Robust M-M Unscented Kalman Filter

The adaptive estimator described in Chapter 5 rebalances the contribution of the dynamic model and the measurements, and hence effectively improves the performance of the filter. The estimator, however, relies on the robustness of the measurements. It also rescales the covariance matrix of the dynamic model in terms of the system discrepancy, namely, innovation vector. The accuracy of the estimator, however, degrades if the measurements contain outliers. The robust M-M estimator presented in this chapter is to obtain more accurate estimate from both contaminated dynamic predictions and measurement.

6.1 M-M Estimation

Yang (1991) introduced three robust estimators based on the M-estimation technique for measurements in the following three cases 1) the measurements follow the contaminated normal distribution (M-LS), 2) The prior estimate has outliers (LS-M), and 3) both measurements and prior estimate follow the contaminated normal distribution (M-M). This section reviews the methodology of the three estimators.

Let the linear measurement equation be,

$$y = HX + \Delta \tag{6.1}$$

where y is the $n \times 1$ measurement vector; H is the $n \times m$ design matrix; Δ is the $n \times 1$ error vector; and X is the $m \times 1$ state vector with prior estimated $\bar{X}$ and covariance matrix $\Sigma_{\bar{X}}$.

The error equation of the measurement is,

$$V = A\hat{X} - y \tag{6.2}$$

where V is the $n \times 1$ residual vector and $\hat{X}$ is the estimated state of X.

If the predicted residuals, $\Delta\bar{X} = \bar{X} - X$, and the measurements are independent and identically distributed with Gaussian distribution, the risk function based on the least squares (LS) Bayesian estimation is,

$$\Omega = V^T \Sigma_\Delta V + \left(\bar{X} - \hat{X}\right)^T \Sigma_{\bar{X}}^{-1} \left(\bar{X} - \hat{X}\right) \tag{6.3}$$

where Σ_Δ is the measurements covariance matrix.

Assuming that the measurement y is contaminated by outliers and the contaminated distribution is,

$$F_\Delta(\varepsilon) = (1 - \varepsilon)\phi_\Delta + \varepsilon M \tag{6.4}$$

where $0 < \varepsilon < 1$, M is any symmetric distribution, and ϕ_Δ is the norm distribution.

Applying the M-estimation, the risk function becomes,

$$\Omega_y = \sum_{i=1}^{n} \rho(v_i) + \left(\bar{X} - \hat{X}\right)^T \Sigma_{\bar{X}}^{-1} \left(\bar{X} - \hat{X}\right)/2 \tag{6.5}$$

where v_i is the ith row of the measurement residual; $\rho(\cdot)$ is the robust score function used to cut off the outliers and the contaminated Gaussian noise. The Huber's score function can be applied to suppress the influence of the outliers,

$$\rho(v_i) = \begin{cases} \frac{v_i^2}{2} & |v_i| < \tau \\ \tau|v_i| - \frac{\tau^2}{2} & |v_i| \geq \tau \end{cases} \tag{6.6}$$

where τ is chosen to give a desired efficiency at the Gaussian model (Kovacevic et al., 1992).

The estimator is then,

$$\hat{X} = \bar{X} - \Sigma_{\bar{X}} H^T [\Psi(V)] \tag{6.7}$$

Define $p(v_i) = \psi(v_i)/v_i$, eq. (6.7) is then rewritten as,

$$\hat{X} = \bar{X} - \Sigma_{\bar{X}} H^T P(V) V \tag{6.8}$$

where $P(V)$ is usually a diagonal matrix with the elements $p(v_i)$.

Considering another case, in which the predicted state $\bar{X}$ follows a contaminated normal distribution. The model is defined by

$$F_{\Delta\bar{X}}(\varepsilon_x) = (1 - \varepsilon_x)\phi_x + \varepsilon_x M \tag{6.9}$$

where ϕ_x is a normal distribution.

The risk function with M-estimation is,

$$\Omega_{\bar{X}} = \frac{V^T \Sigma_\Delta V}{2} + \sum_{j=1}^{m} \beta(\delta\tilde{x}_j) \tag{6.10}$$

where $\delta\tilde{x}_j = \sum_{j=1}^{m} \left(\Sigma_{\bar{X}}^{-\frac{1}{2}}\right)_{jk} (\delta\hat{x}_k)$, $\delta\hat{x}_k = \hat{X}_k - \bar{X}_k$; and $\beta(\cdot)$ functions are similar to as $\rho(\cdot)$.

The estimator determined by the condition (6.10) is known as the LS-M estimators.

The estimated state is then,

$$\hat{X}_k = \left(H^T \Sigma_\Delta^{-1} H + P\left(\delta\hat{X}_k\right)\right)^{-1} \left(H^T \Sigma_\Delta^{-1} y + P\left(\delta\hat{X}_k\right)\bar{X}_k\right) \tag{6.11}$$

where $P\left(\delta\hat{X}_k\right)$ is also a diagonal matrix with elements $p(\delta\hat{x}_i) = \eta(\delta\hat{x}_i)/\delta\hat{x}_i$, and $\eta(\cdot)$ is similar to the $\psi(\cdot)$ function.

If both the measurement vector y and the prior estimate vector $\bar{X}$ are contaminated, two score functions of M-estimates can be used. This function is,

$$\Omega = \sum_{i=1}^{n} \rho(v_i) + \sum_{j=1}^{m} \beta\left(\delta\tilde{x}_j\right) \tag{6.12}$$

The estimator determined by the condition function (6.12) known as the M-M estimator, as the M-estimation principle is applied for both the measurement and the predicted state vectors. The robust estimator is expressed as,

$$\hat{X}_k = \left(H^T P(V) H + P\left(\delta\hat{X}_k\right)\right)^{-1} \left(H^T P(V) y + P\left(\delta\hat{X}_k\right)\bar{X}_k\right) \tag{6.13}$$

which is the combination of the LS-M and M-LS estimators. It also can be written as follows (Koch, 1999; Yang, et al., 2001a),

$$\hat{X}_k = \bar{X}_k + \bar{\Sigma}_{\bar{X}} H_k^T (H_k \bar{\Sigma}_{\bar{X}} H_k^T + \bar{\Sigma}_\Delta)^{-1} (y_k - \bar{y}_k) \tag{6.14}$$

where $\bar{\Sigma}_{\bar{X}} = \left(P\left(\delta\hat{X}_k\right)\right)^{-1}$ and $\bar{\Sigma}_\Delta = \left(P(V)\right)^{-1}$ are the equivalent covariance matrices of the predicted state and measurement vectors.

6.2 Robust M-M Unscented Kalman Filter

The above M-M estimator is related only to the measurement and predicted state vectors' residuals rather than the state space model. The outliers of the dynamic model and the measurements are down weighted by their iterated residuals with the robust equivalent covariance matrices of both predicted state vector and measurement noise vector. Thus, the RMUKF can be derived by embedding the formulated robust covariance, which iteratively suppresses the effects of the outliers in both dynamic model and measurements. Considering the estimated state vector from a nonlinear state space model by the UKF expressed in eqs. (2.15) to (2.29) presented in Chapter 2, the residual vectors of the measurement and predicted state can be obtained using the estimated state vector below,

$$\hat{y}_k = h(\hat{X}_k) \tag{6.15}$$

$$V_k = \hat{y}_k - y_k \tag{6.16}$$

$$V_{\bar{X}_k} = \hat{X}_k - \bar{X}_k \tag{6.17}$$

where $\hat{y}_k$ is the estimated measurement.

Based on the M-estimation principle, the risk function is,

$$V_{\bar{X}_k}^T \bar{P}_{\bar{X}_k} V_{\bar{X}_k} + V_k^T \bar{P}_k V_k = min \tag{6.18}$$

where $\bar{P}_{\bar{X}_k}$ and $\bar{P}_k$ are the robust equivalent weight matrices of the respective predicted state and measurement vectors;

An alternative expression of the risk function can be expressed as,

$$V_{\bar{X}_k}^T \bar{\Sigma}_{\bar{X}_k}^{-1} V_{\bar{X}_k} + V_k^T \bar{\Sigma}_k^{-1} V_k = min \tag{6.19}$$

where $\bar{\Sigma}_{\bar{X}_k}$ and $\bar{\Sigma}_k$ are the equivalent covariance matrices of $\bar{X}_k$ and y_k respectively, with such elements as,

$$\begin{aligned} \bar{\sigma}_i^2 &= \lambda_{ii}\sigma_i^2 \quad \lambda_{ii} \geq 1 \\ \bar{\sigma}_j^2 &= \lambda_{jj}\sigma_j^2 \quad \lambda_{jj} \geq 1 \\ \bar{\sigma}_{ij} &= \lambda_{ij}\sigma_{ij} \end{aligned} \tag{6.19a}$$

where λ_{ii} and λ_{jj} denote the shrink factors, $\lambda_{ij} = \sqrt{\lambda_{ii}\lambda_{jj}}$; $\bar{\sigma}_i^2$, $\bar{\sigma}_j^2$, as well as $\bar{\sigma}_{ij}$ are equivalent variances and covariance elements.

The new covariance matrix has thus kept the original correlations unchanged,

$$\bar{\Sigma} = \begin{bmatrix} \bar{\sigma}_{11}^2 & \cdots & \bar{\sigma}_{1n}^2 \\ \vdots & \ddots & \vdots \\ \bar{\sigma}_{n1}^2 & \cdots & \bar{\sigma}_{nn}^2 \end{bmatrix} = \begin{bmatrix} \lambda_{11}\sigma_{11}^2 & \cdots & \lambda_{1n}\sigma_{1n}^2 \\ \vdots & \ddots & \vdots \\ \lambda_{n1}\sigma_{n1}^2 & \cdots & \lambda_{nn}\sigma_{nn}^2 \end{bmatrix} \tag{6.19b}$$

It should be noted that the measurements are independent within the loosely coupled integration; the predicted state elements, however, are correlated. The traditional method normalizes the error equation, which not only requires additional calculation, but also transforms or masks the errors, and may result in conversion of the outliers to measurements or state elements. This conversion would lead to improper weighting for the measurements. To handle the correlated predicted information, a bi-factor reduction model is employed to evaluate the weight matrix of the state: a matrix is similar to that used in correlated observations presented in (Yang et al., 2002).

If both the predicted state and measurement vectors are assumed to be contaminated by outliers, the equivalent weight matrices of the measurements and the predicted state vector can be constructed as,

$$\bar{p}_{ij} = \gamma_{ij} p_{ij} \tag{6.20}$$

$$\bar{p}_{\bar{x}_{ij}} = \gamma_{ij} p_{\bar{x}_{ij}} \tag{6.30}$$

where $\bar{p}_{ij}$ and $\bar{p}_{\bar{x}_{ij}}$ are the elements of the respective weight matrix $\bar{P}_k$ and $\bar{P}_{\bar{X}_k}$; p_{ij} and $p_{\bar{x}_{ij}}$ are the $ijth$ elements of the measurement and predicted state vectors,

$$P_k = \Sigma_k^{-1} \tag{6.31}$$

$$P_{\bar{X}_k} = \Sigma_{\bar{X}_k}^{-1} \tag{6.32}$$

and γ_{ij} is the reduction factor of the weight elements,

$$\gamma_{ij} = \sqrt{\gamma_{ii} \gamma_{jj}} \tag{6.33}$$

γ_{ii} and γ_{jj} are two reduction factors of the weight elements, the so-called bi-factor, and the values for which can be,

$$\gamma_{ii} = \begin{cases} 1 & |\tilde{v}_i| \le c \\ \frac{|\tilde{v}_i|}{c} & |\tilde{v}_i| > c \end{cases} \tag{6.34}$$

where c is a constant, and a value in 1.0-1.5 is usually chosen ; $\tilde{v}_i$ is the standardized residual with,

$$\tilde{v}_i = \text{median}|V|/0.6745 \tag{6.35}$$

where V is the residual vector of the measurement or the predicted state; and the constant 1/0.6745 is a correction factor for Fisher consistency at the Gaussian distribution (Fakharian et al., 2011).

The equivalent weight matrix of the measurement is then in the form of,

$$\bar{P} = \begin{bmatrix} \gamma_{11} & \cdots & \gamma_{1n} \\ \vdots & \ddots & \vdots \\ \gamma_{n1} & \cdots & \gamma_{nn} \end{bmatrix} \cdot P \tag{6.36}$$

The equivalent weight matrix of the predicted state vector can be obtained in the same form as eq. (6.36). Thus, the robust covariance matrix of the predicted state vector $\bar{\Sigma}_{\bar{X}_k}$ and covariance matrix $\bar{\Sigma}_k$ of the measurement vector are obtained,

$$\bar{\Sigma}_{\bar{X}_k} = P_{\bar{X}_k}^{-1} \tag{6.37}$$

$$\bar{\Sigma}_k = \bar{P}_k^{-1} \tag{6.38}$$

The robust estimates of the state vector and its covariance matrix then can be derived via eqs. (2.27) and (2.28), while the iterations can effectively suppress the influences of the outliers to the state estimate.

It can be found from the above derivation that the robust estimation process requires iteration at each estimation epoch. The estimated state vector at the first iteration acts as the reference for calculating the measurement residuals and predicted state residuals, based on which the robust equivalent weight matrices for M-M estimation are obtained. Figure 6.1 presents the estimate procedure of the RMUKF method.

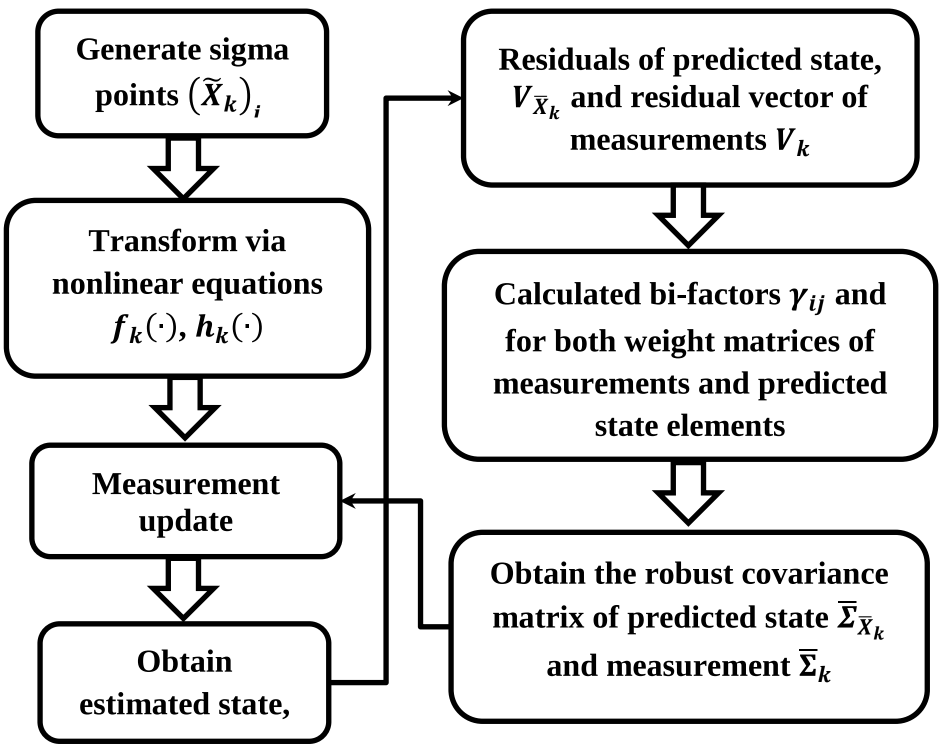

Figure 6.1 Flow chart for the RMUKF procedure

To summarize, the following characteristics can be stated,

(i) The M-M estimation technique is not limited to linear models. It can be also applied to nonlinear models with unscented transform.

(ii) The RMUKF can effectively attenuate the disturbances of the dynamic model and measurement outliers by an iteration procedure.

(iii) The algorithm can be modified into an adaptive algorithm by adding an adaptive factor to the covariance matrix of the innovation vector if the measurement error is normal distributed. The equivalent weight matrix of the innovation vector can decrease the contribution of the dynamic model to the estimated state vector based on system discrepancy.

(iv) The equivalent weight matrix determined by eq. (6.36) is symmetric and keeps the correlation coefficients of the original predicted state unchanged.

(v) The derivation is carried out with a nonlinear state space model. In practice, however, it may appear that the state space model consisting of a nonlinear model and a linear model, for which the algorithm is also suitable for this situation.

6.3 Computation and Analysis

To verify the proposed RMUKF, a simulation and a field test were conducted. The loosely coupled integration strategy was used to fuse the GPS and IMU data. A nine-state nonlinear error model, presented in Chapter 3, was used as the dynamic model equation. Data were processed using the Matlab R2010a 64-bit program on a PC with Intel Core i7-3770 CPU at 3.40 GHz, 16-GB RAM equipped with Win10.

6.3.1 Simulation Test

The configuration for the simulation is listed in Table 6.1. Simulation duration is 549s. The measurement outliers, listed in Table 6.2, are manually input.

Table 6.1 Simulation configuration

gyro constant drift	100°/h
angular random walk	5°/√h
velocity random walk	1000 ηg/√Hz
accelerometer bias	2000 ηg
Initial position	[22.31° 114.18° 41 m]
Initial positioning error	[1 m 1 m 3 m]
Initial velocity error	[0.2 m/s 0.2 m/s 0.2 m/s]
Initial Misalignment angle	[-20° 37° 80°]

Table 6.2 Magnitude of input outliers

Epoch	East [m/s]	North [m/s]	Altitude [m/s]	Latitude [m]	Longitude [m]	Altitude [m]
150s	+ 4.8	-	-	+ 10.01	-	-
200s	+ 1.33	+ 0.97	-	+ 9.95	+ 9.96	-
300s	+ 1.13	- 0.92	-	+ 10.01	+ 10.21	-
450s	+ 0.44	-	-	+ 9.95	-	-
138s	-	-	-	-	-	+ 10

The estimation results were compared with the simulated value (as the reference. The positioning errors of the simulation results in the three components are illustrated in Figure 6.2. Figure 6.3 is for the velocity error. It can be observed that the UKF result is sensitive to the outliers, and the error magnitude is more than 10 m in the longitude component, while that of the RMUKF is less than 5 m. The position error of the RMUKF is much smaller than that of the UKF, and its peak value is confined. This pattern is more obviously in the velocity estimation. The maximum errors of the UKF and RMUKF are plotted in Figure 6.4, which shows that the magnitude of estimate error of the RMUKF is smaller than that of the UKF. The RMSEs given in Table 6.3 show that the UKF and RMUKF have a similar performance in terms of position errors in the three components, however, the RMUKF suppressed the influences of the outliers and the velocity estimated from the RMUKF is superior to that of the UKF.

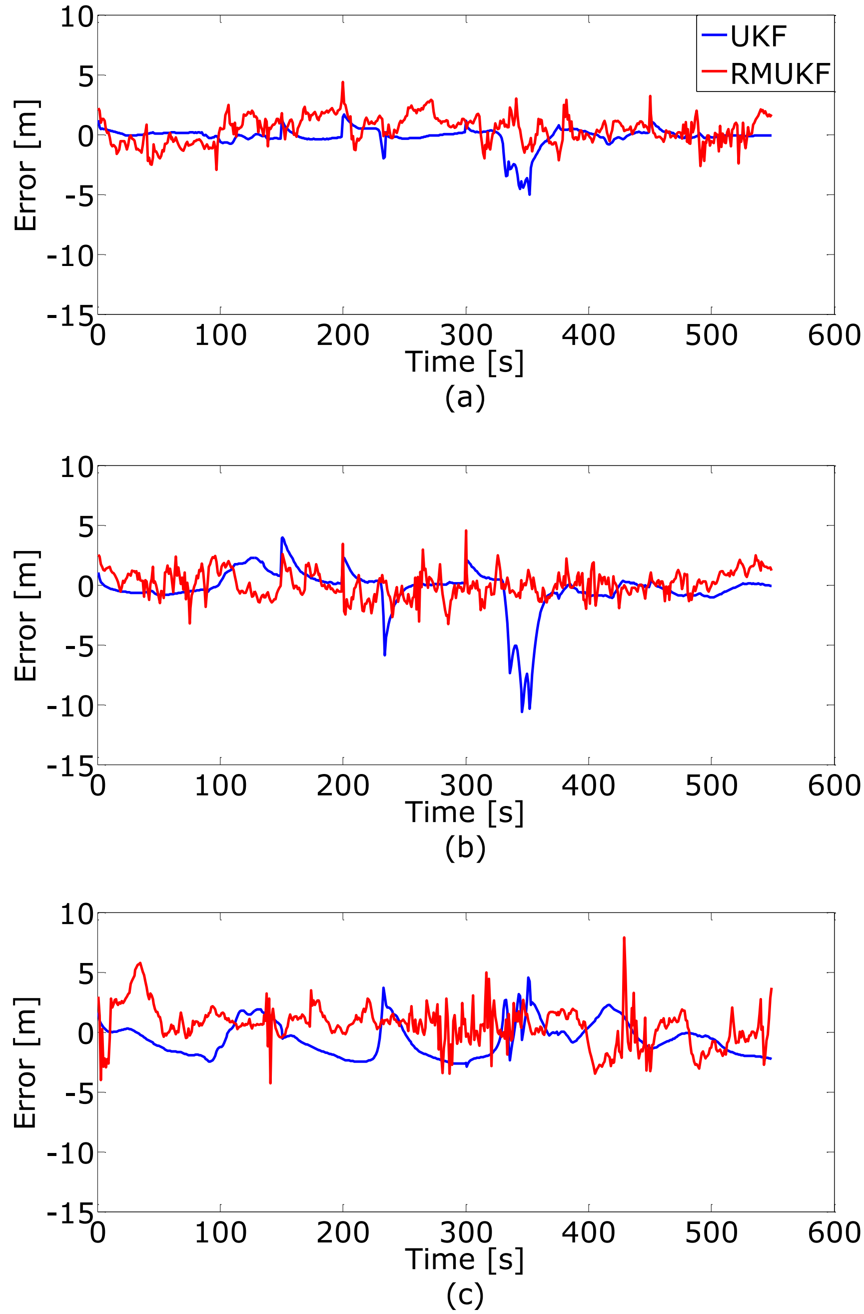

Figure 6.2 Position error of two filters in Latitude (a), Longitude (b), and Altitude (c)

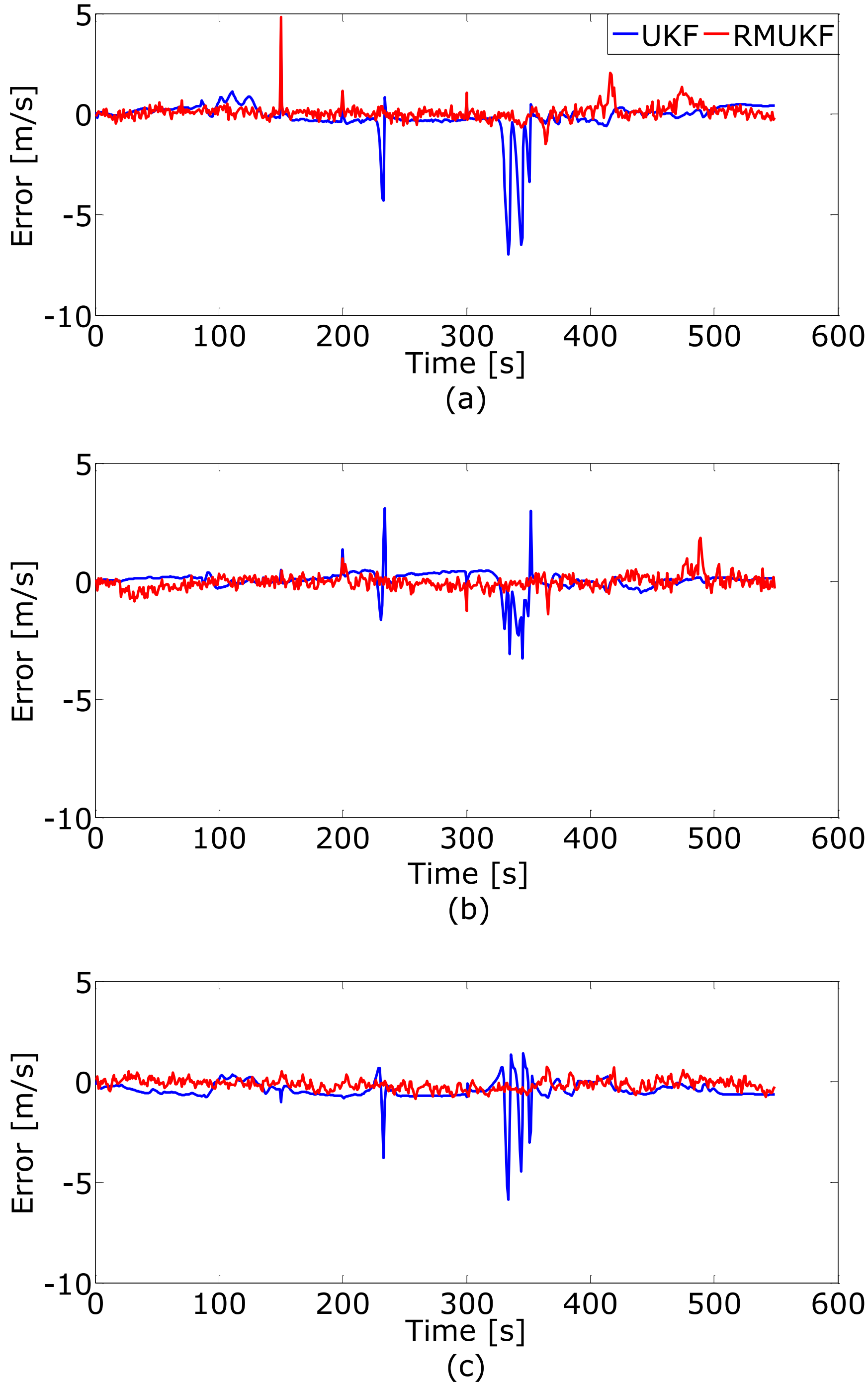

Figure 6.3 Velocity error of two filters in East (a), North (b), and Altitude (c)

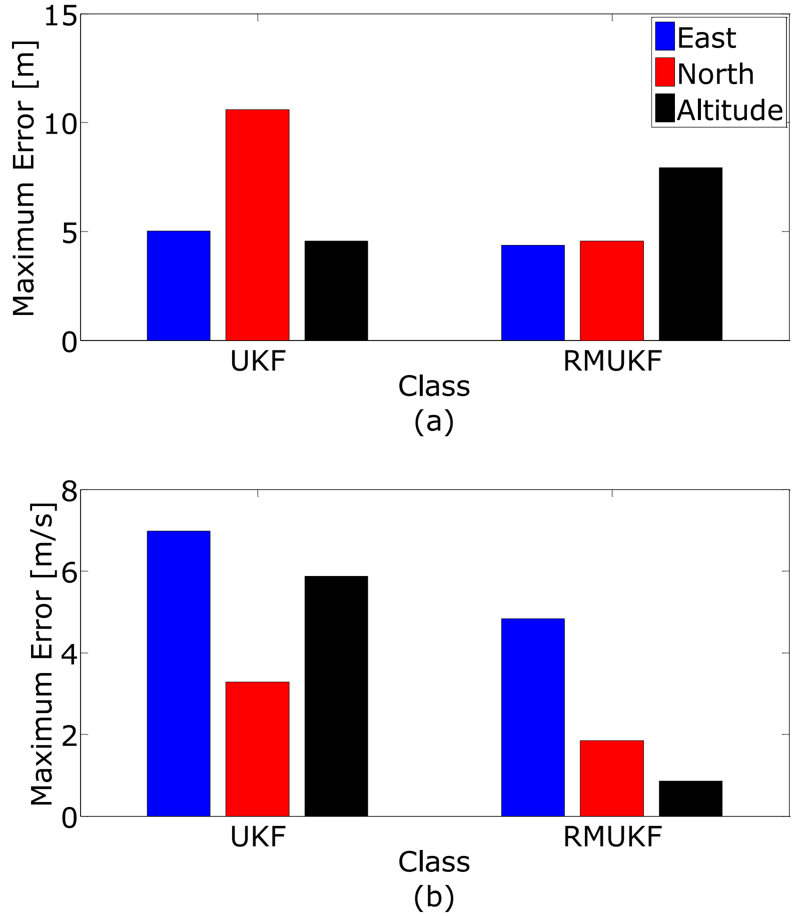

Figure 6.4 Maximum error of position (a) and velocity (b) of two filters

Table 6.3 RMSE of UKF and RMUKF

	Latitude [m]	Longitude [m]	Altitude [m]	East [m/s]	North [m/s]	Up [m/s]
UKF	0.84	1.83	1.57	0.90	0.46	0.72
RMUKF	1.21	1.10	1.75	0.40	0.30	0.30

6.3.2 Field Test

The proposed RMUKF applied to IMU/GPS integrated vehicle navigation was also tested in field and the test lasted about one and a half hours. The IMU and GPS parameters and initial conditions are listed in Table 6.4.

Table 6.4 IMU and GPS parameters and initial conditions

IMU Sampling Frequency	100 Hz
GPS Sampling Frequency	10 Hz
IMU Accelerometer bias	500 μg
IMU gyro bias	1 deg/h
Initial Position Error	[7 m, 7 m 7 m]
Initial Velocity Error	[0.1 m/s 0.1 m/s 0.1 m/s]
Initial Attitude Error	[10° 20° -15°]

The robust equivalent weight function is applied in the M-M UKF. The estimated results are compared with GPS robust SPP solution, and the result of position errors are presented in Figure 6.5. It can be seen that the RMUKF position is much closer to the GPS measured position. Compared with those UKF results, the RMUKF restricted the positioning error. The velocity result presented in Figure 6.6 indicates that the RMUKF outperformed UKF, especially in the east component during the early period. The RMSE presented in Figure 6.7 also proves the superior performance of the RMUKF.

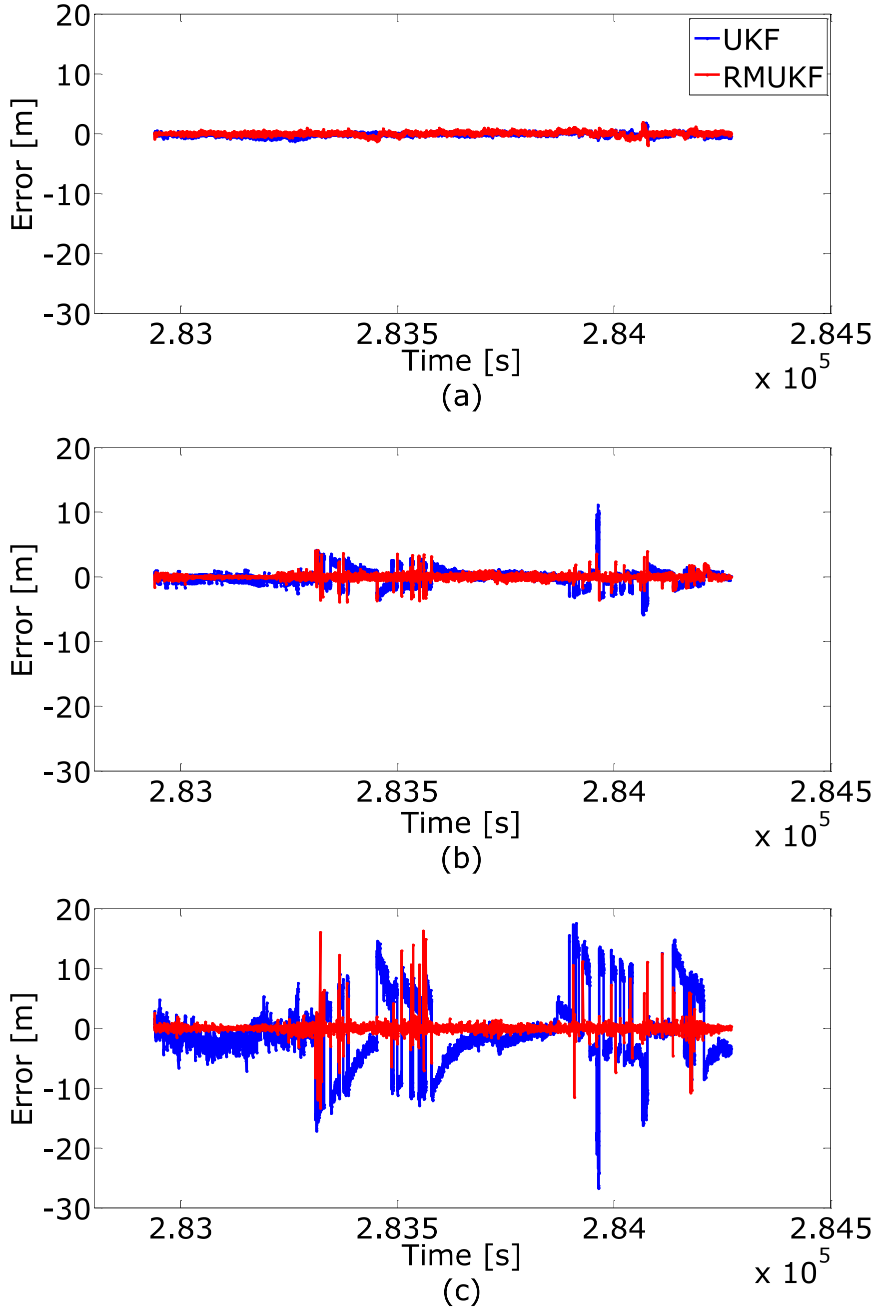

Figure 6.5 Position error of two filters at East (a), North (b), and Altitude (c) Components

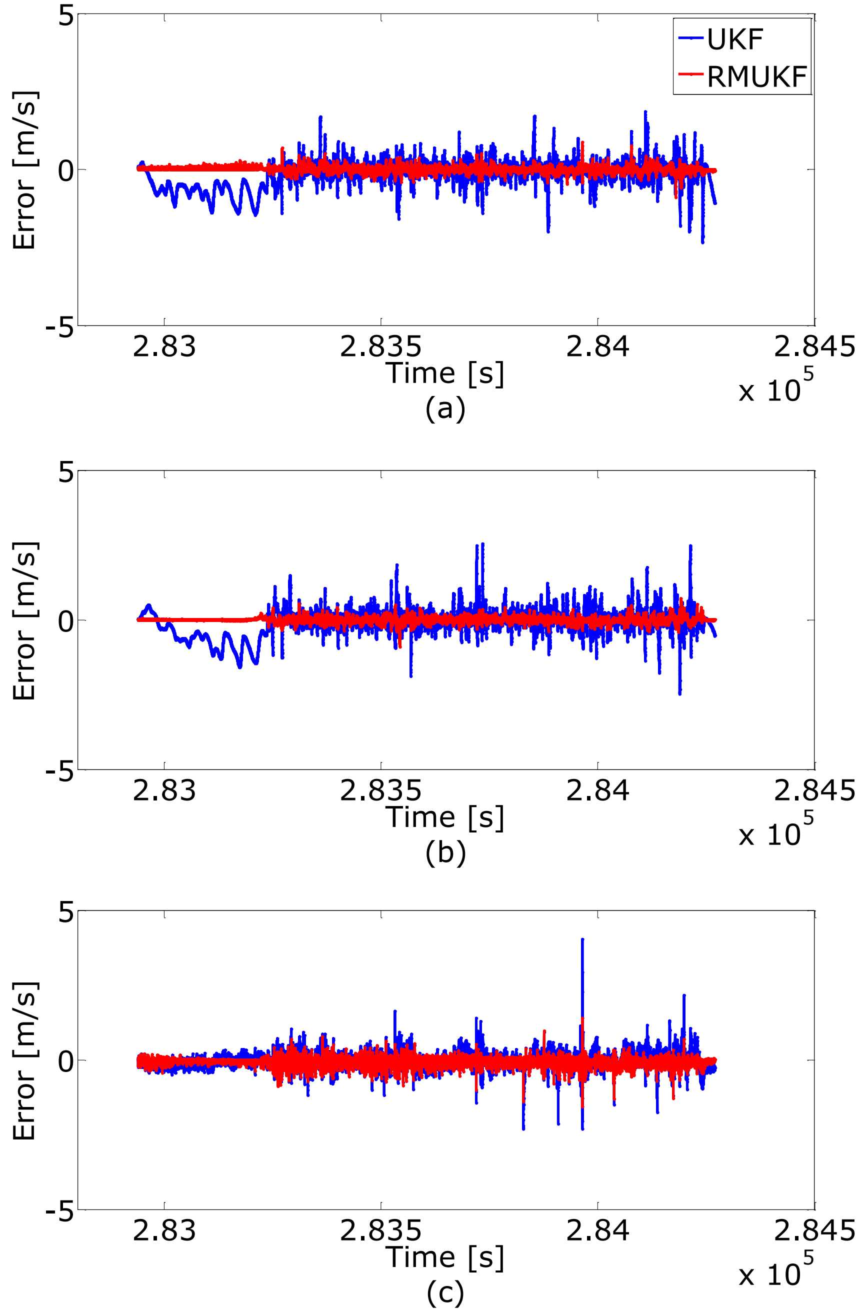

Figure 6.6 Velocity errors of two filters at East (a), North (b), and Altitude (c) Components

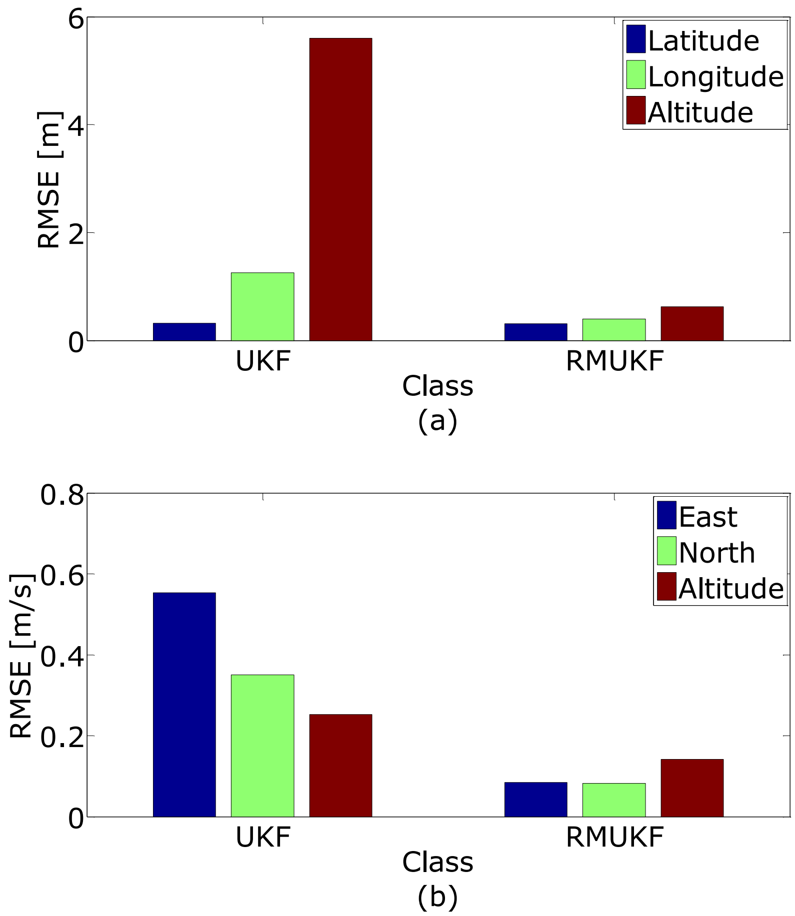

Figure 6.7 RMSE of position (a) and velocity (b)

6.4 Summary

This chapter presented a robust Unscented Kalman filter based on the M-M estimation method. The filter can suppress the state outliers from both the dynamic model and the measurements and hence provides a robust solution in an iterative manner. Furthermore, the correlations between the predicted state elements are solved by a correlated bi-factor algorithm that keeps the original correlation unchanged. The performance of the filter was tested by both simulation and field experiments. In the field test, the RMSE of RMUKF positioning estimate in East, North, and Altitude components are 0.31 meter, 0.40 meter, and 0.63 meter correspondingly; while the RMSE of those of UKF are 0.32 meter, 1.25 meter, and 5.60 meter. The measurement outliers and uncertainties of the system are both handled well by the RMUKF, while the UKF result fluctuated with outlier and could hardly maintain the accuracy.

Chapter 7 Conclusions and Future Recommendations

The main aim of the study is to investigate a robust and adaptive nonlinear filter to effectively improve the performance of GPS/IMU integrated navigation system. A comprehensive investigation the performances of various filters in the loosely coupled strategy have been conducted using both simulation and field tests.

The main contribution of this research includes:

(i) The correlational inference of the Kalman fileting method has revealed the fundamental relationship among the estimated state vector, the innovation vector and the predicted state vector, as well as their covariance and cross-covariance matrices. The new expression of the state estimator can be easily expressed into the standard Kaman filter, EKF and UKF. In addition, the new target function of UKF is firstly presented, and the estimator is rigorously derived.

(ii) Proposed an adaptive Unscented Kalman filter (AUKF) based on the correlational inference to deal with the contaminated predicted information and the nonlinear model with an adaptive factor which is constructed based on the system discrepancy at the present epoch.

(iii) Developed a robust M-M UKF (RMUKF) to further reduce the influences of the measurement outliers, with the consideration of the dynamic disturbances and nonlinear model. The robust equivalent weight matrices of the predicted state vector and measurement noise are constructed based on the residual vectors of the predicted states and measurements in an iterative manner. The correlations between the state parameters have been kept unchanged by using the bi-factor algorithm to construct the weight matrix.

7.1 Conclusions

The AUKF and RMUKF presented in this thesis improved the effectiveness and the accuracy of the UKF in the case of dynamic disturbances and system outliers. Kalman filtering is an effective and versatile method to estimate kinematic state from the measurements and dynamic model information in the integrated navigation systems. However, its functional models are based on the linear assumption, which are not very suited for real-world applications. To estimate nonlinear system states, the EKF has been widely applied. It analytically approximates the nonlinear equation by the first-order Taylor expansion. The cumbersome derivation and determination of the Jacobian matrix not only increases the complexity of the mathematical computation, but also introduces linearization errors. The UKF is another Gaussian approximation method that approximates a transformed probability statistically based on a set of sigma points.

Kalman filtering and its alternatives are all based on the weighted least squares principle, which are susceptible to measurement outliers, the abnormal disturbances of moving vehicles or the uncertainties of the dynamic models, and also the model errors introduced from the linearization process. In this research, the comparative studies for the UKF and EKF using different feedback modes were conducted, and test results revealed that the UKF outperformed the EKF. In the case of inaccurate stochastic information of physic or geometric errors of a dynamic model, the adaptive estimation introduced for this study is used to address the nonlinear model problems and dynamic model abnormality. In addition, the robust adaptive UKF introduced is to attenuate the influences of measurement outliers and stochastic uncertainties of the dynamic model on state estimates.

The following conclusions can be drawn from the theoretical analysis, simulation and field tests:

The Kalman filter derived using a correlational inference is very flexible and furthermore, the standard Kalman filter and the UKF can be easily accomplished in the same framework. The statistical relationships between the UKF and Kalman filter are thus obtained by the correlational inference. The performance of the UKF and EKF were analytically analyzed. The UKF uses the UT technique to approximate the predicted state vector $\bar{X}_k$ with its covariance matrix $\Sigma_{\bar{X}_k}$. In contrast, the EKF acquires the predicted state vector $\bar{X}_k$ with its covariance matrix $\Sigma_{\bar{X}_k}$ using the analytical method, variance-covariance propagation law, together with linearization. The performance of prediction accuracy of two approaches was also compared. The Monte Carlo approach was used to provide the reference information for this comparison. The simulation and field tests with different feedback modes, such as direct and indirect modes, in which the former uses the nonlinear state space model and the latter uses the linear state space model, were used to compare the overall performance of the UKF and EKF. The UKF has a better performance in nonlinear state estimation, while the EKF requires the linearize model to propagate the state mean and covariance matrix. Therefore, the UKF is easier in model design. The trace of the covariance matrix of the predicted UKF state is, in theory, larger than that of the EKF. This suggests that the UKF places less weight on historical information to reduce the contribution of the dynamic model information to the state estimates. Furthermore, the sigma points used in the UKF are sampled according to the updated state covariance matrix, which indicates that the predicted state parameters and their covariance matrix are closely related to the updated information. It is also noted that the estimation process of the EKF is less complicated than that of UKF.

The adaptive UKF (AUKF) was derived based on the correlational inference. From the theoretical point of view, the AUKF improved the performance of the filter in dealing with contaminated predicted state parameters and nonlinear models. If the predicted state has been seriously contaminated or the statistical information is insufficient for an accurate description of the present situation, a pertinent adaptive factor can effectively balance the contribution between the updated parameters and measurements by reducing the weight of the contaminated predicted information. Thus the influences of the contaminated dynamic model information are controlled by the adaptive factor. The adaptive factor is obtained from the innovation vector at the present epoch, which avoids the storage of innovation sequences and is more sensitive to the discrepancy of the predicted system state parameters and those estimated from the measurements. Both simulation and the field test, using loosely coupled configuration with a nonlinear dynamic model, have shown that the AUKF has superior performance in velocity and positioning parameter estimates, compared to the UKF.

The robust adaptive UKF based on the M-M estimation method can suppress the effects of both dynamic model disturbances and measurement outliers on the state estimates, and also provide a robust solution in an iterative manner. Furthermore, the correlations of the predicted state parameters are rigorously taken into account by the correlated bi-factor algorithm, in which the original correlations of the predicted parameters have been kept unchanged. The performance of the robust M-M UKF (RMUKF) was tested also by a simulation and a field test. The measurement outliers and dynamic model disturbances as well as the stochastic model uncertainties, were well handled by RMUKF.

7.2 Recommendations

Based on the studies in this thesis, the following recommendations for future work are suggested.

In urban canyons, the lack of GNSS observations is the main factor affecting the accuracy of a GNSS/IMU integrated navigation system, especially in the case that the integrated system uses low-cost inertial sensors. Such a system suffers from low precision and high sensitivity to surrounding environment. The accuracy of the system degrades quickly during outage of satellite signals due to the accumulation of IMU errors. The horizontal or vertical constraints, such as the known lateral and vertical acceleration components, should be taken into account in the state estimation, which will be known as constrained UKF. This topic could contribute to further study in for improvements of the navigation accuracy.

The tightly coupled integration GNSS/IMU strategy has the advantages that GNSS raw measurements are involved in the positioning solution. A robust tightly coupled integrated navigation strategy can be another research direction, especially as regards multiple GNSS signals integrated with inertial navigation system. It is expected that the robust coupled integrated navigation can be effective in improving the reliability of kinematic state estimation as well as the continuity of navigation solutions.

The robustness of the integrated system can be further improved by the inclusion of a new data source, such as map information, new sensors, and vision inputs. The new data sources, not only improve the availability, accuracy and reliability, but also the robustness owing to the redundant measurements.

The proposed algorithm can be further extended to smart phone positioning, in which the consumer grade IMU and radio signals as well as GNSS signals are integrated for the estimation or tracking of the phone position. The adaptive robust algorithm proposed in this study can be applied in improving the performance of the smart phone positioning by rebalancing the weights among various measurements as well as the dynamic model information.

References

Agarwal, M., & Mehra, R. (2014). Review of Matrix Decomposition Techniques for Signal Processing Applications. *International Journal of Engineering Research and Applications, 4*(1), 90-93.

Alspach, D., & Sorenson, H. (1972). Nonlinear Bayesian estimation using Gaussian sum approximations. *IEEE Transactions on Automatic Control, 17*(4), 439-448.

Anaolog Devices Inc. (2004). Angular Rate Sensor , ADXRS300 Data sheets, Rev. B. Analog Devices Inc.; Norwood, MA, USA.

Arulampalam, M. S., Maskell, S., Gordon, N., & Clapp, T. (2002). A tutorial on particle filters for online nonlinear/non-Gaussian Bayesian tracking. *IEEE Transactions on Signal Processing, 50*(2), 174-188.

Bancroft, S. (1985). An Algebraic Solution of the GPS Equations. *IEEE Transactions on Aerospace and Electronic Systems, AES-21*(1), 56-59.

Baarda, W. (1967). Statistical concepts in geodesy, Publication on Geodesy, 2*(4)*, Netherlands Geodetic Commission, Delft, Netherlands.

Baarda W. (1968). A testing procedure for use in geodetic networks, Publication on Geodesy, 2*(5)* Netherlands Geodetic Commission, Delft, Netherlands.

Betz, J. W., Blanco, M. A., Cahn, C. R., Dafesh, P. A., Hegarty, C. J., Hudnut, K. W., Kasemsri, V., Keegan, R., Kovach, K., Lenahan, L., Ma, H., Rushanan, J., Sklar, D., Stansell, T., Wang, C. Yi, S. (2006). *Description of the L1C Signal.* In Proceedings of the 19th International Technical Meeting of the Satellite Division of The Institute of Navigation (ION GNSS 2006).

Caputi, M. J., & Moose, R. L. (1993). A modified Gaussian sum approach to estimation of non-Gaussian signals. *IEEE Transactions on Aerospace and Electronic Systems, 29*(2), 446-451.

Challa, S. (2011). *Fundamentals of object tracking*. Cambridge University Press.

Chan, S. C., Zhang, Z. G., & Tse, K. W. (2005). *A new robust Kalman filter algorithm under outliers and system uncertainties.* In Circuits and Systems, 2005. ISCAS 2005. IEEE International Symposium on (pp. 4317-4320). IEEE.

Chang, G., & Liu, M. (2015). M-estimator-based robust Kalman filter for systems with process modeling errors and rank deficient measurement models. *Nonlinear Dynamics, 80*(3), 1431-1449.

Chang, L., Hu, B., Chang, G., & Li, A. (2012). Huber-based novel robust unscented Kalman filter. *IET Science, Measurement & Technology, 6*(6), 502-509.

Cui, N., Hong, L., & Layne, J. R. (2005). A comparison of nonlinear filtering approaches with an application to ground target tracking. *Signal Processing, 85*(8), 1469-1492.

Daum, F. (2005). Nonlinear filters: beyond the Kalman filter. *IEEE Aerospace and Electronic Systems Magazine, 20*(8), 57-69.

Davydov V., Revnivykh S.: GLONASS Today and Tomorrow, GPS World, vol. 23, no. 2, 2012, p. 16-17

Ding, W., Wang, J., Rizos, C., & Kinlyside, D. (2007). Improving Adaptive Kalman Estimation in GPS/INS Integration. *Journal of Navigation, 60*(03), 517-529.

Doucet, A., Godsill, S., & Andrieu, C. (2000). On sequential Monte Carlo sampling methods for Bayesian filtering. Statistics and Computing, 10(3), 197-208.Doucet, A., De Freitas, N., & Gordon, N. (2001). *Sequential Monte Carlo methods in practice*. New York: Springer.

Durgaprasad, G., & Thakur, S. S. (1998). Robust dynamic state estimation of power systems based on M-Estimation and realistic modeling of system dynamics. *IEEE Transactions on Power Systems, 13*(4), 1331-1336.

Durovic, Z. M., & Kovacevic, B. D. (1999). Robust estimation with unknown noise statistics. *IEEE Transactions on Automatic Control, 44*(6), 1292-1296.

El-Sheimy, N. (2012). Inertial Techniques and INS/DGPS Integration, ENGO 623-Course Notes, University of Calgary, Calgary, 2006.

European GNSS Agency (2016). Galileo goes live, https://www.gsa.europa.eu/newsroom/news/galileo-goes-live.

Fakharian, A., Gustafsson, T., & Mehrfam, M. (2011). *Adaptive Kalman Filtering Based Navigation: An IMU/GPS Integration Approach.* In Networking, Sensing and Control (ICNSC), 2011 IEEE International Conference on (pp. 181-185). IEEE.

Falco, G., Einicke, G., Malos, J., & Dovis, F. (2012). Performance Analysis of Constrained Loosely Coupled GPS/INS Integration Solutions. *Sensors, 12*(11), 15983-16007.

Faragher, R. (2012). Understanding the basis of the kalman filter via a simple and intuitive derivation [lecture notes]. *IEEE Signal processing magazine, 29*(5), 128-132.

Fitzgerald, R. (1971). Divergence of the Kalman filter. *IEEE Transactions on Automatic Control, 16*(6), 736-747.

Friedland, B. (1986). *Control system design : an introduction to state-space methods*. Courier Corporation.

Gandhi, M. A., & Mili, L. (2010). Robust Kalman Filter Based on a Generalized Maximum-Likelihood-Type Estimator. *IEEE Transactions on Signal Processing, 58*(5), 2509-2520.

Gao, J., Petovello, M., & Cannon, M. E. (2008). Integration of Steering Angle Sensor with Global Positioning System and Micro-Electro-Mechanical Systems Inertial Measurement Unit for Vehicular Positioning. *Journal of Intelligent Transportation Systems, 12*(4), 159-167.

Gao, S. S., Hu, G., & Zhong, Y. M. (2015). Windowing and random weighting-based adaptive unscented Kalman filter. *International Journal of Adaptive Control and Signal Processing, 29*(2), 201-223.

Gelb, A. (1974). *Applied optimal estimation*: MIT press.

Gordon, N. J., Salmond, D. J., & Smith, A. F. M. (1993). Novel Approach to Nonlinear Non-Gaussian Bayesian State Estimation. In IEE Proceedings F (Radar and Signal Processing) (Vol. 140, No. 2, pp. 107-113). IET Digital Library.

Grejner-Brzezinska, D. A., & Yi, Y. (2003). Experimental GPS/INS/Pseudolite System for Kinematic Positioning. *Survey Review, 37*(288), 113-126.

Grewal, M. S., Weill, L. R., & Andrews, A. P. (2007). *Global positioning systems, inertial navigation, and integration*: John Wiley & Sons.

Gustafsson, F., Gunnarsson, F., Bergman, N., Forssell, U., Jansson, J., Karlsson, R., & Nordlund, P. J. (2002). Particle filters for positioning, navigation, and tracking. *IEEE Transactions on Signal Processing, 50*(2), 425-437.

Gustafsson, F., & Hendeby, G. (2012). Some Relations Between Extended and Unscented Kalman Filters. *IEEE Transactions on Signal Processing, 60*(2), 545-555.

Guo, J. (2015). A Note on the Conventional Outlier Detection Test Procedures. Boletim de Ciências Geodésicas, 21*(2)*, 433-440.

Hajiyev, C., & Soken, H. E. (2014). Robust adaptive unscented Kalman filter for attitude estimation of pico satellites. *International Journal of Adaptive Control and Signal Processing, 28*(2), 107-120.

Hamilton, J. D. (1994). *Time series analysis*. Princeton, N.J: Princeton University Press.

Han, J., Song, Q., & He, Y. (2009). *Adaptive unscented Kalman filter and its applications in nonlinear control*: INTECH Open Access Publisher.

He, Y. Q., & Han, J. D. (2010). Acceleration-Feedback-Enhanced Robust Control of an Unmanned Helicopter. *Journal of Guidance, Control, and Dynamics, 33*(4), 1236-1250.

Hide, C., Moore, T., & Smith, M. (2003). Adaptive Kalman Filtering for Low-cost INS/GPS. *Journal of Navigation, 56*(1), 143-152.

Hitachi. (2007). User's Manual, Hitachi H48C 3-Axis Accelerometer Module.Hofmann-Wellenhof, B., Legat, K., & Wieser, M. (2003). *Navigation : principles of positioning and guidance*. Wien: Springer.

Hu, C., Chen, W., Chen, Y., & Liu, D. (2003). Adaptive Kalman filtering for vehicle navigation. *Positioning, 1*(4), 42-47.

Huang, B., & Wang, Q. (2006). *Overview of emerging Bayesian approach to nonlinear system identification.* In Round tables on Non-linear Model Identification, International Workshop on Solving Industrial Control and Optimization Problems (pp. 6-7).

Jin, S., Cardellach, E., & Xie, F. (2014). GNSS remote sensing: theory, methods and applications. Dordrecht: Springer.

Julier, S. J. (1998). *Skewed approach to filtering.* In Aerospace/Defense Sensing and Controls (pp. 271-282). International Society for Optics and Photonics.

Julier, S. J. (2002). *The scaled unscented transformation.* In American Control Conference, 2002. Proceedings of the 2002 (Vol. 6, pp. 4555-4559). IEEE.

Julier, S. J., & Uhlman, J. K. (1997). A New extension of the Kalman filter to nonlinear systems. Proceedings of the Society of Photo-Optical Instrumentation Engineers 3068:182–193

Julier, S. J., & Uhlmann, J. K. (2004). Unscented Filtering and Nonlinear Estimation. *Proceedings of the IEEE, 92(3), 401-422.*

Kaplan, E., & Hegarty, C. (2005). *Understanding GPS: principles and applications*: Artech house.

Koch, K. R. (1977). Least squares adjustment and collocation. *Bulletin géodésique, 51*(2), 127-135.

Koch, K. R. (1999). *Parameter estimation and hypothesis testing in linear models* (2nd updated and enl. ed.). Berlin, New York: Springer.

Koch, K. R., & Yang, Y. (1998). Robust Kalman filter for rank deficient observation models. *Journal of Geodesy, 72*(7), 436-441.

Kong, X. (2000). *Inertial navigation system algorithms for low cost IMU.* (Ph.D.), University of Sydney.

Kong, X. (2004). INS algorithm using quaternion model for low cost IMU. *Robotics and Autonomous Systems, 46*(4), 221-246.

Kovacevic, B., Durovic, Z., & Glavaski, S. (1992). On robust Kalman filtering. *International Journal of Control, 56*(3), 547-562.

Leick, A. (2004). *GPS satellite surveying* (3rd ed.). Hoboken, N.J: John Wiley & Sons.

Li, W., Sun, S., Jia, Y., & Du, J. (2016). Robust unscented Kalman filter with adaptation of process and measurement noise covariances. *Digital Signal Processing, 48*, 93-103.

Markov, B., & Tsankova, D. (2014). Mit rule based model reference adaptive control of linear induction motor. *Annals of the Faculty of Engineering Hunedoara - International J.* 12(3), 95-100.

Mohamed, A. H., & Schwarz, K. P. (1999). Adaptive Kalman Filtering for INS/GPS. *Journal of Geodesy, 73*(4), 193-203.

Moritz, H. (1978). *Statistical foundations of collocation*. (No. DGS-272). Ohio State University Columbus Department of Geodetic Science.

Noureldin, A., Karamat, T. B., & Georgy, J. (2013). Fundamentals of inertial navigation, satellite-based positioning and their integration. Berlin: Springer.

Orderud, F. (2005). *Comparison of kalman filter estimation approaches for state space models with nonlinear measurements.* In Proc. of Scandinavian Conference on Simulation and Modeling (pp. 1-8).

Park, M., & Gao, Y. (2006). Error Analysis and Stochastic Modeling of Low-cost MEMS Accelerometer. *Journal of Intelligent and Robotic Systems, 46*(1), 27-41.

Petovello, M. (2003). *Real-time integration of a tactical-grade IMU and GPS for high-accuracy positioning and navigation.* (Ph.D.), The University of Calgary.

Rigatos, G. G. (2012). Nonlinear Kalman Filters and Particle Filters for integrated navigation of unmanned aerial vehicles. *Robotics and Autonomous Systems, 60*(7), 978-995.

Sage, A. P., & Husa, G. W. (1969). Adaptive filtering with unknown prior statistics. *Joint Automatic Control Conference, 7*, 760-769.

Savage, P. G. (2000). *Strapdown Analytics*: Strapdown Associates.

Shin, E. H. (2005). *Estimation techniques for low-cost inertial navigation.* (Ph.D.), The University of Calgary.

Simon, D. (2006). Optimal state estimation Kalman, H Infinity, and nonlinear approaches. John Wiley & Sons.

Wan, E. A., & van der Merwe, R. (2000). *The unscented Kalman Filter for nonlinear estimation.* In Adaptive Systems for Signal Processing, Communications, and Control Symposium 2000. AS-SPCC. The IEEE 2000 (pp. 153-158). IEEE.

Wang, J., Gopaul, S., & Guo, J. (2010). *Adaptive Kalman Filtering Based on Posteriori Variance-Covariance Components Estimation.* In Proceeding of the CPGPS Technical Forum Satellite Navigation and Positioning, Shanghai, China (Vol. 1720, p. 111).

Wang, J. H. (2006). *Intelligent MEMS INS/GPS integration for land vehicle navigation.* (Ph.D), The University of Calgary.

Wang, Y., Sun, S., & Li, L. (2014). Adaptively Robust Unscented Kalman Filter for Tracking a Maneuvering Vehicle. *Journal of Guidance, Control, and Dynamics, 37*(5), 1696-1701.

Wu, F., & Yang, Y. (2010). An Extended Adaptive Kalman Filtering in Tight Coupled GPS/INS Integration. *Survey Review, 42*(316), 146-154.

Yan, G., Yan, W., & Xu, D. (2008). Application of simplified UKF in SINS initial alignment for large misalignment angles. *Journal of Chinese Inertial Technology, 16*(3), 253-264.

Yang, C., Shi, W., & Chen, W. (2016). Comparison of Unscented and Extended Kalman Filters with Application in Vehicle Navigation. *The Journal of Navigation*, 70(2), 411-431.

Yang, Y. (1991). Robust bayesian estimation. *Bulletin géodésique, 65*(3), 145-150.

Yang, Y., Cui, X., & Gao, W. (2004). Adaptive integrated navigation for multi-sensor adjustment outputs. *Journal of Navigation, 57*(02), 287-295.

Yang, Y., & Gao, W. (2005). Comparison of adaptive factors in Kalman filters on navigation results. *Journal of Navigation, 58*(03), 471-478.

Yang, Y., & Gao, W. (2006). An Optimal Adaptive Kalman Filter. *Journal of Geodesy, 80*(4), 177-183.

Yang, Y., He, H., & Xu, G. (2001a). Adaptively robust filtering for kinematic geodetic positioning. *Journal of Geodesy, 75*(2), 109-116.

Yang, Y., Song, L., & Xu, T. (2002). Robust estimator for correlated observations based on bifactor equivalent weights. *Journal of Geodesy, 76*(6), 353-358.

Yang, Y., & Xu, T. (2003). An adaptive Kalman filter based on Sage windowing weights and variance components. *The Journal of Navigation, 56*(02), 231-240.

Yang, Y., Xu, T., & He, H. (2001b). *On adaptively kinematic filtering.* Paper presented at the Selected Papers for English of Acta Geodetica et Cartographica Sinica.

Yang, Y., Zeng, A., & Zhang, J. (2009). Adaptive collocation with application in height system transformation. *Journal of Geodesy, 83*(5), 403-410.

Zhe Chen and Emery N. Brown (2013) State space model. Scholarpedia, 8(3):30868.

Zhong, Y., Gao, S., & Li, W. (2012). A Quaternion-Based Method for SINS/SAR Integrated Navigation System. *IEEE Transactions on Aerospace and Electronic Systems, 48*(1), 514-524.